

Design and synthesis of small
molecule probes targeting malaria,
diabetic neuropathy and
thrombocytopenia

Meena Purohit, *BITS Pilani*



**Design and synthesis of small molecule probes
targeting malaria, diabetic neuropathy and
thrombocytopenia**

THESIS

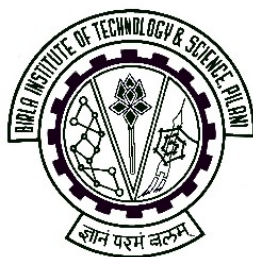
Submitted in partial fulfillment
of the requirements for the degree of
DOCTOR OF PHILOSOPHY

By

Meena Purohit

Under the supervision of

Prof. Lakshmi P. Kotra



BIRLA INSTITUTE OF TECHNOLOGY AND SCIENCE

PILANI (RAJASTHAN) INDIA

2013

BIRLA INSTITUTE OF TECHNOLOGY & SCIENCE
PILANI, RAJASTHAN

CERTIFICATE

This is to certify that the thesis entitled, “**Design and synthesis of small molecule probes targeting malaria, diabetic neuropathy and thrombocytopenia.**” was submitted by **Meena Purohit, ID. No. 2006PH08145** for award of Ph.D. degree of the Institute embodies the original work done by her under my supervision.

Signature of the supervisor:

Name in capital block letters: **PROF. LAKSHMI P. KOTRA**

Designation: **Adjunct Professor, BITS- Pilani
and Associate Professor, University of Toronto**

Date:

This thesis is dedicated to my parents

Thank you papa and mummy for your endless support and love

Acknowledgments

Research is always a team effort. I want to take this opportunity to thank many people for helping me in research and making my stay at University of North Carolina, Greensboro, US (2008-2009) and University Health Network, Toronto (2009-2012) a memorable one.

I would like to express my deep gratitude to my research advisor, Prof. Lakshmi P. Kotra for his guidance and support for last four years. I have learned from him how to grow and think as a scientist. He was always available whenever I needed his help and advice. He is a constant source of great innovative research ideas. I feel privileged to have an opportunity to work under his excellent mentorship and amazing research facilities. The work experiences gained from him will be remembered throughout my life.

My gratitude to Prof. Bijendra Nath Jain, Vice Chancellor of BITS (Pilani). I owe my gratitude to former Dean, Research and Consultancy Division, BITS (Pilani) Prof. Ravi Prakash for giving me an opportunity to carry out my doctoral research work in US and Canada. I owe my deepest gratitude to Prof. R. N. Saha, Deputy Director, Research, and Education Development, BITS (Pilani), for his support and encouragement to pursue my doctoral thesis. My sincere thanks to Dr. R. Mahesh, Dean, Faculty Affairs, BITS (Pilani) for his guidance. I owe my gratitude to Dr. Hemant Jadhav, Head of Department, Pharmacy Group, BITS (Pilani). He was in constant communication with me throughout my off-campus PhD programme, thus making it easy.

I also owe my deepest gratitude to our collaborators Dr. Emil Pai (Univ of Toronto), Dr. Donald Branch (Canadian Blood Services), Dr. Paul Fernyhough (Univ of Manitoba) and Dr. Nigel Calcutt (UCSD).

Very special thanks to all my all former and present labmates. Dr. Chandrasekhar Vanampally and Dr. Mallinath Hadimani are like my family members more than colleagues. Their help during my transition from US to Canada was unforgettable. My parents too owe them hearty thanks.

Dr. Angelica Bello, Dr. Meza Avina Elena and Dr. Sai Kumar Chakka are three additional mentors who helped me to be what I am today. They introduced and guided me in the world of organic chemistry, analytical chemistry, medicinal chemistry and life chemistry. Doing research away from family was not very easy but these three wonderful people made my life in US and Canada easy and comfortable.

I am very much thankful to Ms. Ewa Poduch for teaching me practical aspects of biochemistry. She is one of the perfectionists I have come across so far. I would like to thank Dr. William Wei for his computational contribution in ODCase project. William, I would never forget long lunch breaks and interesting conversations with you.

I am grateful to Gabriella Iftime for her guidance and friendship. I also owe my gratitude to Melissa Lewis, Amelia Navarate, Ram Kumar Mishra and Joseph. Friends are family members selected by us. I am very much thankful to all my friends especially Erica, Nicole, Peter, Terence, John, Lilly, Yatong, Srihari, Sourabh, Rohini, Rajeev, Niloufer and Veenu.

My warmest thanks belong to my family for their never ending love, encouragement and support. Very special thanks to my father for his belief that I can do it. His immense trust and confidence on me has made it possible for me to finish my thesis. I owe my doctorate degree to my parents for boosting my confidence. I wish to dedicate this thesis to my sisters, sister-in-law and my dear nieces for their love and affection.

I want to thank my fiancé for his love and all efforts he took to preserve our long distance relationship.

Thank you, God for a beautiful and meaningful life.

Meena Purohit

List of figures

Figure No.	Description	Pg.No.
Figure 1.1	Schematic representation of the drug development process. The stages of drug development confronted in this thesis are target identification, hit identification and lead generation and optimization	2
Figure 2.1	De Novo biosynthesis of pyrimidine nucleotides	10
Figure 2.2	Schematic representation of unconventional reactions by ODCase. A. The conversion of 6-CN-UMP (4) to BMP (3) by native ODCase, B. Covalent bond formation with native ODCase active amino acid Lys75 and 6-I-UMP (5)	13
Figure 2.3	Schematic representation of 6-azaUMP bound to the active site of ODCase from <i>M.thermoautotrophicum</i>	14
Figure 2.4	Inhibition of <i>Mt</i> ODCase by compound 14 . (A) Thermograms representing the reaction rate in the absence and presence of compound 14 . (B) The rate of decarboxylation of OMP in the absence and presence of compound 14 . (C) Line weaver Burk plot for the inhibition of ODCase by compound 14	26
Figure 2.5	Co-crystallization of compound 14 and 27 with <i>Hs</i> ODCase	28
Figure 2.6	Co-crystals of compound (A) 14 and (B) 27 with <i>Hs</i> ODCase	28
Figure 2.7	IR Spectrums for (A) Cyd- N^3 -oxide (13), (B) Cyd- N^4 -OH (15), (C) CMP- N^3 -oxide (14) and (D) CMP- N^4 -OH (27)	32
Figure 2.8	^1H NMR (400 MHz) spectrum of compound 14 (A) and 27 (B)	33
Figure 2.9	Ferric Chloride color test distinguishing between compounds 14 and 27 . (A) Blank, (B) CMP (11), (C) CMP- N^3 oxide (14) and (D) N^4 -OH-CMP (27)	33
Figure 2.10	Hydrogen bonding interactions between UMP and the various active site residues of <i>Hs</i> ODCase	37
Figure 2.11	X-ray crystal structure of the complex generated by incubating ODCase with compound 14 . Panel (A) shows both rearranged products 5-OH-CMP and N^4 -OH-CMP from 14 bound to the active site of the <i>Hs</i> ODCase. Panel (B) exhibits the rearranged product N^4 -OH-CMP and 5-OH-CMP from 14 during co-crystallization with <i>Hs</i> ODCase. Panels (C) and (D) 5-OH-CMP and N^4 -OH-CMP bound to the	39

active site of the *Hs* ODCase, respectively. *Hs* ODCase presented as cartoon model and colored with respect to the secondary structure (α -helix: Red. β -sheet: yellow. Turns: green). The rearranged products from **14** are shown as stick model with electron density map ($2F_o-F_c$) at 1σ value. Catalytic residues of K92, D123, K125, and D128 from human ODCase are also shown as capped-stick model. (E) and (F) Hydrogen bonding network between the rearranged product N^4 -OH-CMP and 5-OH-CMP from ligand **14** (respectively) with the various active site residues of *Hs* ODCase. (G) Plausible mechanism of rearrangement of the ligand **14** to yield N^4 -OH-CMP and 5-OH-CMP.

- Figure 2.12 X-ray crystal structure of the complex generated by incubating *Hs* ODCase with compound **27**. (A) Active site region of the *Hs* ODCase with ligand **27** bound in different conformations. (B) Amino-imino tautomers of **27** and the cis-trans imino isomers of the exocyclic N^4 -OH moiety with respect to the N3 of the pyrimidine. Panel (C) and (D) represents compound **27** bound in the *cis* and *trans*-conformation respectively, in the active site of the *Hs* ODCase. *Hs* ODCase presented as cartoon model, colored with respect to the secondary structure (α -helix: Red. β -sheet: yellow. Turns: green). Compound **27** is shown in capped-stick representation with electron density map ($2F_o-F_c$) at 1σ value. Catalytic residues of K92, D123, K125, and D128 of *Hs* ODCase are shown as stick model 46
- Figure 2.13 Active sites of ODCase from the X-ray crystal structures of the complexes of (A) *Hs* ODCase with UMP (yellow) overlapped with *Mt* ODCase bound by CMP (blue), (B) *Hs* ODCase with UMP overlapped with *Hs* ODCase bound by N^4 -OH-CMP (**27**) (green), (C) *Mt* ODCase with CMP bound by *Hs* ODCase bound by **27** 47
- Figure 3.1 A schematic depiction of metabolic, functional and structural abnormalities in a peripheral diabetic neuron, which could play a role in neuropathy development 56
- Figure 3.2 Schematic presentation of procedure to isolate the molecular proteins binding to ligand immobilised on the solid matrix. Step a. Addition of cell lysate to suspension of resin loaded ligand in buffer, step b. Incubation of the cell lysate with ligand in buffer, step b. Incubation of the cell lysate with ligand immobilised on resin at 4 °C, 4h, step c. Centrifugation 12000 rpm, 2 min, step d. Removal of the supernatant (S1) followed by gentle and thorough washing of the residual resin (R1), step e. Addition of surfactant (20 μ l), step f. Incubation of the surfactant solution with ligand immobilised resin (R1), rt, 15 min. Repetition of step c and d 79

	to isolate the proteins fished by the ligand immobilised on the solid matrix	
Figure 3.3	(A) IR spectra of Neat affinity resin-Toyopearl Carboxy AF 650M, (B) IR spectra of ligand 19 , (C) IR spectra of resin 20 after loading of ligand 19 , (D) IR spectra obtained after subtraction of resin 20 spectra from spectrum A	85
Figure 3.4	(E) IR spectra of resin 21 after capping with ethanolamine, (F) IR spectra acquired after subtraction of resin 21 spectra from spectrum A, (G) IR spectra of resin 22 after removal of protective groups of vicinal 1,2-diols and (H) IR spectra obtained after subtraction of resin 22 spectra from spectrum A	86
Figure 3.5	Rat sensory neuron cultures from the DRG of adult normal rats were grown for 1 day in the presence of a cocktail of growth factors, with 10 mM D-glucose and were exposed to a range of concentrations of compounds. Total neurite outgrowth was assessed by counting the neurite intersects with a Weibel grid. All data adjusted to number of cells (presented as number of intersects per cell). Values are means \pm SEM (n = 6 replicate cultures). * P < 0.05 vs control (oneway ANOVA with Tukeys); ** P < 0.02 vs control and 0.1 μ M (oneway ANOVA with Tukeys) and *** P < 0.02 vs control. Panel A is an image of 24h culture of adult rat STZ-diabetic sensory neurons. Panel B and C are images of 24h adult rat STZ diabetic sensory neurons incubated with compound 1 (1.0 μ M) and compound 9 (0.01 μ M) respectively. The graphs showing total axonal regeneration and outgrowth from adult rat STZ diabetic sensory neurons stimulated by compounds 1 and 6 are presented in Panel D, whereas compounds 9 , 10 , 7 , and 8 are presented in Panel E, F, G and H respectively. White arrows show swellings or dystrophic regions on axon and black arrow non-neurons	87
Figure 3.6	Prevention study of guaifenesin (1) investigating its effect on diabetes induced MNCV slowing (A) and thermal latency (B) in STZ-diabetic mice. Intervention study of guaifenesin (1) investigating its effect on diabetes induced MNCV slowing (C) and thermal latency (D) in STZ-diabetic mice	91
Figure 3.7	Effect of (<i>R</i>)-guaifenesin (9) on diabetes induced MNCV slowing in STZ-diabeticmice. MNCV was measured at weekly intervals. Data are group mean \pm SEM	92
Figure 3.8	SDS PAGE for protein isolated by serial affinity chromatography. Lane T1 shows protein captured by resin 22 , lane of control shows protein captured by control resin and lane of MWt shows molecular weight ladde	95

Figure 4.1	Fc γ mediated clearance of autoantibody sensitized platelets	104
Figure 4.2	Monocyte monolayer assay (MMA) for screening drugs inhibiting phagocytosis. (MMA was carried out by Dr. Donald Branch laboratory ²²) a. Isolation of peripheral blood mononuclear cells (PBMCs; containing monocytes) by density gradient centrifugation; b. After overnight incubation at 37°C, 5% CO ₂ , layering of PBMCs onto chamber slides followed by incubation at 37°C, 5% CO ₂ for 1h; c. Incubation of the adhered monocytes with drug at 37°C, 5% CO ₂ for 1h; d Incubation of drug treated monocytes with anti-D opsonized RBCs at 37°C, 5% CO ₂ for 2h; e. Fixing of slides and f. Read out of phagocytosis by microscopy with phase contrast.	107
Figure 4.3	Template for first generation SH/SS pyrazole derivatives inhibiting phagocytosis	109
Figure 4.4	Strategic structural modifications around the hit molecule 10	109
Figure 4.5	MMA slide under microscope. (A) Opsonised RBCs (white arrows) phagocytised by M ϕ (black arrows); (B) Opsonized RBCs (white arrows) attached on M ϕ (black arrows)	153
Figure 4.6	(A) Chromatogram of purchased 4i found to be a mixture of sulfide 4i and disulfide 5i (B) Mass Spectrum of peak 18.43 min 5i , (C)) Mass Spectrum of peak 14.23 min 4i	156
Figure 4.7	Chromatograph of compounds (A) 4i and (B) 5ii	157
Figure 4.8	Chromatograph of compound 5iv as polysulfide mixture	158

List of tables

Table No.	Description	Pg.No.
Table 2.1	Purity data for cytidine derivatives	23
Table 2.2	Diffraction and refinement data for co-crystal complexes of compound 14 and 27 with <i>Hs</i> ODCase.	29
Table 2.3	Inhibition constants for nucleotide ligands against ODCases from <i>Mt</i> , <i>Hs</i> and <i>Pf</i> . All inhibitors were evaluated in competitive assays against the ODCase. “No inhibition” indicates that the activity was not inhibited at up to 20 mM concentration of the inhibitor	35
Table 2.4	UV spectra for compounds 14 and 27 after incubation in the crystallization buffer for 24 h at room temperature	44
Table 3.1	Purity data for guaifenesin derivatives	69
Table 3.2	Stock solutions preparation	80
Table 3.3	Lysis buffer-1 recipe	80
Table 3.4	Final lysis buffer recipe	80
Table 3.5	SDS buffer recipe	80
Table 3.6	Pharmacokinetic parameters of racemate guaifenesin (1) and (<i>R</i>)-guaifenesin (9) in control and STZ- diabetic mice	93
Table 4.1	Severity and clinical outcomes of thrombocytopenia	103
Table 4.2	Summary of the compounds synthesized in the Scheme 1	112
Table 4.3	Semi - preparatory purification method for compound 9	147
Table 4.4	HPLC methods used for the purity assessment of synthesized compounds	149
Table 4.5	Purity data for the first generation synthesized compounds	150
Table 4.6	Purity data for the second generation synthesized compounds	151
Table 4.7	Biological activity for first generation compounds 4i-4ii , 5i , 5iii-iv , 9 and 10 at 5 μ M concentration, in comparison to the positive control IVIG. Results represent the mean percentage phagocytosis inhibition \pm SEM of three	163

independent experiments

Table 4.8	Biological activity for second generation inhibitors at 5 μ M concentration, in comparison to the positive control IVIG Results represent the mean percentage phagocytosis inhibition \pm SEM of three independent experiments	164
Table A.3.1	Neuronal proteins found in the control lane (excluding keratin and repeats) of target deconvolution (serial affinity chromatography) experiment, chapter 3	A6
Table A.3.2	Neuronal proteins found in the T1lane (excluding keratin and repeats) of target deconvolution (serial affinity chromatography) experiment, chapter 3	A12

List of charts

Chart No.	Description	Pg.No.
Chart 1.1	Structures of hit compounds in chapter 2 and 3	4
Chart 2.1	Structures of ODCase substrate, OMP and various inhibitors	12
Chart 2.2	Design of CMP analogs	16
Chart 2.3	Chemical structures of purine nucleotides	35
Chart 3.1	Different classes of drugs inducing neurite outgrowth	58
Chart 4.1	Preceding compounds inhibiting Fc γ receptor mediated phagocytosis of opsonized RBCs	106
Chart 4.2	Lead molecules chemical structures	109

List of abbreviations

ACN	Acetonitrile
ANOVA	Analysis of variance
ATR-IR	Attenuated Total Reflectance-Infra Red
BLAST	Basic Local Alignment Search Tool
br	broad
BOC	<i>tert</i> -Butyl carbonate
CDCl ₃	Deuterated chloroform
CMP	Cytidine-5'-monophosphate
d	doublet
dd	Doublet of doublet
DEAD	Diethyl azodicarboxylate
D ₂ O	Deuterated water
DCM	Dichloromethane
DRG	Dorsal Root Ganglion
DMAP	4-Dimethylaminopyridine
DMF	Dimethylformamide
DMSO	Dimethylsulfoxide
DTT	Dithiothreitol
ESI	Electrospray ionization
EDTA	Ethylene Diamine Tetracetic Acid
EDAC	1-Ethyl-3-(3-dimethylaminopropyl)carbodiimide
EtOAc	Ethylacetoacetate
Et ₃ N	Triethylamine
HATU	(<i>O</i> -(7-azabenzotriazol-1-yl)- <i>N,N,N',N'</i> -tetramethyluronium hexafluorophosphate)

^1H NMR	Proton Nuclear Magnetic Resonance
HPLC	High Pressure Liquid Chromatography
HTS	High Throughput Screening
[I]	Inhibitor
i.p.	intraperitoneal
i.v.	Intravenous infusion
IC ₅₀	half maximal inhibitory concentration
ITP	Idiopathic Immune Thrombocytopenia
ITC	Isothermal Titration Calorimetry
IVIG	Intravenous Immunoglobulins
K _i	Inhibition Constant
LAH	Lithium Aluminum Hydride
m	multiplet
MS	Mass spectrometry
MSDS	Material safety data sheet
MMA	Monocyte monolayer assay
mM	Millimolar
MWt	Molecular weight
mg	Milligram
mmol	Millimoles
nM	Nanomolar
NGF	Neutrophic Growth Factors
NHS	<i>N</i> -hydroxy succinimide
ODCase	Orotidine-5'-monophosphate decarboxyale
Py	Pyridine
PTFE	Polytetrafluoroethylene

rt	Room temperature
Rt	Retention time
s	singlet
s.c.	subcutaneous
[S]	Substrate
SDS	Sodium dodecyl sulfate
SEM	Standard Error of Mean
STZ	Streptozotocin
$t_{1/2}$	half life
TBDMSCl	<i>tert</i> -Butyldimethylsilyl chloride
TFA	Trifluoroacetic acid
TLC	Thin layer Chromatography
Tris	tris(hydroxymethyl)aminomethane
UMP	Uridine-5'-monophosphate
μ M	Micromolar

Abstract

This thesis describes work done in design and synthesis of small molecule probes targeting malaria, diabetic neuropathy and thrombocytopenia.

Orotidine-5'-monophosphate decarboxylase (ODCase) has been a subject of intense investigation over the past two decades. Inhibition of *Plasmodium* ODCase is a strategy to develop novel drugs targeting malaria. Several C-6 substituted UMP derivatives were developed as potent ODCase inhibitors and their interactions with the active site of ODCase were studied comprehensively. As compared to UMP, cytidine-5'-monophosphate (CMP) is a weak inhibitor of ODCase. Unlike uridine mononucleotides, the cytosine ring of CMP cannot engage optimally with the enzyme active site. Hence, the investigation was undertaken using two novel CMP derivatives that bind to ODCase with high potency and engage in productive interactions with the ODCase active site. These CMP analogs were co-crystallized with human ODCase and their interactions were studied. A detailed discussion on the molecular interactions of CMP analogs with ODCase and their therapeutic potential is presented in Chapter Two.

Chapter Three discusses target identification and drug development for diabetic neuropathy, a common complication of diabetes mellitus. In diabetics, several morphological and structural changes such as microangiopathy, axonal degeneration, and segmental demyelination are seen due to increased level of glucose in peripheral nerves. Guaifenesin was identified as a potential molecule engaging in enhancing neuronal outgrowth and restore neuronal

conduction. Target deconvolution was attempted for the most potent (*R*)-enantiomer of the guaifenesin by affinity chromatography approach.

Immunological destruction of platelets in response to unknown stimulus is known as “idiopathic thrombocytopenic purpura” or “primary immune thrombocytopenia” (ITP). Current treatments for ITP include corticosteroids, rituximab (decreases anti-platelet autoantibody production), intravenous immunoglobulins (IVIg and anti-D) and splenectomy (surgical removal of spleen). Since the Fc γ receptor mediated phagocytosis of the opsonized platelets is the underlying pathogenesis of ITP, small molecules targeting Fc γ receptors expressed on mononuclear phagocytes could be an alternative treatment to ITP. The work presented in Chapter Four of this thesis describes the synthesis, analysis and biological evaluation of a small set of sulfhydryl and disulfide compounds as inhibitors of Fc γ receptors mediated phagocytosis for potential use as therapeutics for ITP.

Key words: Malaria, ODCase, CMP, ITC, diabetic neuropathy, affinity chromatography, guaifenesin, enantiomers, pharmacokinetic, thrombocytopenia, thiols and disulfides, MMA.

Table of contents

Certificate	iii
Acknowledgments	v
List of figures	viii
List of tables	xii
List of charts	xiv
List of abbreviations	xv
Abstract	xviii
<i>Introduction-Thesis overview</i>	
1.1 Introduction	1
1.2 References	8
<i>Project 1-Design and synthesis of CMP derivatives to investigate the mechanistic details of orotidine-5'-monophosphate decarboxylase (ODCase)</i>	
2.1 Introduction and literature review	10
2.2 Objective	15
2.3 Experimental Section	17
2.3.1 Synthetic schemes and procedure	17
2.3.2 Enzymology	24
2.3.3 Crystallography	27
2.3.4 In-vitro parasitology	30
2.4 Chemistry discussion	31
2.5 Result, discussion and conclusion	34
2.6 References	49

Project 2-Phenoxy propanediol derivatives targeting neuroaxonal growth in diabetic neuropathy.

3.1	Introduction and literature review	55
3.2	Objective	61
3.3	Experimental Section	62
3.3.1	Synthetic schemes and procedures	62
3.3.2	In vitro screening assay	70
3.3.3	Motor nerve conduction velocity measurement (MNCV)	70
3.3.4	Thermal latency (Thermal hypoalgesia)	71
3.3.5	Pharmacokinetics studies	71
3.3.6	Experimental section for target deconvolution	73
3.4	Chemistry discussion	81
3.5	Result, discussion and conclusion	88
3.6	References	96

Project 3-Design and synthesis of novel pyrazole derivatives inhibiting Fcγ receptor mediated phagocytosis in idiopathic immune thrombocytopenia (ITP)

4.1	Introduction and literature review	103
4.2	Objective	108
4.3	Experimental Section	110
4.3.1	Synthetic schemes and procedures	110
4.3.2	Monocyte monolayer assay	152
4.4	Chemistry discussion	154
4.5	Result, discussion and conclusion	163
4.6	References	170

Appendices

List of publications	A1
Work presented in conferences	A2
Biography of Lakshmi P. Kotra, B. Pharm.(Hons), Ph.D	A3
Biography of Ms. Meena K. Purohit	A5

Introduction-Thesis Overview

1.1 Introduction

Medicinal chemistry, a multidisciplinary branch, encompasses “drug” and “drug target”. A drug is defined as any substance that brings about a change in the biological function through its chemical actions and prevents or cures diseases in humans, animals or plants. A drug molecule interacts with a specific macromolecule intimately related to the disease in the question and elicits its pharmacological effect. This macromolecule is called as drug target or druggable protein. A comprehensive knowledge about the properties of the drug-like molecule, the druggable protein, and the associated disease knowledge provides an initial stage for a medicinal chemist to design and synthesis a potential drug for treating human disease. ¹

Discovery and development of a new drug are challenging and time consuming process. Figure 1.1 describes the stages involved in the drug development process. Drug discovery initiates after a thorough understanding of the disease pathology and related biochemical research. Based on the information collected, drug design team then decides what intervention would most likely give the desired results. On selection of the point of intervention and identification of a target (druggable protein, e.g., an enzyme or a receptor) relevant in a disease model, a bioassay or screening assay is developed. Phenotypic screening assay (cell-based assay) is developed when the target or the druggable protein remains unidentified. Next, large numbers of molecules are screened (high throughput screening, HTS) in the developed bioassays, resulting in identification of the hit compounds. If the 3D-structure of the druggable protein is known then the virtual screening (computational) is employed and hits are identified. A medicinal chemist then analyses the hits

considering their physiochemical properties and functional groups present on them. Selected hits are then subjected to chemical exploration in search of lead compound. A lead molecule has a potential to develop into a drug. A lead molecule is then further optimized for its physiochemical, pharmacokinetic, and pharmacodynamic properties. Among the compounds of lead series, prospective drug candidates with potential to develop into safe and effective drugs are selected and forwarded for preclinical trials. Drug candidates from preclinical stage are then promoted to clinical trials.^{2, 3}

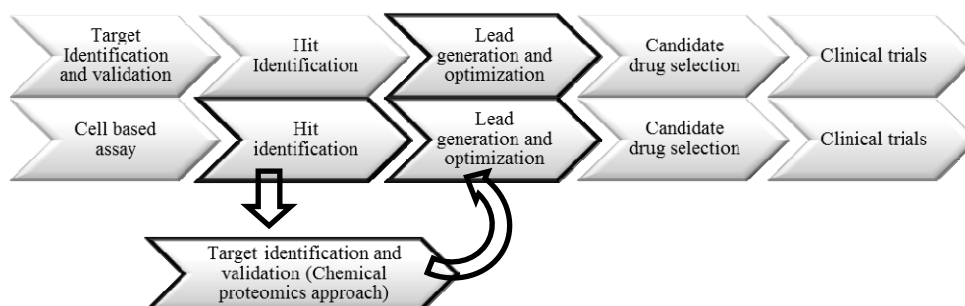


Figure 1.1: Schematic representation of the drug development process. The stages of drug development confronted in this thesis are target identification, hit identification and lead generation and optimization.

This thesis consists of three different projects presenting diversity of challenges encountered in early stages of drug development process.

- a) *Project 1:* Design and synthesis of CMP derivatives to investigate the mechanistic details of orotidine-5'-monophosphate decarboxylase (ODCase).
- b) *Project 2:* Phenoxy propanediol derivatives targeting neuroaxonal growth in diabetic neuropathy.
- c) *Project 3:* Design and synthesis of novel pyrazole derivatives inhibiting Fc γ receptor mediated phagocytosis in idiopathic immune thrombocytopenia (ITP).

In project one, the druggable protein, orotidine -5'-monophosphate decarboxylase (ODCase), is well studied. Project one with the aim to design and synthesize small molecules to probe ODCase in order to illuminate the key small-molecule protein interactions required for preferred conformational binding and potency, are described in detail in chapter 2 of the thesis. A brief overview of chapter 2 is as follow as:

Background: ODCase catalyses the decarboxylation of orotidine-5'-monophosphate (OMP) to uridine-5'-monophosphate (UMP) during *de novo* pyrimidine biosynthesis. In humans, pool of pyrimidine nucleotides is synthesized by both *de novo* and salvage pathways. Malaria parasite lacks salvage pathway for pyrimidine synthesis. Hence, selective inhibition of ODCase in *Plasmodium* parasites results in the eradication of malaria.⁴ ODCase has been an excellent target for the structure based drug design and its 3D structure is available. Numbers of ODCase inhibitors were designed and co-crystallized.^{5,6} Pyrimidine and purine nucleotides exhibit different modes of binding with the ODCase.⁷ Crystal structures of the complexes of ODCase with its inhibitors have exposed the unique architecture of its active site and the intense hydrogen bonding network.⁸

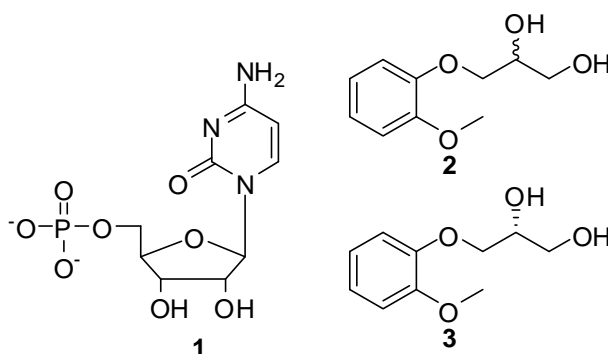
Research gap: CMP, a pyrimidine nucleotide, is a weak inhibitor of ODCase with a K_i of 1200 ± 700 and 1400 ± 100 μM against *Mt* and *Hs* ODCase, respectively.⁷ Regardless of its close similarity to UMP, CMP binds to ODCase in an unusual position, retaining its low energy conformation, with its nucleic base projecting away from the active site.

Objective:

- To design and synthesis the N3 and N4 oxygen substituted derivatives of cytidine-5'- monophosphate (CMP) (**1**), to improve the affinity and potency of ODCase weak inhibitor CMP (**1**).
- To evaluate the enzyme inhibition activity of the synthesized cytidine based derivatives.
- To co-crystallize the cytidine derivatives with ODCase and learn the hydrogen bonds interactions with the active site of ODCase and understand their preference towards nucleotide conformation.

Results of this project further revealed the mysterious nature of the target, ODCase.

Chart 1.1: Structures of hit compounds in chapter 2 and 3.



Chapter three of the thesis explains project two where the druggable protein is unknown and the small molecule probes (tool compounds) are synthesized for target identification.

Background: Diabetes mellitus causes diffuse or focal damage of the somatic or autonomic nerve fibers results into diabetic neuropathy. In diabetic neuropathy, altered glucose metabolism and decrease in synthesis of the neurotrophic factors there leads to slowing of nerve conduction velocity (NCV), decreased blood supply to neurons which further causes neuronal degeneration. Degenerated hyperglycemic neurons lack the ability of regeneration and collateral sprouting.

Research gap: In second project, cell based assay was used to screen 600 compounds for their potential to stimulate axonal regeneration in diabetic neuropathy.⁹ A guaifenesin racemate was identified as hit in this screen. The effect of the guaifenesin chirality on the axonal regeneration was never studied. Moreover, the guaifenesin druggable protein in neurons inducing axonal regeneration and collateral sprouting is yet to be discovered.

Objective:

- a) To design and synthesize a library of compounds around the hit (\pm) guaifenesin (**2**) (Chart 1.1) to generate a lead structure stimulating axonal regeneration.
- b) To synthesize the guaifenesin (**2**) enantiomers and study the effect chirality on neurite outgrowth.
- c) To deconvolute the target protein of the (*R*)-guaifenesin (**3**). On target deconvolution the drug's mechanism of the action would become clear

and rational drug design approach could be adopted for the designing of the drug molecules stimulating axonal regeneration.

Chapter four (project three) of this thesis delineates challenges involved in the hit identification and lead generation stages of drug development process for immune thrombocytopenia purpura (ITP).

Background: A thrombocyte count less than 150,000 per μL of blood is defined as thrombocytopenia.¹⁰ Decrease in platelet count could be either immune-mediated or non-immune-mediated destruction of thrombocytes.^{11, 12} Immunological destruction of platelets in response to unknown stimulus is known as “idiopathic thrombocytopenic purpura” or “primary immune thrombocytopenia” (ITP).¹³ The most preferred treatment for ITP is IVIG. Limited supply of IVIG, the possible exposure to blood borne infectious disease due to its human source requirement and high cost of treatment for ITP has raised a need for new drug treatment.

Research gap: A robust in-vitro cell based Fc- γ receptor dependent phagocytosis assay (monocyte monolayer assay, MMA) was developed.¹⁴ Compounds inhibiting phagocytosis of opsonized RBC's in MMA could be potential candidates for treating ITP. Compounds with sulfhydryl and disulfide groups reported in literature were screened for their potential to inhibit phagocytosis of opsonized red blood cells.¹⁵ But these molecules do not possess drug-like characteristics.

Objective: A logical medicinal chemistry approach was undertaken to search for new hits inhibiting Fc γ R dependent phagocytosis. These newly synthesized small molecule probes inhibiting phagocytosis of opsonized blood cells could provide strong clues to the underlying mechanism of phagocytosis inhibition.

- a) To the synthesize, analysis and biological evaluate a small set of sulfhydryl and disulfide compounds designed based on the lead candidate **4i**, inhibitors of phagocytosis for potential use as therapeutics for ITP
- b) Based on the biological activities of the first generation derivatives, design and synthesize second generation of compounds and screen for their potential to inhibit phagocytosis of opsonized RBC's.

1.2 References

- (1) Nogrady, T.; Weaver, D.F. "Medicinal Chemistry A Molecular and Biochemical Approach" 3rd ed. **2005**.
- (2) Burger, A.; Abraham, D. J. (editor) "Medicinal Chemistry and Drug Discovery" 6th ed., Volume 1, **1998**.
- (3) Gareth, T.; "Fundamentals of medicinal chemistry" Thomas, G. **2004**.
- (4) Kotra, L. P.; Pai, E. F.; Bello, A. M.; Fujihashi, M.; ODCase inhibitors for the treatment of malaria. PCT Patent Application WO 2007/038859 A1, **2007**.
- (5) Bello, A. M.; Poduch, E.; Liu, Y.; Wei, L.; Crandall, I.; Wang, X.; Dyanand, C.; Kain, K. C.; Pai, E. F.; Kotra, L. P. Structure-activity relationships of C6-uridine derivatives targeting plasmodia orotidine monophosphate decarboxylase. *J Med. Chem.* **2008**, *51*(3), 439-448.
- (6) Bello, A. M.; Konforte, D.; Poduch, E.; Furlonger, C.; Wei, L.; Liu, Y.; Lewis, M.; Pai, E. F.; Paige, C. J.; Kotra, L. P. Structure-activity relationships of orotidine-5'-monophosphate decarboxylase inhibitors as anticancer agents. *J. Med. Chem.* **2009**, *52*(6), 1648-1658.
- (7) Poduch, E.; Wei, L.; Pai, E. F.; Kotra, L. P. Structural diversity and plasticity associated with nucleotides targeting orotidine monophosphate decarboxylase. *J. Med. Chem.* **2008**, *51*(3), 432-438.
- (8) Wu, N.; Gillon, W.; Pai, E. F. Mapping the active site-ligand interactions of orotidine 5'-monophosphate decarboxylase by crystallography. *Biochemistry.* **2002**, *41*(12), 4002-4011.
- (9) Paul Fernyhough, University of Manitoba, Canada. Axon regeneration

- from adult sensory neurons. US patent 2008/0255062 A1, October, 16, **2008**.
- (10) Gauer, R. L.; Braun, M. M. Thrombocytopenia. *Am. Fam. Physician* **2012**, 85 (6), 612-622.
- (11) Veneri, D.; Franchini, M.; Randon, F.; Nichele, I.; Pizzolo, G.; Ambrosetti, A. Thrombocytopenias: a clinical point of view. *Blood Transfus.* **2009**, 7 (2), 75-85.
- (12) Cines, D. B.; Bussel, J. B.; Liebman, H. A.; Luning Prak, E. T. The ITP syndrome: pathogenic and clinical diversity. *Blood*. **2009**, 113 (26), 6511-6521.
- (13) Neunert, C.; Lim, W.; Crowther, M.; Cohen, A.; Solberg, L. Jr.; Crowther, M. A. The American Society of Hematology 2011 evidence-based practice guideline for immune thrombocytopenia. *Blood* **2011**, 117 (16), 4190-41207.
- (14) Foo, A. H.; Fletcher, S. P.; Langler, R. F.; Porter, C. H.; Branch, D. R. Structure-function studies for in vitro chemical inhibition of Fc gamma receptor-mediated phagocytosis. *Transfusion*. **2007**, 47(2), 290-298.
- (15) Rampersad, G. C.; Suck, G.; Sakac, D.; Fahim, S.; Foo, A.; Denomme, G. A.; Langler, R. F.; Branch, D. R. Chemical compounds that target thiol-disulfide groups on mononuclear phagocytes inhibit immune mediated phagocytosis of red blood cells. *Transfusion*. **2005**, 45(3), 384-393.

Design and synthesis of CMP derivatives to investigate the mechanistic details of orotidine-5'-monophosphate decarboxylase (ODCase)

2.1 Introduction and literature review

Orotidine-5'-monophosphate decarboxylase (ODCase, EC 4.1.1.23) catalyzes the decarboxylation of orotidine-5'-monophosphate (OMP, **2**) to uridine-5'-monophosphate (UMP, **1**) during *de novo* pyrimidine biosynthesis (Figure 2.1). This pathway converts the amino acid, aspartic acid, to UMP which further is utilized in the construction of DNA and RNA. The catalytic activity of ODCase is independent of any cofactors, metal ions, or intermittent covalent bond formation. The half-time ($t_{1/2}$) for uncatalyzed decarboxylation reaction of OMP is about 78 million years in a neutral aqueous solution at 25 °C, but when catalyzed by ODCase, it is 18 ms.^{1,2}

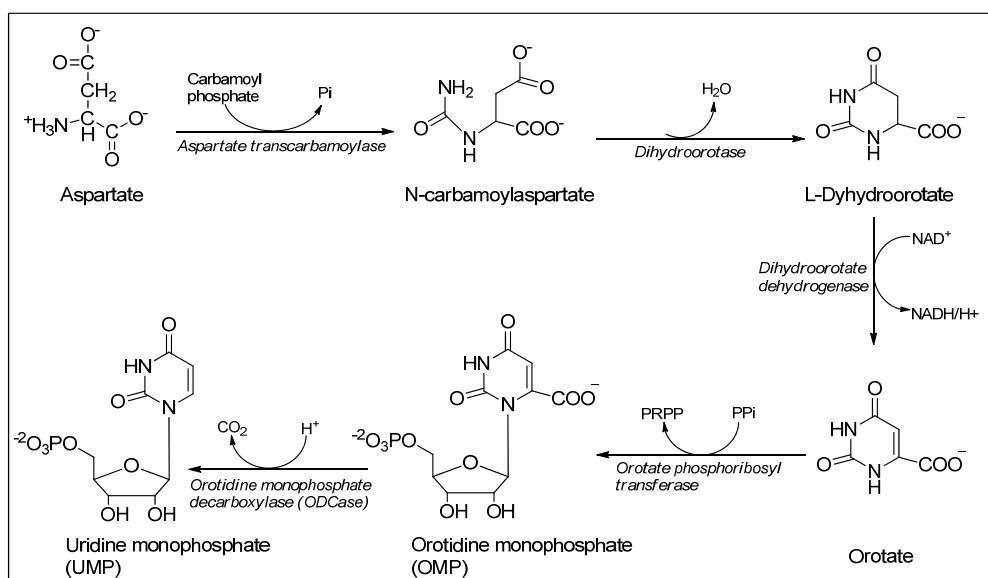
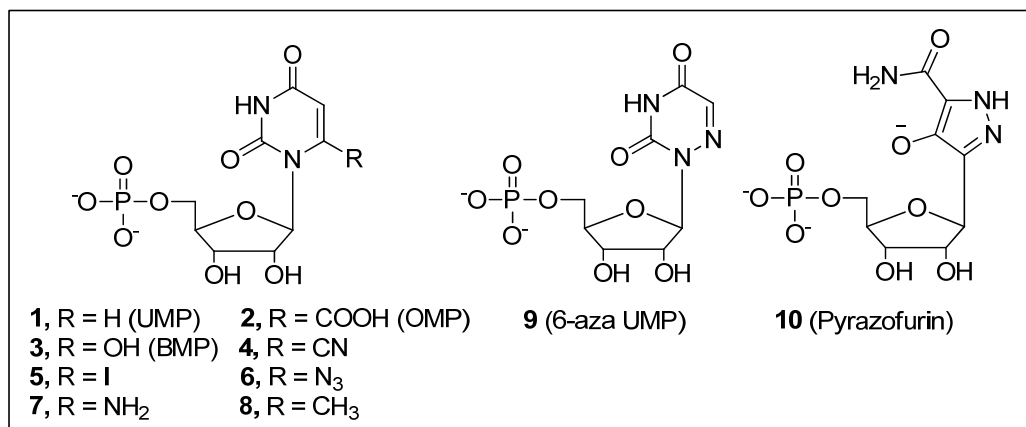


Figure 2.1: De Novo biosynthesis of pyrimidine nucleotides³

ODCase is present in most living organisms including humans, bacteria, and parasites. In humans, ODCase is one of the catalytic domains of the bifunctional protein UMP synthase with other catalytic domain as orotate phosphoribosyl transferase (OPRTase). In some organisms including malaria parasite, ODCase is a monofunctional enzyme. In all species irrespective of its status as a monofunctional or bifunctional enzyme it is active in its dimeric unit.^{4,5} Due to the significant physiological role of ODCase in living organisms, for the synthesis of the pyrimidine nucleotides, this proficient enzyme is a desirable drug target.⁵

Since OMP is a substrate for ODCase, several analogues of OMP have been investigated as ODCase inhibitors. Among these analogues, 6-aza-UMP (**9**) and 6-hydroxy-UMP (BMP) (**3**) are potent inhibitors of ODCase. Other C-6 pyrimidine derivatives designed on the basis of the mechanistic understanding of ODCase that a carbon dioxide molecule is eliminated and the resulting anionic center at C-6 is protonated to produce UMP are 6-cyano-UMP(**4**), 6-iodo-UMP (**5**), 6-azido-UMP (**6**) and 6-amino-UMP (**7**) which are found to be potential inhibitors of ODCase (Chart 2.1).⁶ Kotra and coworkers have developed a variety of C-6 substituted UMPs that exhibit potent ODCase inhibition and antiparasitic activity. These inhibitors were developed based on the principles of bioisosterism and substructure volume. From this study it was revealed that 6-iodo UMP (**5**) and 6-azido UMP (**6**) are covalent inhibitors and 6-cyano UMP (**4**) and 6-amino UMP (**7**) are competitive inhibitors of ODCase (Chart 2.1 and Figure 2.2). Recent discoveries of fluorinated nucleosides as ODCase inhibitors, that exhibit anticancer and antiviral activities, have added a strong potential as a target for drug design.^{7,8}

Chart 2.1: Structures of ODCase substrate, OMP and various inhibitors.

To date, 152 ODCase crystal structures from both prokaryotic and eukaryotic organisms have been solved and appear in the Protein Data Bank (PDB).⁹ Regardless of this large collection of ODCase structures and various mechanistic studies the underlying chemical mechanism for its catalytic biochemical activity is still unclear. However, the active site of the enzyme has been very well mapped. Apart from the decarboxylation, ODCase can also perform pseudo-hydrolysis and covalent reaction involving one of its catalytic residues (Figure 2.2).^{10,11,12}

Based on the crystal structures of ODCase, the catalytic site of ODCase from *Methanobacterium thermoautophicum* consists of two aspartate residues (Asp70 and Asp75B, the latter contributed by the second subunit of the dimeric ODCase) and two lysine residues (Lys42 and Lys72) that are held via a strong network of hydrogen bonds. Analyses of several co crystal structures of ODCase with a variety of ligands confirm that these residues are held tightly in their respective positions of the side chains of these residues.

This Asp-Lys-Asp-Lys tetrad is in close proximity of the groups at the C6-position of the pyrimidine ring (Figure 2.3).

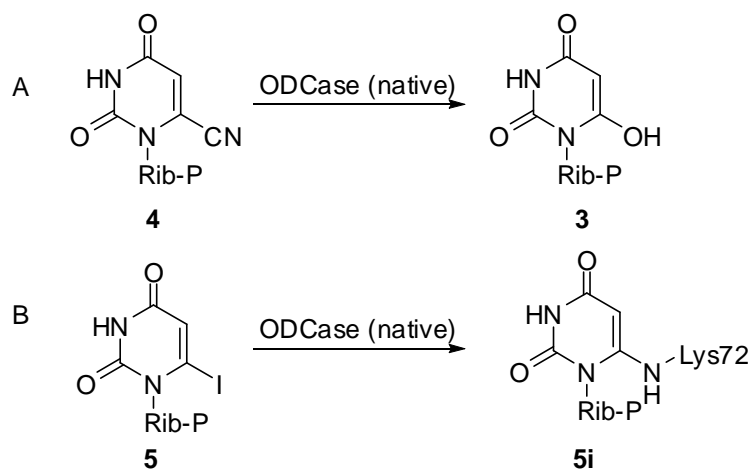


Figure 2.2: Schematic representation of unconventional reactions by ODCase. A. The conversion of 6-CN-UMP (4) to BMP (3) by native ODCase, B. Covalent bond formation with native ODCase active amino acid Lys75 and 6-I-UMP (5).

The ribosyl moiety and the 5'-monophosphate are involved in extensive hydrogen bonding network and the resulting binding energy between the enzyme and the ligands is the driving force to place the pyrimidine base into the active site pocket.¹³ In addition to pyrimidine nucleotides, purine nucleotides are also accepted at the active site of ODCase.¹⁴ In the recent study it has been shown that purine nucleotides XMP, GMP, AMP and IMP inhibit ODCase.¹⁴ Even though these nucleotides do not form hydrogen bonding with the active site of the enzyme they block the catalytic site and thus inhibit the substrate from binding to the active site of the enzyme.¹⁴ In the past few years, many other structures of ODCase have become available. This has intensified structural investigations and enhanced understanding of various 3D structures of ODCase which may aid new drug design.

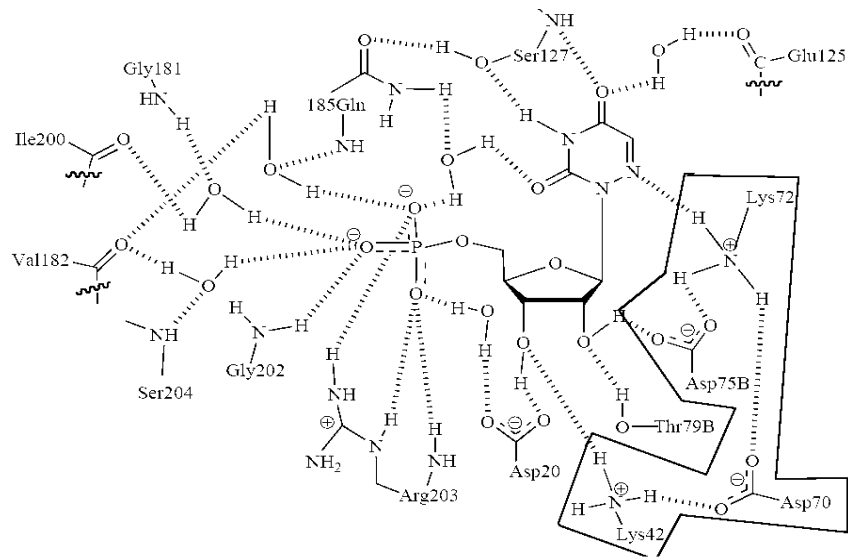


Figure 2.3: Schematic representation of 6-azaUMP bound to the active site of ODCase from *M. thermoautotrophicum*

2.2 Objective

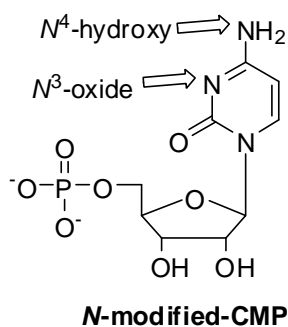
The active site of ODCase is rigid, comprising of four conserved catalytic amino acid residues *i.e.* Lys42, Asp70, Lys72 and Asp75^B.¹⁵ Despite its restricted environment, both pyrimidine and purine based nucleotides fit in the ODCase active site exposing its plasticity.^{14,16} ODCase naturally evolved to bind to uracil-type nucleic bases, considering its dedicated function in the cell for the decarboxylation of OMP to yield UMP. Additionally, the binding conformation of UMP in the enzymatic pocket of ODCase gives insight into the types of preferable interactions and binding positions within the active site. It has been reported that the nucleic base of cytidine-5'-monophosphate (CMP) binds to the active site of the ODCase with an alternate binding mode to UMP. In this binding mode the phosphate and ribosyl moieties sit in a similar fashion to that of UMP, but the pyrimidine assumes a completely different orientation as well as conformation, almost reaching outside of the binding pocket.^{13,17} Due to its unusual binding conformation in the active site of ODCase, CMP (**11**) fails to undergo optimum interactions and is thus unable to effectively inhibit the catalytic site. This is further demonstrated by the difference in K_i values between UMP and CMP for the inhibition of *Hs* ODCase (220 ± 10 and $1200 \pm 700 \mu\text{M}$, respectively).¹⁴

N-Modified CMP derivatives, especially at the N^3 and N^4 positions of CMP were conceived as novel ligands to ODCase (Chart 2.2), with the anticipation to create novel interactions for the CMP ligands in the ODCase binding site, as well as to improve on its affinity. The objectives of the study undertaken to learn insight of the ODCase are as follow as:

- a) To design and synthesize N^3 and N^4 oxygen substituted cytidine based derivatives to inhibit ODCases.
- b) To evaluate the synthesized substituted cytidine derivatives for their ODCase inhibition in ITC based enzymatic assay.
- c) To co-crystallize the synthesized cytidine derivatives with ODCase and study their interactions with the ODCase binding site.

In this chapter, the chemistry and biochemistry of N^3 - and N^4 - substituted CMP derivatives in the context of the therapeutic target, ODCase are disclosed.

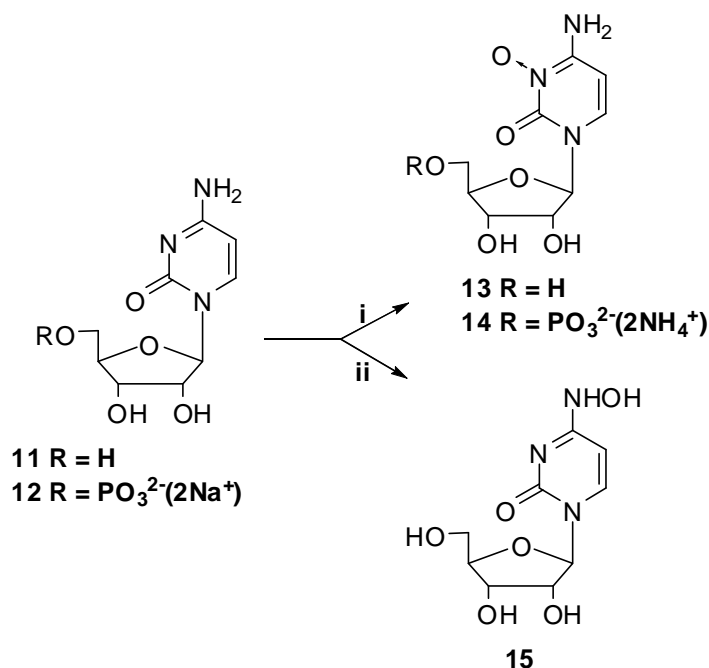
Chart 2.2: Design of CMP analogs



2.3 Experimental Section

2.3.1 *Synthetic schemes and procedure*

General: All solvents and reagents were obtained from commercial sources. Column chromatography purifications were performed on Biotage flash chromatography system using normal silica gel (60 Å, 70-230 mesh) and reverse-phase (C18) cartridges. Reactions were monitored by thin layer chromatography Merck. NMR spectra were recorded on Bruker spectrometer (400 MHz for ^1H and 162.03 MHz for ^{31}P). Chemical shifts are reported in δ ppm using residual solvent peak as the reference for the ^1H NMR spectra, and phosphoric acid as external standard for ^{31}P spectrum. Purity of the synthesized compounds was determined by WatersTM HPLC system (Delta 600) and/or LC-MS system (WatersTM 2545 binary gradient module) including eluting system. Mass spectra (ESI) were recorded on a WatersTM LC/MS system equipped with a WatersTM 3100 mass detector. All enzyme assays were performed at 37 °C or 55 °C using VP-ITC microcalorimeter (MicroCal, Northampton, MA) according to previously published procedures.¹⁸ The pH of the buffers was measured with a CorningTM 430 pH meter.



Scheme 2.1. Synthesis of cytidine based derivatives as ODCase inhibitors. Reagents and conditions: (i) *m*-CPBA, methanol, rt; (ii) Hydroxylammonium acetate (5N), pH 6.5, 35 °C.

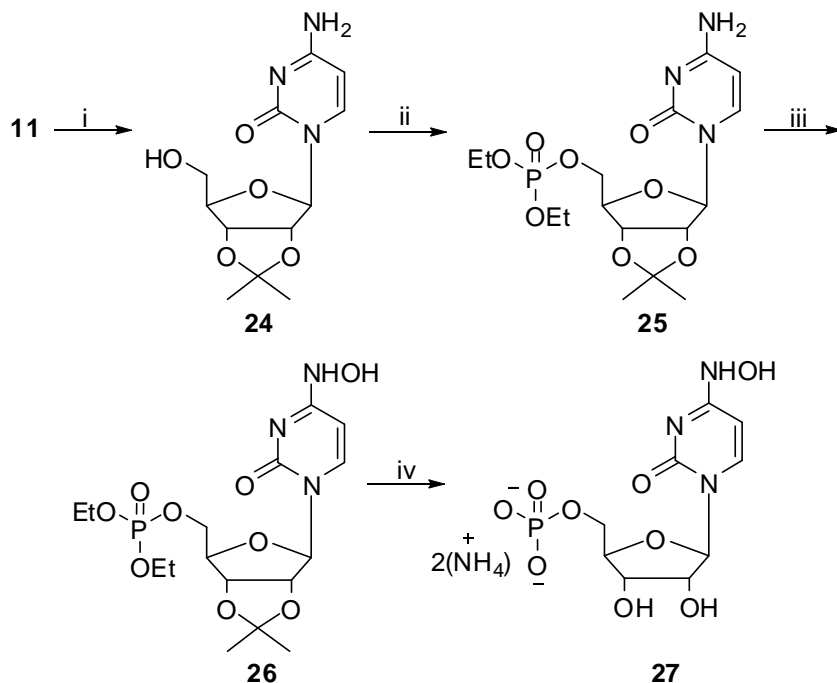
4-Amino-1-(3,4-dihydroxy-5-hydroxymethyl-tetrahydrofuran-2-yl)-1H-pyrimidin-2-one-3-oxide (Cyd-*N*³-oxide) (13): Cytidine (100 mg, 0.41 mmol) was suspended in anhydrous methanol (4 mL). *m*-Chloroperbenzoic acid (213 mg, 1.23 mmol) was added in fractions to above reaction suspension at 0 °C. Reaction mixture was allowed to stir at 0 °C for 15 min. After 24 hr of stirring at room temperature, reaction solvent was evaporated to dryness. Water (4 mL) was added to precipitate *m*-chloroperbenzoic acid. The byproduct was filtered off and the filtrate was purified by reverse phase chromatography (Note 1). Fractions containing compound of interest were mixed together and lyophilized to give compound **13** as white solid (62 mg, 58%). ¹H NMR (D₂O) δ 3.85 (dd, *J* = 12, 44 Hz, 2H, 5' and 5"), 4.13-4.193 (m, 2H, 4' and 3'), 4.35 (dd, *J* = 3.36, 1.16 Hz, 1H, 2'), 5.87 (d, *J* = 3.24 Hz,

1H, 1'), 6.31 (d, $J = 8.00$ Hz, 1H, 5), 8.04 (d, $J = 8.04$ Hz, 1H, 6). ESI (+ve) [M+H⁺] calculated 260.09, found 260.11.

(5-(4-Amino-3-oxido-2-oxopyrimidin-1-yl)-3,4-dihydroxyoxolan-2-yl)methyldihydrogen phosphate (CMP-*N*³-oxide) (14). Compound **14** was synthesized similarly to compound **13** from CMP (100 mg, 0.27 mmol). Product was purified by HPLC using reverse phase semi preparatory column (Note 1). Fractions containing desired compound were collected and lyophilized. Free acid form of compound **14** was neutralized by NH₄OH to yield ammonium salt of CMP-*N*³-oxide (48 mg, 42.27%). ¹H NMR (D₂O) δ 4.04 (dd, $J = 12.24, 37.16$ Hz, 2H, 5' and 5''), 4.26 (m, 1H, 4'), 4.30-4.36 (m, 2H, 3' and 2'), 5.98 (d, $J = 2.6$ Hz, 1H, 1'), 6.36 (d, $J = 7.84$ Hz, 5), 8.10 (d, $J = 7.6$ Hz, 6). ³¹P (D₂O) δ -3.647. ESI (-ve) [M-H⁺] calculated 339.05, found 338.21.

1-(3,4-Dihydroxy-5-(hydroxymethyl)tetrahydrofuran-2-yl)-4-(hydroxyamino)pyrimidin-2[1H]-one (*N*⁴-OH-Cyd, **15).** Hydroxyl ammonium acetate ¹⁹ was synthesized by adjusting the pH of 5*N* NH₂OH by acetic acid to 5.98. Cytidine (50 mg, 0.20 mmol) was dissolved in 2.5 mL of hydroxyl ammonium acetate at room temperature. Reaction mixture was then warmed up to 37 °C and stirred for 15 h. Reaction solvent was evaporated and the reaction crude was dissolved in 2 mL of water. It was then purified by reverse phase chromatograph (Note 1). Aqueous fractions containing the target compound were collected and lyophilized to yield compound **15** (32 mg, 60%). ¹H NMR (D₂O) δ 3.85 (dd, $J = 12, 44$ Hz, 2H, 5' and 5''), 4.07 (br, m, 1H, 4'), 4.18 (br, dd, $J = 4.68, 5.40$ Hz, 1H, 3'), 4.29 (br, dd, $J = 5.28, 5.00$

Hz, 1H, 2'), 5.84-5.86 (m, 2H, 1' and 5), 7.34 (d, $J = 8.28$ Hz, 1H, 6). ESI (+ve) $[M+H^+]$ calculated 260.09, found 260.11.



Scheme 1.2. Synthesis of compound **27**. Reagents and conditions: (i) Acetone, H^+ , rt; (ii) Diethylchlorophosphate, py, 0 °C to rt; (iii) Hydroxylammonium acetate (5*N*), 35 °C, 13 h; (iv) TMSBr, DCM, 0 °C to rt.

4-Amino-1-(6-(hydroxymethyl)-2,2-dimethyltetrahydrofuro[3,4-

d][1,3]dioxol-4-yl)pyrimidin-2[1H]-one (24): In a flame dried flask, a suspension of cytidine (500 mg, 2.05 mmol) in anhydrous acetone (40 mL) was cooled to 0 °C and treated with conc. H_2SO_4 (0.25 mL) drop wise. After being stirred at room temperature for 12 h the reaction mixture was then neutralized by NH_4OH and purified over silica gel (10% MeOH in DCM). Organic fractions containing compound of interest were evaporated to obtain compound **24** as a white solid (547 mg, 93%). 1H NMR ($CDCl_3$) δ 1.34 (s, 3H, *iso* CH_3), 1.55 (s, 3H, *iso* CH_3) 3.83 (dd, $J = 35.42, 11.16$ Hz, 2H, 5' and 5''),

4.30 (br, m, 1H, 4'), 4.96 (br, m, 1H, 3'), 5.02 (br, m, 1H, 2'), 5.57 (br, s, 1H, 1'), 6.00 (d, $J = 7.36$ Hz, 1H, 5), 7.57 (d, $J = 7.44$ Hz, 1H, 6).

(6-(4-Amino-2-oxopyrimidin-1(2H)-yl)-2,2-dimethyltetrahydrofuro[3,4-d][1,3]dioxol-4-yl)methyl diethyl phosphate (25): Compound **24** (547 mg, 1.93 mmol) was dissolved in 2 mL of anhydrous pyridine. Reaction mixture was cooled to 0°C and diethyl chlorophosphate (333 mg, 1.93 mmol) was added drop wise. Reaction was stirred at 0°C for 30 min and then for additional 15 min at room temperature. Reaction was quenched with 2 mL of MeOH and purified over silica gel (10% MeOH in DCM) to give compound **25** as white solid (479 mg, 67.5%). ^1H NMR (CDCl_3) δ 1.25-1.27 (br, m, 9H, 3 CH_3), 1.48 (s, 3H, *iso* CH_3), 3.65-4.27 (m, 7H, 5', 5'', 4' and *diethyl* 2 CH_2), 4.80-4.89 (m, 2H, 3' and 2'), 5.75 (br, s, 1H, 1'), 6.28 (br, s, 1H, 5), 7.63 (br, s, 1H, 6), 8.593 (br, s, 1H, NH), 9.156 (br, s, 1H, NH).

Diethyl(6-(4-(hydroxyamino)-2-oxopyrimidin-1(2H)-yl)-2,2-dimethyltetrahydrofuro[3,4-d][1,3]dioxol-4-yl)methyl phosphate (26): Compound **25** (450 mg, 1.07 mmol) was dissolved in 1 mL of ethanol. 5 *N* hydroxyl ammonium acetate (pH 6.5, 2 mL) was added to it and stirred at 37 °C for 17 h. Reaction crude was then purified over silica gel (9% MeOH in DCM). Organic fractions containing desired compound were mixed together and concentrated to yield compound **26** (45 mg). ^1H NMR (CDCl_3) δ 1.30-1.31 (m, 9H, *iso* CH_3 and *diethyl* 2 CH_2), 1.53 (s, 3H, *iso* CH_3), 4.08-4.24 (m, 7H, 5', 5'', 4', and *diethyl* 2 CH_2), 4.80 (br, m, 1H, 3'), 4.88 (br, m, 1H, 2'), 5.68 (br, s, 1H, 1'), 6.70 (d, $J = 7.36$ Hz, 1H, 5), 6.92 (br, s, 1H, NH), 7.48 (d, $J = 6.52$ Hz, 1H, 6).

(3,4-Dihydroxy-5-(4-(hydroxyamino)-2-oxopyrimidin-1(2H)-yl)tetrahydrofuran-2-yl)methyl phosphate (27): Compound **26** (37 mg, 0.08 mmol) was dissolved in 1 mL of anhydrous DCM and cooled to 0°C. TMSBr (130 mg, 0.84 mmol) was added to the reaction mixture and stirred for 10 min at 0°C. After additional stirring at room temperature for 30 min, reaction mixture was evaporated and 1 mL of water was added to it. Aqueous reaction mixture was then purified over HPLC by reverse phase chromatography (Note 1). Aqueous fractions containing compound **27** were lyophilized and neutralized by NH₄OH to yield ammonium salt of target compound **27** (10 mg, 33%). ¹H NMR (D₂O) δ 3.93 (br, m, 2H, 5' and 5''), 4.18 (m, 1H, 4'), 4.29 (dd, *J* = 2.84, 2.30 Hz, 1H, 3'), 4.36 (dd, *J* = 5.60, 6.12 Hz, 1H, 2'), 5.80 (d, *J* = 8.24 Hz, 1H, 5), 5.92 (d, *J* = 6.44 Hz, 1H, 1'), 7.26 (d, *J* = 8.08 Hz, 1H, 6). ³¹P (D₂O) δ 3.39. ESI (-ve) [M-H⁺] calculated 339.05, found 338.21.

Purity of the synthesized compounds:

Purity for nucleosides was evaluated on Water LC-MS system (Waters™ 2545 binary gradient module) with a photodiode array detector using a X-Bridge C18 column (4.6 x 150 mm, 5 μ m). The HPLC methods used for the purity assessment were Method A: (Isocratic conditions, 95% Water with 0.05% TFA and 5% MeOH with 0.05% TFA, 10 min), Method B: (Isocratic conditions, 100% Water with 0.05% TFA, 15 min). Purity for nucleotides was evaluated on Water HPLC system with a photodiode array detector using a Spherisorb C18 column (4.5 x 250 mm, 5 μ m). The HPLC methods used for the purity assessment were Method B: (Isocratic conditions, 100% Water with 0.05% TFA, 10 min), Method C: (Gradient conditions, 100% Water to 95% Water and 5% ACN with 0.05% TFA, 15 min). All HPLC solvents were filtered through the membrane filters (47 mm GHP 0.45 μ m, Pall Corporation). Injection samples were filtered using Pall Acrodisc® Syringe filters 4 mm PTFE (0.2 μ m).

Table 2.1: Purity data for cytidine derivatives.

Compound No	Method	Rt (min)	Purity
13	Method A	2.87	>99.9%
	Method B	2.68	>99.9%
15	Method A	3.93	>99.9%
	Method B	4.33	>99.9%
14	Method B	4.73	>99.9%
	Method C	4.77	>99.9%
27	Method B	4.76	>99.9%
	Method C	4.77	>99.9%

Note 1. *Semi preparatory Purification Method:* Final compounds were purified on Water HPLC using semi prep Spherisorb ODS2 C18 column (20 x150 mm, 4 mL/min). The HPLC method used for the purification was Method B: (Isocratic, 100% Water with 0.05% TFA)

2.3.2 Enzymology

Enzymology experiments were done in collaboration with Ewa Poduch. ODCases from *Methanobacterium thermoautotrophicum* (*Mt*), *Plasmodium falciparum* (*Pf*) and *Homo sapiens* (*Hs*) were cloned, expressed and purified, as described earlier.^{6,17} Enzyme reactions were performed at 55 °C (*Mt* ODCase) and 37 °C (*Pf* and *Hs* ODCase) on the isothermal titration calorimeter (VP-ITC MicroCal, Northampton, MA) as described previously.¹⁸

Enzyme Inhibition: The inhibition of ODCase from different species, by compounds **14** and **27** was evaluated by competitive inhibition method.¹⁸ Enzyme stock samples were prepared in assay buffer, 50 mM Tris, 40 mM NaCl and 20 mM DTT and incubated overnight at room temperature. Assay samples were prepared in 50 mM Tris, 20 mM DTT buffer, pH 7.5. Small aliquots of enzyme stock were diluted in the assay buffer to give final enzyme concentration of 20 nM (*Mt*), 60 nM (*Hs*), and 60 nM (*Pf*). Control reaction, without inhibitor, was initiated by a single injection of OMP **2**. Final substrate concentration was 40 μM (*Mt*), 20 μM (*Hs*), and 12 μM (*Pf*). The final assay concentrations of compound **14** were: *Mt* ODCase: 0, 15, 30, 50, and 100 μM, *Hs* ODCase: 0, 25, 50, 100 and 150 mM, *Pf* ODCase: 0, 25, 50, and 100 μM. The concentration of compound **27** in the assay sample was: *Hs* ODCase: 0, 25, 50, 100 and 150 mM. In the competitive inhibition assay of compound **14** and **27**, the reaction was initiated by addition of the substrate OMP (**2**) to the mixture of enzyme and inhibitor. Reactions were performed in triplicates.

Data Analysis. The kinetic raw data obtained from isothermal titration calorimetry (ITC) experiments were analyzed using Origin 7.0 program. Kinetic raw and analyzed data sets of inhibitor **14** with *Mt* ODCase are

provided (Figure 2.4). The reaction progress curves obtained from the ITC experiment at various concentrations of inhibitor (raw data) is represented in Figure 2.4A. The inhibition constant (K_i) was derived by converting the raw data from inhibited reactions to Michaelis-Menten curves (Figure 2.4B) by use of the Substrate Only mode in the Origin software to fit the raw data. From this typical rate versus substrate $[S]$ plot reaction rate at each substrate concentration in the absence and presence of the inhibitor could be computed. The data from inhibition assays were plotted using the double reciprocal plots ($1/\text{rate}$ vs. $1/[S]$) at various concentrations of inhibitor to confirm that the inhibition is competitive in nature (Figure 2.4C). For detailed description of the data analyses, please refer to reference 18.

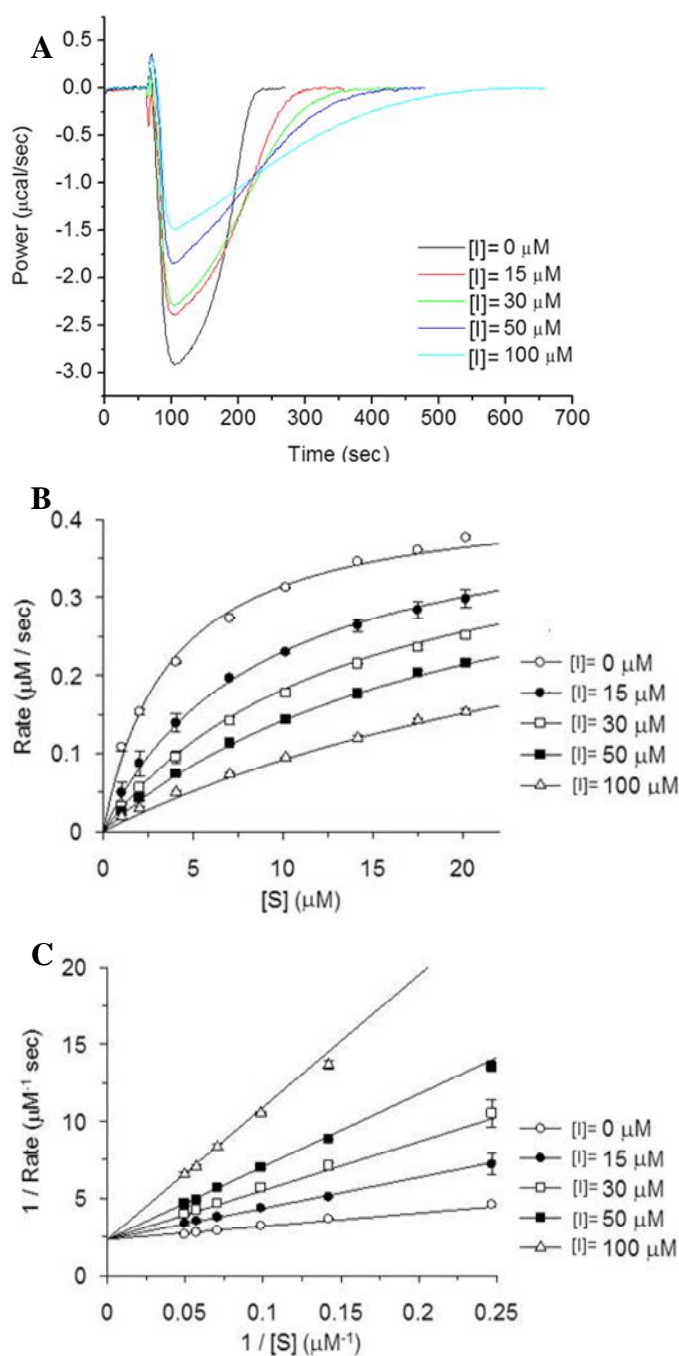


Figure 2.4: Inhibition of *Mt* ODCase by compound 14. (A) Thermograms representing the reaction rate in the absence and presence of compound 14. (B) The rate of decarboxylation of OMP in the absence and presence of compound 14. (C) Line weaver Burk plot for the inhibition of ODCase by compound 14.

2.3.3 Crystallography

Crystallography was done in collaboration with Emil Pai. All *Hs* ODCase concentrations were determined using a BioRAD protein assay kit and BSA as a standard. ODCase protein was dissolved in 20 mM Tris (pH 8.0), 10 mM NaCl. *Hs* ODCase complex crystals were grown in hanging drops using 1.6M-1.7M ammonium sulphate, pH 7.0-9.0, as the precipitant (Figure 2.5). All crystals grew in space group *P*1211, with unit cell dimensions deviating less than 1% from $a = 69.78 \text{ \AA}$, $b = 61.64 \text{ \AA}$, and $c = 71.37 \text{ \AA}$ (Figure 2.6). For data collection, the crystals were cryo-protected by 25% glycerol and Parotone-N oil before flash-freezing in a stream of boiling nitrogen. Diffraction data for the crystals of *Hs* ODCase co-crystallized with Compound **27** was collected at 100 K and $\lambda = 0.979490 \text{ \AA}$ on beamline 08ID-1 at Canadian Macromolecular Crystallography Facility, Canadian Light Source, Inc.²⁰ All data were reduced and scaled using XDS.²¹ Data collection statistics are given in Table 2.2. The structures of all complexes were determined using molecular replacement techniques with the help of the program package MOLPREP;²² subsequent refinements were done with Refmac-5.5.0110²³ and model building used COOT version 0.6.1.²⁴ The refinement statistics are also given in Table 2.2. The diffraction data for *Hs* ODCase co-crystallized with compound **14** was collected at 100 K and $\lambda = 1.54179 \text{ \AA}$ on beamline MAR. Data were reduced and scaled using HKL2000.²⁵ Data collection statistics are given in Table 2.2. The structures of all complexes were determined using molecular replacement techniques with the help of the program package MOLPREP; subsequent refinements were done with Refmac-5.234²³ and model building using COOT.²⁴ The refinement statistics are also given in

Table 2.2. Atomic coordinates and structure factors have been deposited into the Protein Data Bank (PDB IDs: 2QAF, 2Q8Z, and 3BAR).

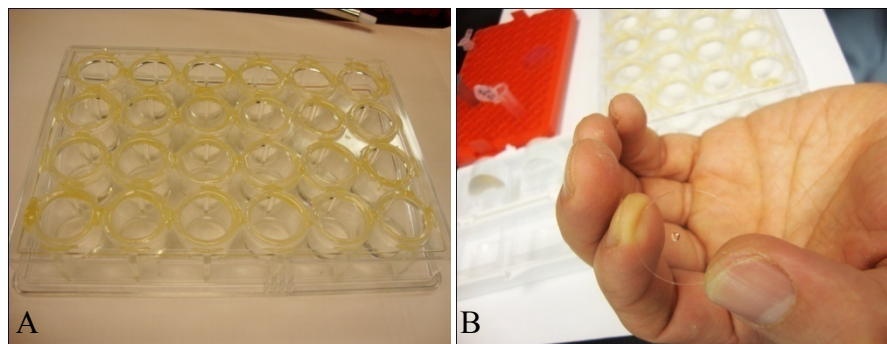


Figure 2.5: Co-crystallization of compound **14** and **27** with *Hs* ODCase by hanging drop technique. (A) 24-well plate used for crystallization and (B) A drop of solution of protein and inhibitor placed on the cover slip

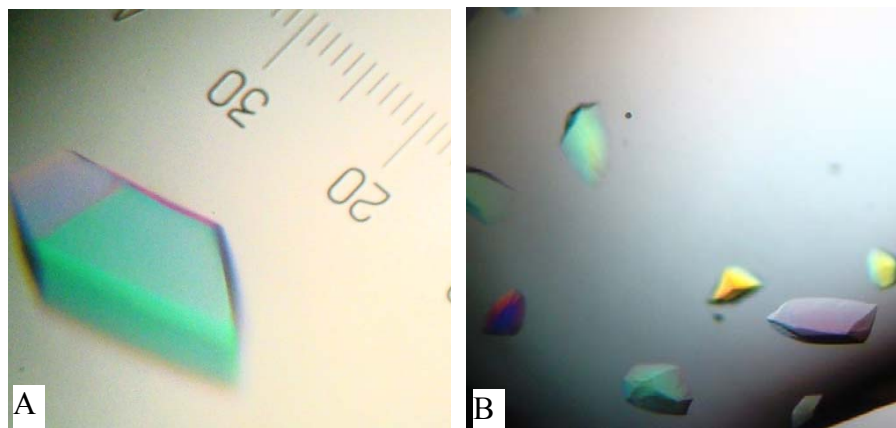


Figure 2. 6: Co-crystals of compound (A) **14** and (B) **27** with *Hs* ODCase

Table 2.2: Diffraction and refinement data for co-crystal complexes of compound **14** and **27** with *Hs* ODCase.

Diffraction Data	Human ODCase + Compound 14	Human ODCase + Compound 27
Resolution	1.80-1.75	1.95 - 1.90
Measured Reflection	4126	3234
Unique reflections	4449	3319
Completeness	92.7	97.4
Rsym	0.248	0.0882
Space Group	P1 21 1	P1 21 1
	a=69.29 =90.00	a=69.78=90.00
	b=61.77=112.90	b=61.64 =112.08
	c=70.52=90.00	c=71.37 =90.00
Refinement Statistics		
Resolution	64.97 –1.75	66.08 – 1.90
Protein Atoms	3962	4048
Water molecules	304	190
Reflections Used for	50805	42064
R _{cryst} %	16.05	19.02
R _{free} %	18.50	22.33
Root Mean Square Deviation Bond Length	0.016	0.026
Root Mean Square Deviation Bond Angle	1.598	2.076
Average B-factor	17.899	28.478

2.3.4 *In-vitro parasitology*

Parasitology studies were done in collaboration with Ian Crandall. Human malaria parasites were grown in O blood obtained by venipuncture of volunteers. Cultures of the laboratory line ItG was maintained by the method of Trager and Jensen²⁶ using RPMI 1640 supplemented with 10% human serum and 50 μ M hypoxanthine. *In vitro* viability assays were performed using the SYBR Green method.²⁷ Briefly the compound was dissolved in RPMI 1640 to a final concentration of 10mg/mL and was then sterilized by passing it through a 0.22 μ m filter. The compound was then serially diluted across a 96 well plate (top concentration 500 μ g/mL) containing a constant number of parasites per well, with the final wells in the series receiving no compound. After 48 hours in an atmosphere of 3% CO₂, 2% O₂ and 95% N₂ the growth of the parasites in individual wells will be determined by adding 100 μ L of a solution containing 2 μ L of SYBR Green stock solution in 11mLs of a solution containing buffer and Triton X-100. The relative fluorescence was determined using GMG fluorescent plate reader and was compared to the results obtained with a chloroquine control. Assays were done in quadruplicate. The concentration of compound that inhibited the growth of 50% of the cultures (IC₅₀ values) was determined using a non-linear regression analysis of the dose-response curve using the computer program Sigma Plot 2000 (Jandel Scientific).

2.4 Chemistry discussion

Compounds **13**, **14**, **15** and **27** were synthesized from either cytidine or CMP. The basic tertiary nitrogen of cytidine (pKa 4.2)²⁸ and CMP (pKa 5.6)³⁸ was oxidized with *meta*-chloroperbenzoic acid (*m*-CPBA) to yield cytidine-*N*³-oxide (Cyd-*N*³-oxide, **13**) and CMP-*N*³-oxide (**14**) respectively (Scheme 2.1).²⁹ The *N*⁴-hydroxy-cytidine (*N*⁴-OH-Cyd, **15**) was obtained by reacting cytidine with hydroxylammonium acetate at pH 6.5. Synthesis of *N*⁴-OH-CMP (**27**) required the protection of 2' and 3' hydroxyl moieties of cytidine with isopropylidene and the 5'-hydroxyl moiety with diethyl chlorophosphate followed by treatment with hydroxylammonium acetate at pH 6.5. All protecting groups were removed by trimethylsilyl bromide (TMSBr) to yield the desired compound **27** (Scheme 2.2). Compounds **13**, **14**, **15** and **27** were unambiguously characterized as the desired cytidine and CMP derivatives by IR (Figure 2.7) ¹HNMR (Figure 2.8) and color test (Figure 2.9). Classical ferric chloride test was employed to confirm N3 oxidized compounds **13**, **14** which gave orange-red color, and N4 oxidized compounds **15**, **27** produced blue color.^{30,31,32}

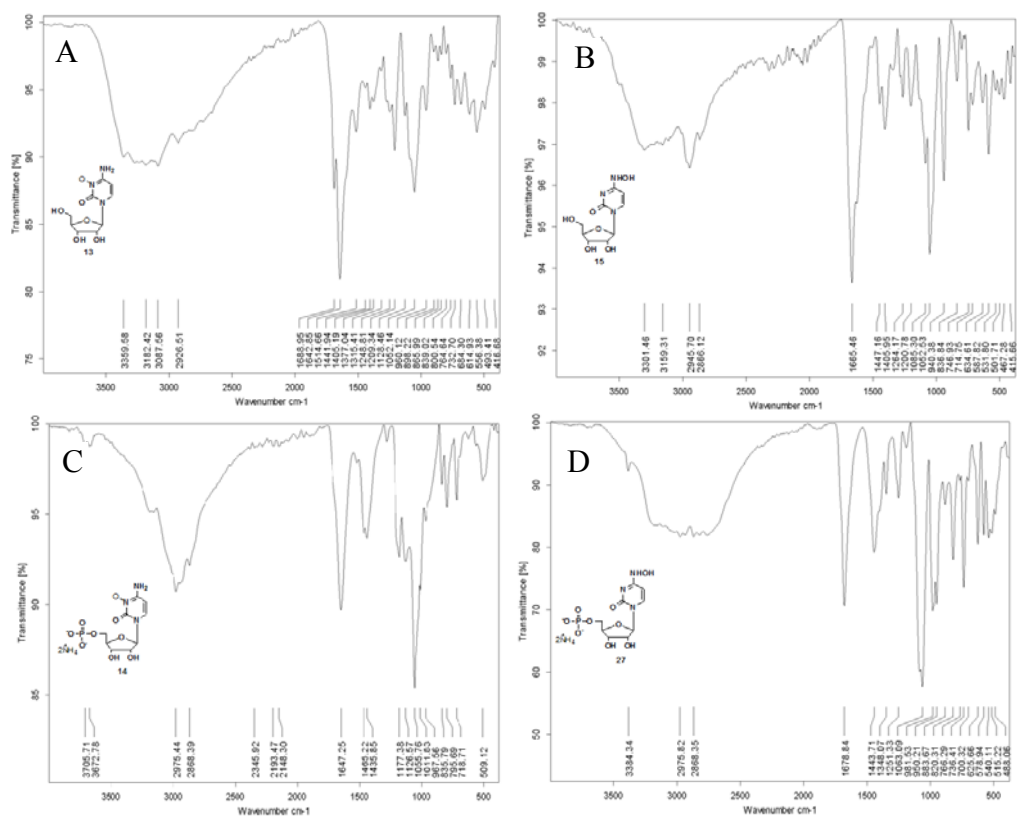


Figure 2.7: IR Spectrums for (A) Cyd-N³-oxide (**13**), (B) Cyd-N⁴-OH (**15**), (C) CMP- N³-oxide (**14**) and (D) CMP- N⁴-OH (**27**).

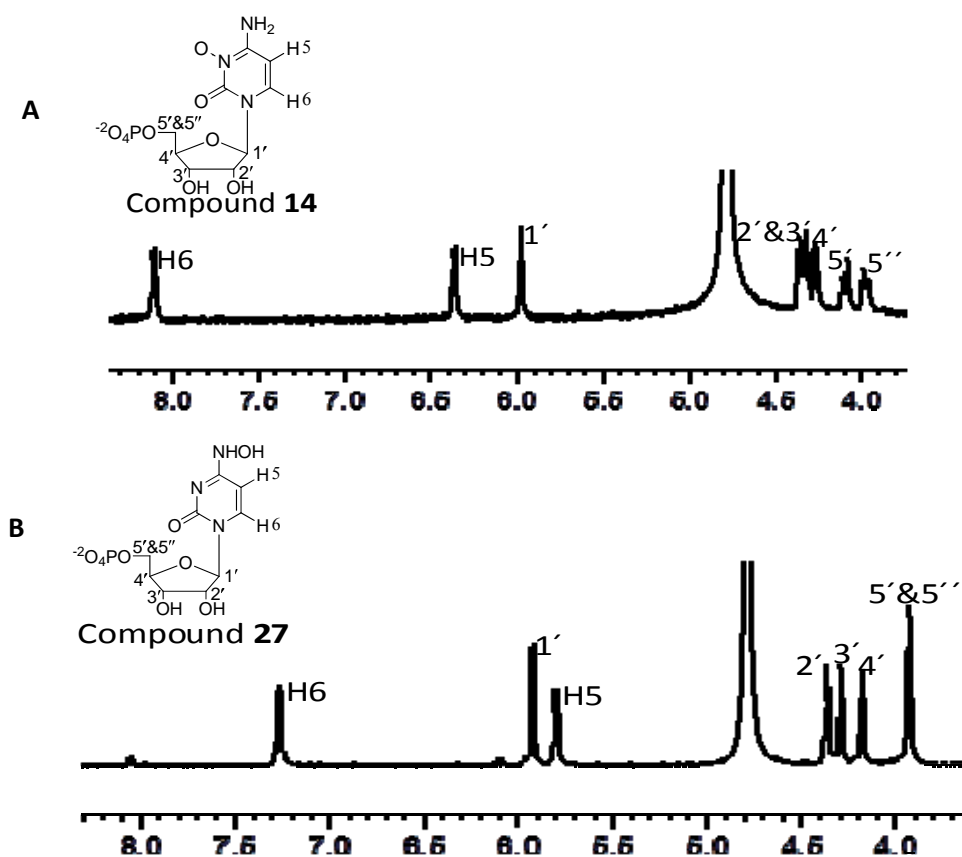


Figure 2.8: ^1H NMR (400 MHz) spectrum of compound **14** (A) and **27** (B).

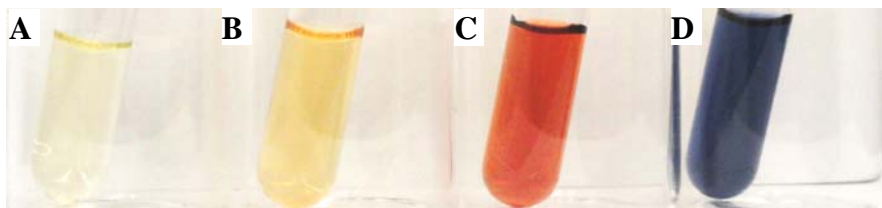
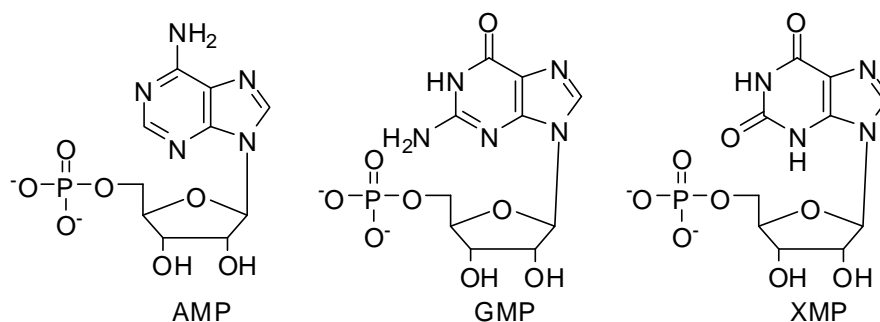


Figure 2.9: Ferric Chloride color test distinguishing between compounds **14** and **27**. (A) Blank, (B) CMP (**11**), (C) CMP- N^3 oxide (**14**) and (D) N^4 -OH-CMP (**27**).

2.5 Result, discussion and conclusion

The plasticity of ODCase catalytic site towards the purine and pyrimidine nucleotide ligands and their unusual mode of binding are reported by Kotra and Pai et al.^{13,14} Purine nucleotides AMP, GMP and XMP (Chart 2.3) along with the pyrimidine nucleotides were evaluated for their inhibitory potential of ODCase activities (Table 2.3). From the inhibition profiles of purine nucleotides, XMP seems to be a potent inhibitor of the ODCase (Table 2.3). The only structural difference between the GMP and XMP is the amino moiety replacing the ketone moiety at C2 position of GMP. A similar structural difference and trend in the inhibition profile was observed for UMP and CMP nucleotides. CMP, a pyrimidine nucleotide, is a weak inhibitor of ODCase with a K_i of 1200 ± 700 and 1400 ± 100 μM against *Mt* and *Hs* ODCases, respectively (Table 2.3). K_i values were determined by ITC based enzymatic assay as reported in earlier work (Figure 2.4).¹⁸ Structurally, the main difference between the CMP and UMP is the amino moiety replaces the ketone moiety at C4 position in CMP. Regardless of its close similarity to UMP, CMP binds to ODCase in an unusual position, retaining its low energy conformation, with its nucleic base projecting away from the active site. In this conformation, the ribose ring is in the 3' *endo* conformation and the base is oriented *anti* to the ribose ring.^{13,14,17}

Chart 2.3 : Chemical structures of purine nucleotides**Table 2.3:** Inhibition constants for nucleotide ligands against ODCases from *Mt*, *Hs* and *Pf*. All inhibitors were evaluated in competitive assays against the ODCase. “No inhibition” indicates that the activity was not inhibited at up to 20 mM concentration of the inhibitor.

Ligand	ODCase Inhibition, K_i (μM)		
	<i>Mt</i>	<i>Hs</i>	<i>Pf</i>
UMP ¹⁴	330±10	220±100	210±10
CMP ¹⁴	1200±700	1400±100	no inhibition
AMP ¹⁴	3500±200	4300 ±200	no inhibition
XMP ¹⁴	130±3.4	0.7±0.3	43±2
GMP ¹⁴	4200±100	no inhibition	2100±100
CMP- <i>N</i> ³ -oxide (14)	11.1±0.4	28.3±1.5	22.1±3.2
<i>N</i> ⁴ -OH-CMP (27)	-	-	> 1000

In the case of uracil based nucleotide ligands, the backbone -NH- of Ser127 in the binding pocket of ODCase interacts with the O4 atom of the uracil ring while the Ser127 side chain -OH serves as a hydrogen bond acceptor to N3 proton. Earlier structural studies by Wu et al. with the S127A ODCase mutant showed that the hydrogen bonds with the side chain of Ser127 residue are important for the correct placement of the uracil ring in the active site.³³ In the case of CMP, the phosphate and ribosyl moieties are held in place by similar hydrogen bonding patterns to that observed with UMP. The cytosine base, however, adopts an *anti* instead of a *syn* conformation. In this conformation the cytosine moiety is away from the Ser127 residue to engage in any interactions and even if the cytosine position were more favorable, the tertiary N3 could not act as hydrogen bond donor to Ser127 nor is there a suitable atom to form a hydrogen bond interaction with the backbone atoms, as was seen in the case of UMP (Figure 2.10). Therefore, it was envisioned that modification of the N3 and N4 position of CMP with oxygen may improve its potential to interact within the active site and its affinity favorably towards ODCase. Thus, compounds **14** and **27** were synthesized. Monophosphate derivatives **14** and **27** were investigated against ODCase, and the nucleoside derivatives **13** and **15** were evaluated in cell-based assays.

CMP-*N*³-oxide (**14**) reversibly inhibited *Mt*, *Hs* and *Pf* ODCases with K_i s 11.1 ± 0.4 , 28.3 ± 1.5 and 22.1 ± 3.2 μ M, respectively (Table 2.3). Compared to CMP, compound **14** showed 100 fold increases in ODCase inhibition activity. The oxygen at N3 position on compound **14** could act as a strong hydrogen bond acceptor. Compound **27**, which is a derivative of CMP at N4 position, was not active upto a concentration of 1 mM of the inhibitor,

against *Pf* ODCase.

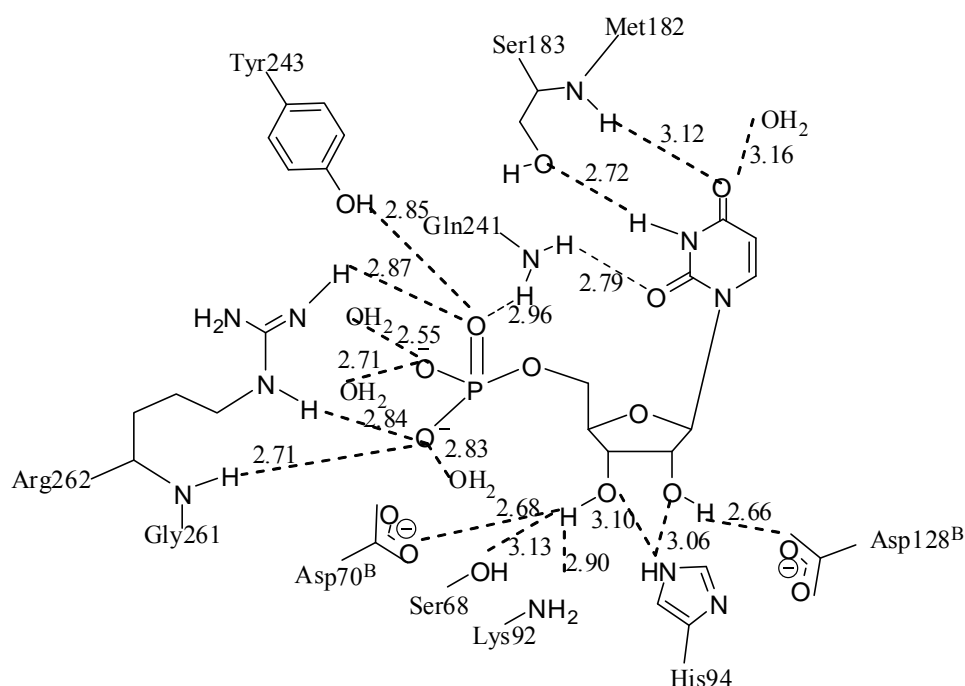


Figure 2.10: Hydrogen bonding interactions between UMP and the various active site residues of *Hs* ODCase.

Antiplasmodial activity of nucleosides **13** and **15** (nucleoside forms of **14** and **27**, respectively) were determined by fluorescence based SYBR-green assay against *P. falciparum*. Inhibitory concentrations (IC_{50} values) for compounds **13** and **15** were 411 ± 22 and 610 ± 38 $\mu\text{g/mL}$ against *P. falciparum* ItG, respectively. Compound **13** showed better potency than the N^4 -hydroxy derivative **15**, a trend that correlates with the weaker enzymatic inhibition by the nucleotide derivative **27**. It must be noted that the potencies of these cytidine nucleosides are also reflection of the phosphorylation and/or transport of the nucleosides since the mononucleotide derivatives would be the ligands inhibiting the target enzyme, ODCase.

CMP- N^3 -oxide (**14**) and N^4 -OH-CMP (**27**) were co-crystallized with *Hs* ODCase to investigate the influence of N^3 -oxide and N^4 -hydroxy

substitutions, respectively, in CMP, on the ligand orientation and interactions in the active site of ODCase. In the X-ray crystal structure of compound **14** bound to *Hs* ODCase, migration of oxygen was observed from N3 to N4, as well as to C5 position (**Figure 2.11**). Compound **27** was bound to *Hs* ODCase in both *cis* and *trans* conformations exhibiting the orientation and conformation similar to that with UMP (**1**) in the ODCase active site (Figure 2.12).

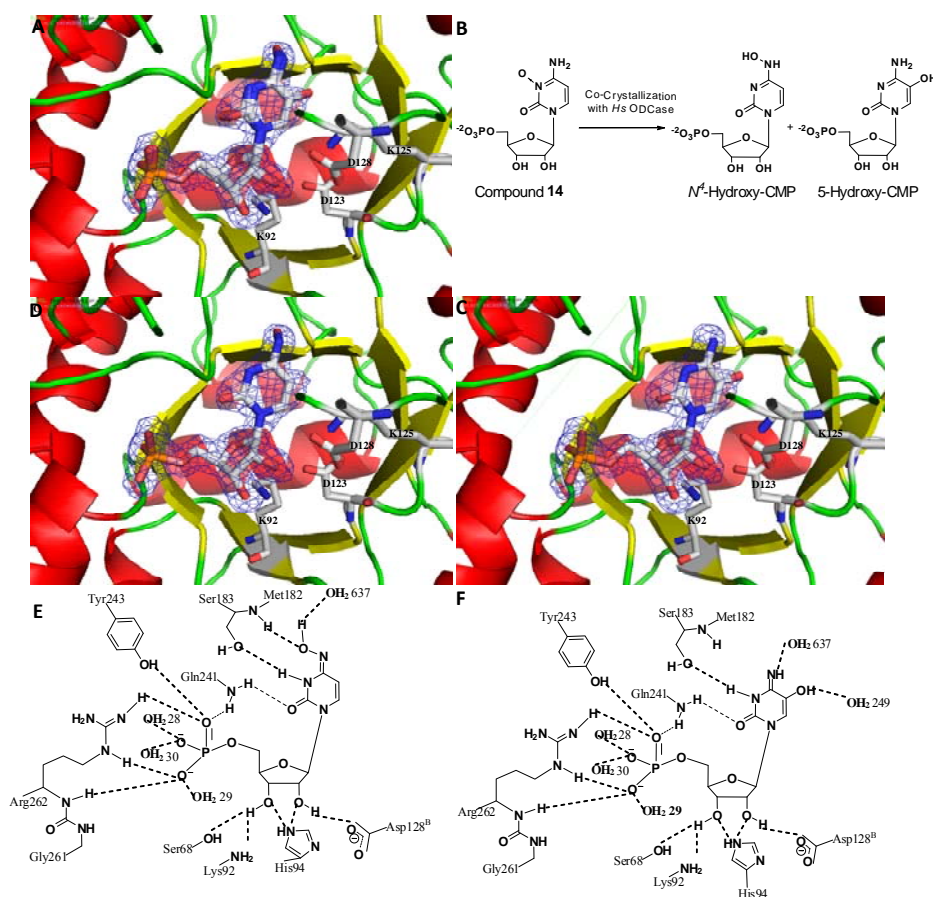


Figure 2.11: X-ray crystal structure of the complex generated by incubating ODCase with compound **14**. Panel (A) shows both rearranged products 5-OH-CMP and N^4 -OH-CMP from **14** bound to the active site of the *Hs* ODCase. Panel (B) exhibits the rearranged product N^4 -OH-CMP and 5-OH-CMP from **14** during co-crystallization with *Hs* ODCase. Panels (C) and (D) 5-OH-CMP and N^4 -OH-CMP bound to the active site of the *Hs* ODCase, respectively. *Hs* ODCase presented as cartoon model and colored with respect to the secondary structure (α -helix: Red. β -sheet: yellow. Turns: green). The rearranged products from **14** are shown as stick model with electron density map ($2F_o - F_c$) at 1σ value. Catalytic residues of K92, D123, K125, and D128 from human ODCase are also shown as capped-stick model. (E) and (F) Hydrogen bonding network between the rearranged product N^4 -OH-CMP and 5-OH-CMP from ligand **14** (respectively) with the various active site residues of *Hs* ODCase.

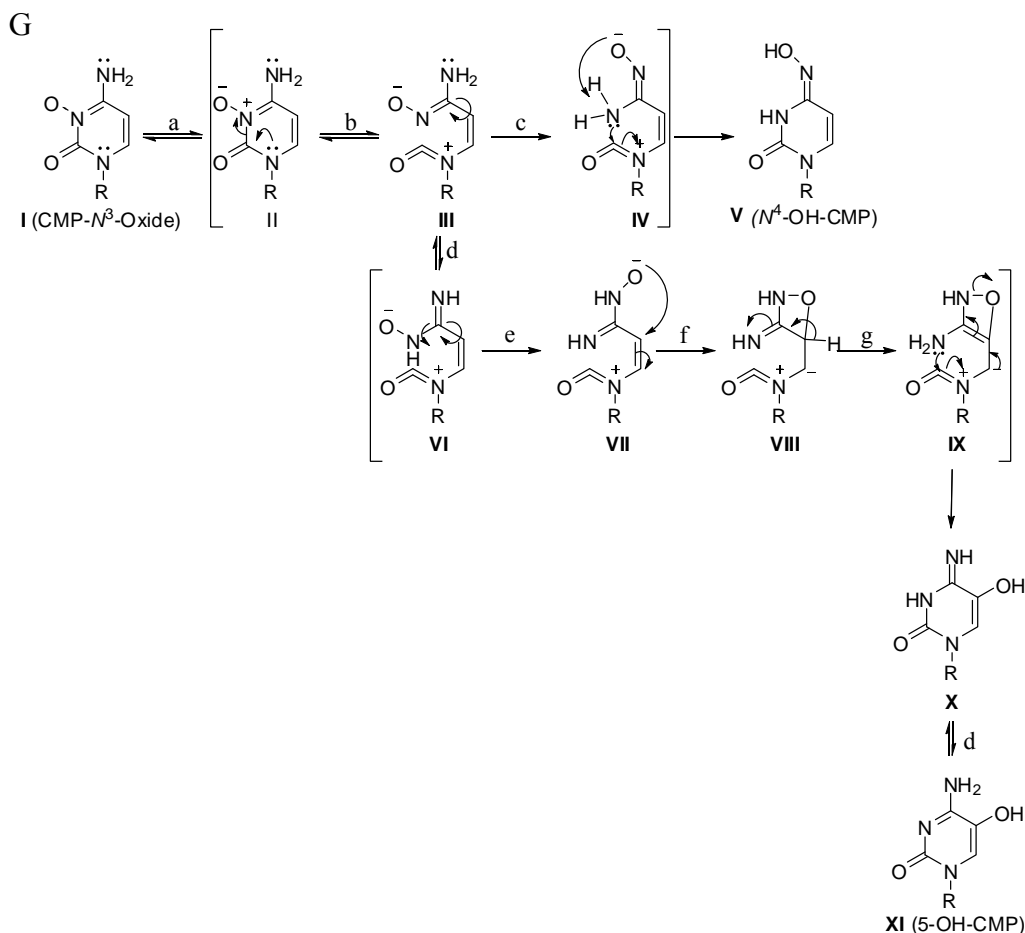


Figure 2.11 (Continued). (G) Plausible mechanism of rearrangement of the ligand **14** to yield N^4 -OH-CMP and 5-OH-CMP.

Crystals of compound **14** with ODCase proved to be difficult to grow in comparison to co-crystals with other pyrimidine derivatives in our laboratory. In the electron density map from this co-crystal with **14**, the pyrimidine portion exhibited changes in the atomic arrangement. The oxygen atom migrated from N^3 to N^4 or $C5$ position on the cytosine ring (Figure 2.11C and D). These rearranged or modified nucleotides, presumably during the crystallization process, were each bound to ODCase in a $2'$ -endo, *syn* conformation. The binding orientation and interactions in the active site of ODCase are similar, between the rearranged products, N^4 -OH-CMP and 5-OH-CMP themselves (due to the overlap density already observed in the co-

crystal structure with **14**). The orientation and the binding site interactions of the rearranged products are also similar to the observed in the co-crystal structure of UMP with the human ODCase (Figure 2.13, 2.11E and 2.11F).

The rearranged ligand N^4 -OH-CMP from compound **14** engaged in three hydrogen bond interactions with Ser183 (one with the backbone –NH–, and the other with side chain hydroxyl moiety) and a crystallographic water molecule (H₂O637) in the active site of the ODCase (Figure 2.11E). The second rearranged ligand 5-OH-CMP from compound **14** formed two hydrogen bonds: one between N3 of the ligand and the side chain of Ser183, and the other hydrogen bond was between the 4-amino moiety and the crystallographic water molecule H₂O637 (Figure 2.11F).

It was indeed intriguing to observe this unusual products N^4 -OH-CMP and 5-OH-CMP, when CMP- N^3 -oxide (**14**) was incubated with *Hs* ODCase. However, our laboratories have observed such unusual and unexpected behavior for various ligands in the presence of ODCase, such as that with the 6-cyano-UMP, 6-iodo-UMP, 6-azido-UMP and others.^{10,11,12} Interestingly, pyrimidine- N -oxides are known to undergo Dimroth rearrangement, a classical mechanism where endocyclic and exocyclic nitrogens switch places.**Error! Bookmark not defined.**³⁴ In fact, Dimroth rearrangement, also known as amidine rearrangement, was reported on cytidine- N^3 -oxide (**13**) under alkaline conditions.³⁵ Presumably, if one were to accept the idea that a Dimroth rearrangement occurred in the binding site of ODCase after the binding of compound **14**, a hypothetical mechanism could be proposed as below (Figure 2.11G). According to the proposed mechanism, the electron withdrawing nature of the N3-oxide of **14** weakens the endocyclic C2-N3 bond (Figure

2.11G, species II) and the labile C2-N3 bond yields to the acyclic a reactive isocyanate species **III** (Figure 2.11G). Subsequently, a 180° rotation around the C4-C5 bond is followed by ring closure via the species **IV** leads to the *N*⁴-OH-CMP product observed as one of the molecules bound in the active site of ODCase. This mechanism follows the classical Dimroth rearrangement observed on cytidine-*N*³-oxides.³⁵ Alternately, species **III** could undergo tautomerization yielding species **VI**, which then sets the stage for a totally different outcome. Species **VI**, after a 180° rotation of the N3-C4 and C4-C5 bonds, yields species **VII**, which could lead to the oxazete-like species **VIII**. Oxazetes are relatively stable entities that could be even isolated with appropriate stabilizing groups.^{36,37} Further rearrangement of C5 proton, N3-C2 ring closure and the more thermodynamically stable C5-C6 double bond formation leading to C5-OH moiety via species **IX** leads to the **X**. Compounds **X** and **XI** are the tautomeric forms for 5-OH-CMP, the second species observed in the catalytic site of ODCase when incubated with CMP-*N*³-oxide (**14**). While there is no proof that these complex rearrangements could happen in the binding site of ODCase, above mechanism provides a plausibility for the outcome observed when ODCase was incubated with CMP-*N*³-oxide (**14**). Several attempts of the co-crystallization taught us that the co-crystallization does not succeed always with **14**, and only on very few occasions, we observed the two products.

In order to rule out the possibility that crystallization buffer (Tris/HEPES) played any role in initiating or accelerating the rearrangement of **14**, we conducted UV spectrophotometric studies on compounds **14**. Thus, compound **14** were incubated with crystallization buffer, devoid of ODCase.

UV spectra were recorded for upto 24 h, an average time it takes to generate crystals from the protein solution. There was no observed change in the UV profiles of **14** even after 24 h (Table 2.3). This suggests that the rearrangement of **14** probably took place during the co-crystallization process and presumably in the active site of the enzyme itself.

Table 2.4: UV spectra for compounds **14** and **27** after incubation in the crystallization buffer for 24 h at room temperature.

Time (h)	CMP- N^3 -oxide (14)	CMP- N^4 -OH (27)
<i>Crystallization conditions:</i> Tris Buffer (pH7), Glycerol (12%), Ammonium Sulfate (1.8M), Inhibitor (0.396 mM). Incubated at room temperature 22 °C		
0		
24		
<i>Crystallization conditions:</i> HEPES (pH7.75), Glycerol (12%), Ammonium Sulfate (1.8M), Inhibitor (0.396 mM). Incubated at room temperature 22 °C.		
0		
24		

In the complex of compound **27** (N^4 -OH-CMP) bound to the active site of *Hs* ODCase, the nucleic base assumed a *syn* conformation and the ribosyl moiety assumed 2'-*endo* conformation. The 5'-*O*-phosphate moiety

on compound **27** maintained strong hydrogen bond interactions with Gly261, Arg262, and three crystallographic water molecules H₂O, 2, 13 and 33. In fact, the binding conformation of **27** is similar to that observed with UMP in the binding site of ODCase (Figure 2.13B).³⁸ *N*⁴-OH-CMP (**27**) could exist in two tautomeric forms, where the N4 group could assume sp² or sp³ hybridization, resulting in an imino or amino moiety, respectively (Figure 2.12B). In an aqueous environment, it was reported that the imino tautomer is more predominant, and the dipole moment of the imino tautomer of *N*⁴-OH cytosine is close to that of uracil.^{39,40} Thus, it is conceivable that *N*⁴-OH-CMP **27** binds to ODCase active site with a binding conformation similar to that of UMP.

Based on the co-crystal structure of **27** bound to ODCase, the imino tautomer of **27** could exist in both *cis* and *trans* conformations with respect to N3 (Figure 2.12A). In the *cis* conformation of **27** (Figure 2.12D), the hydroxyl group at N4 position formed a hydrogen bond (2.26 Å) with –NH– of Ser183. While in the *trans* conformation of **27** (Figure 2.12C), the hydroxyl of Ser183 formed a hydrogen bond with the N3 of the pyrimidine ring (2.72Å). Interestingly, both of these interactions were observed to occur together when UMP is bound in the active site of ODCase.¹⁰ Interactions of **27** with Ser183 residue were important for locking the nucleic base in the *syn* conformation. An earlier study reported by Wu et al. with ODCase mutant S127A and 6-aza UMP (**9**) showed that the interactions between the Ser127 residue and the uracil moiety are determining factors for the binding of the ligand in *syn* conformation to the active site of ODCase.³³

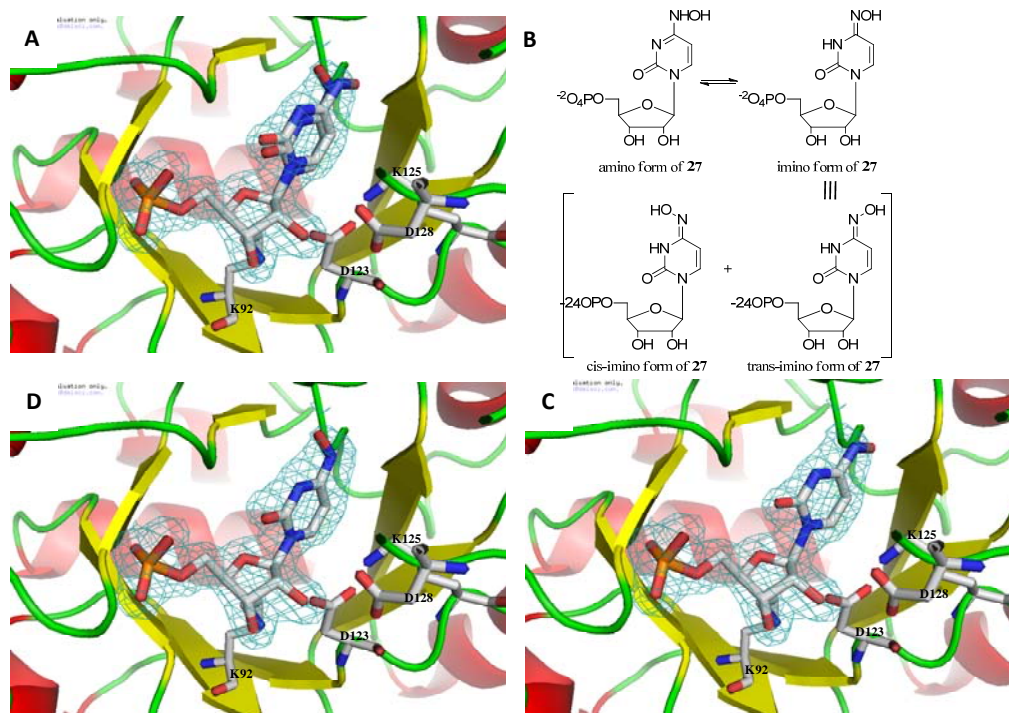


Figure 2.12: X-ray crystal structure of the complex generated by incubating *Hs* ODCase with compound 27. (A) Active site region of the *Hs* ODCase with ligand 27 bound in different conformations. (B) Amino-imino tautomers of 27 and the cis-trans imino isomers of the exocyclic N^4 -OH moiety with respect to the N3 of the pyrimidine. Panel (C) and (D) represents compound 27 bound in the *cis* and *trans*-conformation respectively, in the active site of the *Hs* ODCase. *Hs* ODCase presented as cartoon model, colored with respect to the secondary structure (α -helix: Red. β -sheet: yellow. Turns: green). Compound 27 is shown in capped-stick representation with electron density map ($2F_o - F_c$) at 1σ value. Catalytic residues of K92, D123, K125, and D128 of *Hs* ODCase are shown as stick model.

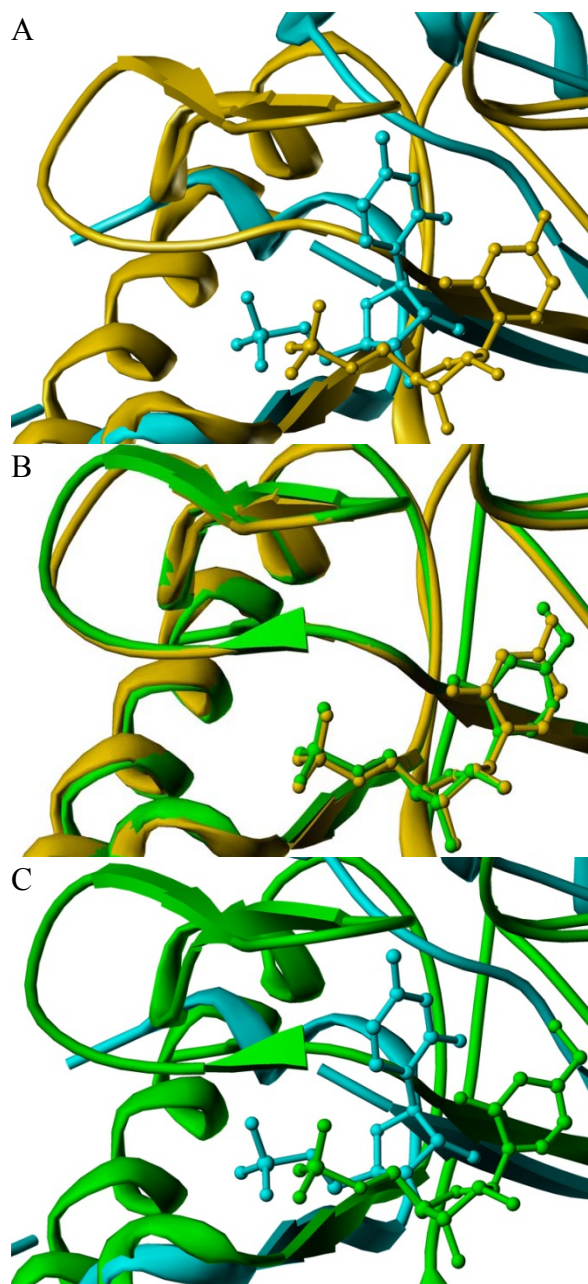


Figure 2.13: Active sites of ODCase from the X-ray crystal structures of the complexes of (A) *Hs* ODCase with UMP (yellow) overlapped with *Mt* ODCase bound by CMP (blue), (B) *Hs* ODCase with UMP overlapped with *Hs* ODCase bound by *N*⁴-OH-CMP (**27**) (green), (C) *Mt* ODCase with CMP bound by *Hs* ODCase bound by **27**.

Based on the results obtained from the overall study, following conclusions were arrived CMP and UMP—pyrimidine mononucleotides differing only by a single moiety at C4 position by an amino *vs* keto moieties, respectively—interact with ODCase quite distinctly. The introduction of the oxygen atom at the N3 position of CMP had a 100-fold increase in inhibitory activity compared to CMP and even a 10 fold increase in inhibitory activity compared to UMP against ODCase.

A yet-to-be-proven rearrangement in the binding site of ODCase contributed to the observed products, when co-crystallized with the N^3 -oxide derivative. On introduction of the oxygen atom in the form of N^4 -hydroxyl substitution on CMP, binding interactions of the CMP derivative are similar to that with UMP in the active site of ODCase, although a minor compromise was observed in the enzymatic inhibition. These results indicated that the *N*-hydroxylated cytidine derivatives behave significantly differently, potentially with improved potency against ODCase. The nucleoside versions of these CMP-based nucleotides could lead to new class of therapeutic agents.

2.6 References

- (1) Miller, B. G.; Wolfenden, R. Catalytic proficiency: the unusual case of OMP decarboxylase. *Annu. Rev. Biochem.* **2002**, *71*, 847-885.
- (2) Radzicka, A.; Wolfenden, R. A proficient enzyme. *Science*. **1995**, *267* (5194), 90-93.
- (3) Kotra, L. P.; Pai, E. F.; Bello, A. M.; Fujihashi, M.; ODCase inhibitors for the treatment of malaria. PCT Patent Application WO 2007/038859 A1, **2007**.
- (4) Yablonski, M. J.; Pasek, B.; Jones, M. E.; Traut, T. W.; Intrinsic activity and stability of bifunctional human UMP synthase and its two separate catalytic domains, orotate phosphoribosyltransferase and orotidine -5'-phosphate decarboxylase. *J.Bio.Chem.* **1996**, *271*, 10704-10708.
- (5) Meza-Avina, M. E.; Wei, L.; Buhendwa, M. G.; Poduch, E.; Bello, A. M.; Pai, E. F.; Kotra, L. P. Inhibition of orotidine 5'-monophosphate decarboxylase and its therapeutic potential. *Mini Rev. Med. Chem.* **2008**, *8*(3), 239-247.
- (6) Bello, A. M.; Poduch, E.; Liu, Y.; Wei, L.; Crandall, I.; Wang, X.; Dyanand, C.; Kain, K. C.; Pai, E. F.; Kotra, L. P. Structure-activity relationships of C6-uridine derivatives targeting plasmodia orotidine monophosphate decarboxylase. *J Med. Chem.* **2008**, *51*(3), 439-448.
- (7) Bello, A. M.; Konforte, D.; Poduch, E.; Furlonger, C.; Wei, L.; Liu, Y.; Lewis, M.; Pai, E. F.; Paige, C. J.; Kotra, L. P. Structure-activity

- relationships of orotidine-5'-monophosphate decarboxylase inhibitors as anticancer agents. *J. Med. Chem.* **2009**, *52*(6), 1648-1658.
- (8) Lewis, M.; Meza-Avina, M. E.; Wei, L.; Crandall, I. E.; Bello, A. M.; Poduch, E.; Liu, Y.; Paige, C. J.; Kain, K. C.; Pai, E. F.; Kotra, L. P. Novel interactions of fluorinated nucleotide derivatives targeting orotidine 5'-monophosphate decarboxylase. *J. Med. Chem.* **2011**, *54*(8), 2891-2901.
- (9). <http://www.rcsb.org/pdb/results/results.do?tabtoshow=Current&qrid=2F386D66> Access Date: 11th December, **2011**.
- (10) Fujihashi, M.; Bello, A. M.; Poduch, E.; Wei, L.; Annedi, S. C.; Pai, E. F.; Kotra, L. P. An unprecedented twist to ODCase catalytic activity. *J. Am. Chem. Soc.* **2005**, *127* (43), 15048–15050.
- (11) Bello, A. M.; Poduch, E.; Fujihashi, M.; Amani, M.; Li, Y.; Crandall, I.; Hui, R.; Lee, P. I.; Kain, K. C.; Pai, E. F.; Kotra, L. P. A potent, covalent inhibitor of orotidine 5'-monophosphate decarboxylase with antimalarial activity. *J. Med. Chem.* **2007**, *50*(5), 915-921.
- (12) Fujihashi, M.; Wei, L.; Kotra, L. P.; Pai, E. F. Structural Characterization of the Molecular Events during a Slow Substrate – Product Transition in Orotidine-5'-Monophosphate Decarboxylase. *J. Mol. Biol.* **2009**, *387*, 1199-1210.
- (13) Wu, N.; Pai, E. F. Crystallographic Studies of Native and Mutant Orotidine 5' Phosphate Decarboxylases. *Top. Curr. Chem.* **2004**, *238*, 23-42.

-
- (14) Poduch, E.; Wei, L.; Pai, E. F.; Kotra, L. P. Structural diversity and plasticity associated with nucleotides targeting orotidine monophosphate decarboxylase. *J. Med. Chem.* **2008**, *51*(3), 432-438.
- (15) Residue numbers refer to the enzyme from *Methanobacterium thermoautotrophicum*. The superscript “B”, as in Asp 75^B, indicates that the residue belongs to B subunit.
- (16) Langley, D. B.; Shojaei, M.; Chan, C.; Lok, H.C.; Mackay, J.P.; Traut, T.W.; Guss, J.M.; Christopherson, R. I. Structure and inhibition of orotidine 5'-monophosphate decarboxylase from *Plasmodium falciparum*. *Biochemistry* **2008**, *47*(12), 3842-3854.
- (17) Wu, N.; Gillon, W.; Pai, E. F. Crystal structures of inhibitor complexes reveal an alternate binding mode in Orotidine-5'-monophosphate decarboxylase. *J.Biol.Chem.* **2002**, *277* (31), 28080-28087.
- (18) Poduch, E.; Bello, A. M.; Tang, S.; Fujihashi, M.; Pai, E. F.; Kotra, L. P. Design of inhibitors of orotidine monophosphate decarboxylase using bioisosteric replacement and determination of inhibition kinetics. *J. Med. Chem.* **2006**, *49*(16), 4937-4945.
- (19) Higuchi, T.; Barnstein, C. H. Hydroxylammonium Acetate as Carbonyl Reagent. *Anal. Chem.* **1956**, *28* (6), 1022-1025
- (20) Grochulski, P.; Fodje, M.N.; Gorin, J.; Labiuk, S.L.; Berg, R. Beamline 08ID-1, the prime beamline of the Canadian Macromolecular Crystallography Facility. *J. Synchrotron Rad.* **2011**, *18* (4), 681-684.
- (21) Kabsch, W. XDS. *Acta Cryst. , Sect. D : Biol. Crystallogr.*, **2010**, *D66*, 125-132.

-
- (22) Vagin, A.; Teplyakov, A. MOLREP: an automated program for molecular replacement. *J.Appl.Crystallogr.* **1997**, *30*, 1022-1025.
- (23) Murshudov, G. N.; Vagin, A. A.; Dodson, E. J. Refinement of macromolecular structures by the maximum-likelihood method. *Acta Crystallogr.* **1997**, *D53*, 240–255.
- (24) Emsley, P.; Cowtan, K. Model building tools for molecular graphics. *Acta Crystallogr.* **2004**, *D60*, 2126–2132.
- (25) Otwinowski, Z.; Minor, W. Processing of X-ray diffraction data collected in oscillation mode. *Methods Enzymol.* **1997**, *276*, 307–326.
- (26) Trager, W.; J. Jensen. Human malaria parasites in continuous culture. *Science.* **1976**. *193*, 673-675.
- (27) Smilkstein, M.; N. Sriwilaijaroen, J.; X. Kelly; Wilairat P.; Riscoe M.. Simple and inexpensive fluorescence-based technique for high-throughput antimalarial drug screening. *Antimicrob. Agents Chemother.* **2004**. *48*, 1803-1806.
- (28) Chang, C.; Lin, P.; Chen, Y.; Chang, C.; Kan, L.; Direct visualization of the triplex DNA molecular dynamics by the fluorescence resonance energy transfer and atomic force microscopy measurements. *App. Phys.Lett.* **2007**, *91*, 203901.
- (29) Harnden, M. R.; Brown, A. G.; Hodge, R. A. Oxidation of ribonucleic acids with m-chloroperbenzoic acid. *J. Chem. Soc. Perkin 1.* **1973**, *4*, 333-335.
- (30) Romo, J.; Rodríguez-Hahn, L.; Jiménez, M. Synthesis of steroidal pyrimidine N-oxides. *Can. J. Chem.* **1968**, *46*, 2807-2815.
- (31) Leung, K.K.; Visser, D.W. A new deoxycytidine analog, 5-hydroxy-2'-

- deoxycytidine, *Biochem. Med.* **1974**, *9*, 237-243.
- (32) Delia, T. J.; Olsen, M. J.; Brown, G. B. Cytosine 3-N-Oxide and its rearrangement on acetylation. *J Org Chem.* **1965**, *30*, 2766-2768
- (33) Wu, N.; Gillon, W.; Pai, E. F. Mapping the active site-ligand interactions of orotidine 5'-monophosphate decarboxylase by crystallography. *Biochemistry.* **2002**, *41*(12), 4002-4011.
- (34) El Ashry, E. S. H.; Nadeem, S.; Shah, M. R.; El Kilany, Y. Recent Advances in the Dimroth Rearrangement: A Valuable Tool for the Synthesis of Heterocycles. *Adv.Heterocycl.Chem.* **2010**, *101*, 161–228.
- (35) Sako, M.; Kawada, H. A new and efficient synthetic method for ¹⁵N₃-labeled cytosine nucleosides: Dimroth rearrangement of cytidine N₃-oxides. *J. Org. Chem.* **2004**, *69*(23), 8148-8150.
- (36) Corkins, H. G.; Storace, L.; Osgood, E. R. A new route to the 4H-1,2-oxazete ring system by the stereospecific oxidation of (Z)-3,3-dimethyl-1,1-bis(methylthio)-2-butanone oxime. *Tetrahedron Lett.* **1980**, *21*, 2025-2028.
- (37) Wieser, K.; Berndt, A. 4H-1,2-Oxazete N-oxides from 1,1-di-tert-butylallenes. *Angew. Chem. Internat.* **1975**, *14*, 69-70.
- (38) Wittmann, J. G.; Heinrich, D.; Gasow, K.; Frey, A.; Diederichsen, U.; Rudolph, M.G. Structures of the human orotidine-5'-monophosphate decarboxylase support a covalent mechanism and provide a framework for drug design. *Structure.* **2008**, *16*(1), 82-92.
- (39) Shugar, D.; Kierdaszuk. New light on tautomerism of purines and pyrimidines and its biological and genetic implications. *Proc.Int.Symp.Biomol.Struct.Interactions*, Suppl. *J.Biosci.* **1985**, *8*,

657-668.

- (40) Les, A.; Adamowicz, L.; Rode, W. Structure and conformation of N4-hydroxycytosine and N4-hydroxy-5-fluorocytosine. A theoretical ab initio study. *Biochim.Biophys.Acta* **1993**, *1173*, 39-48.

Phenoxy propanediol derivatives
targeting neuroaxonal growth in
diabetic neuropathy

3.1 Introduction and literature review

Diabetes mellitus is metabolic disorder caused by inherited and/or acquired deficiency in secretion of insulin by pancreas, or by ineffectiveness of the secreted insulin resulting in elevated blood glucose (hyperglycemia). Over the past decade, diabetes has been recognized as an epidemic and by 2030; an estimated 350 million people are expected to suffer from diabetes according to World Health Organization, doubling the current numbers.¹ According to recent study by Centers of Disease Control and Prevention, 25.8 million people in US are affected by diabetes and the total annual cost of diabetes is estimated to US\$174 billion.² Most of the type 2 diabetes patients progress to type 1 diabetes eventually. The encumbrance of both type 1 and type 2 diabetes on human is consequences of the complications of the disease. Hyperglycemia induced microvascular complications includes retinopathy, nephropathy, neuropathy and heart disease as macrovascular complication. A startling fact is that the incidence of neuropathy in diabetic patients can be as high as 50% and leads to incapacitating pain, sensory loss, foot ulceration, gangrene, poor wound healing and lower limb amputation.^{3,4} There is no cure or treatment for this condition currently and most of the treatments are palliative at best.

An important pathological feature of the diabetic neuropathy seen in type 1 diabetes is the loss of the end regions of the nerves affecting senses such as touch, although such loss can be spread to almost all organs and systems in the peripheral system. In diabetics, increased levels of glucose accumulate in the peripheral neurons independent of insulin. This

accumulation is due to the abnormally high levels of glucose in the interstitial fluid and its abnormal metabolism leading to glucose neurotoxicity.^{5,6} Altered glucose metabolism and a decrease in the synthesis of neurotrophic factors lead to slowing of nerve conduction velocity (NCV), decreased blood supply to neurons which further causes neuronal degeneration. A number of molecular mechanisms are proposed in diabetic neuropathy: (a) polyol or sorbital pathway including glucose induced oxidative stress, (b) hexosamine pathway, (c) protein kinase C activation, and (d) non-enzymatic protein glycation. Each of these pathways leads to functional and structural abnormalities in a peripheral neuron ultimately resulting in neuronal degeneration (Figure 3.1).^{7,8,9,10,11,12}

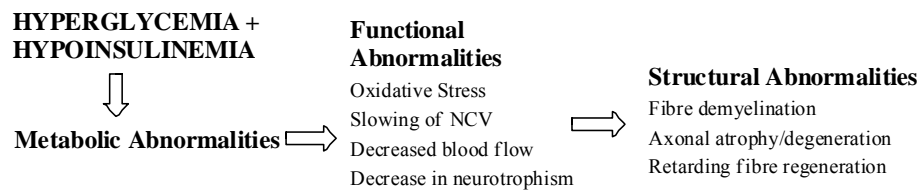
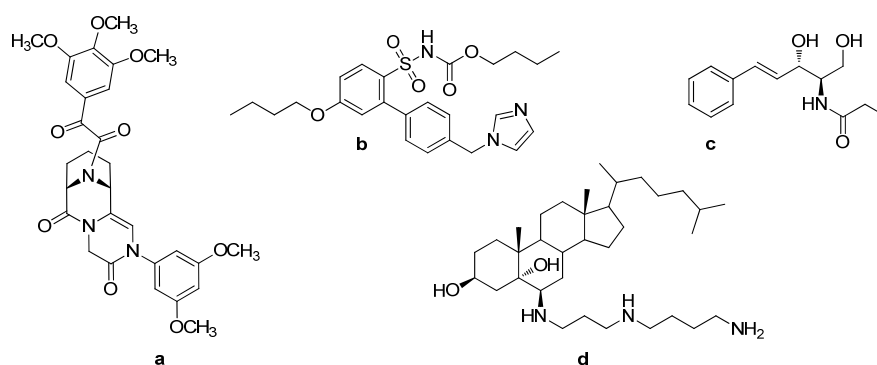


Figure 3.1: A schematic depiction of metabolic, functional and structural abnormalities in a peripheral diabetic neuron, which could play a role in neuropathy development.

Fernyhough and co-workers investigated various endpoints during neuroaxonal degeneration and regeneration processes such as the levels and patterns of axon outgrowth, the modulation of intracellular calcium levels, the maintenance of mitochondrial membrane potential, effect of high glucose on stress-activated protein kinase activity, and the expression of a number of related genes.^{13,14,15,16,17,18,19,20,21} Studies have also shown that these *in vitro* morphological criteria are relevant to the processes of axon regeneration, and collateral sprouting that are observed *in vivo* when peripheral nerve is damaged or the cutaneous target fields are altered.^{22,23}

In Type 1 diabetes a key pathological feature of symmetrical sensory polyneuropathy is the loss of cutaneous sensory innervations. The etiology of the sensory loss remains elusive, however, impaired collateral sprouting and/or regeneration of axons could certainly be pathogenic factors. These may explain the failure of sensory axons, damaged by hyperglycemia or other diabetes-related degenerative events, to re-innervate the peripheral tissues. In this context, collateral sprouting is believed to be a plastic process that results in the terminal fields of sensory neurons being maintained and adjusted according to signals derived from the local environment and neighboring axons, *e.g.* neurotrophic factors.^{24,25}

A strategic approach to identify potential drugs targeting diabetic neuropathy is to find molecules that improve sensory axon sprouting and/or regeneration leading to the prevention and/or reversal of neurodegeneration. The adult sensory neuron culture system allows for such a direct and rapid *in vitro* screening approach for the identification of small molecule drugs.²⁶ A successful example of such an approach has been the identification of neotrofin as a small molecule capable of possibly modulating endogenous NGF activity.²⁷ Few classes of compounds such as (a) polycyclic aza-amide neuroimmunophilin, (b) arylbenzylimidazole AT₂ agonists, (c) short chain ceramide analogs and (d) alkyl amino oxysterols dendrogenin B are reported to induce neurite outgrowth in neuronal cells (Chart 3.1).^{28,29,30,31}

Chart 3.1: Different classes of drugs inducing neurite outgrowth

Three years ago, a library of 600 compounds were screened in-vitro for their ability to enhance axonal regeneration in adult rat sensory neurons by at least 2-fold ($P < 0.05$) in Fernyhough laboratories and this led to the identification of guaifenesin (**1**) as a potent compound in this assay. Guaifenesin is a common active ingredient in various coughs preparations such as Rubitussin™ and is a derivative of phenoxypropane. In the course of the screening program for guaifenesin analogs, the (*R*)-enantiomer **9** of the guaifenesin was found to be 10 times more potent than the racemate mixture. (*S*)-enantiomer **10** of the guaifenesin was not as efficacious as its counterpart, (*R*)-enantiomer **9** and racemate **1**. There was no evidence of (*R*)-guaifenesin's (**9**) site action in diabetic adult sensory neurons. A bead-based chemical proteomics approach was adopted to fish the molecular targets of (*R*)-guaifenesin (**9**) from adult sensory neuronal extract.

Chemical proteomics is an emerging tool in drug discovery unraveling the drug interactome. The underlying principle of chemical proteomics is to immobilize the drug on the solid matrix, followed by incubation with the cell lysate and isolation of the total drug bound interacting protein.^{32,33} The drug bound interactome is then released by treating with surfactant and identified

by mass spectrometry. Affinity chromatography in combination with mass spectrometry is the classical method used in chemical proteomics for target identification.^{34, 35}

Affinity chromatography can be applied in four different ways to pull down the proteins binding to the drug immobilized on affinity matrix.^{36, 37}

- A. Solid phase elution – In this method, solid support immobilized with ligand (drug) is packed in a column and cell lysate is loaded on it. Several column washing is given to get rid of unbound protein. Ligand bound protein is then eluted with buffers which can disrupt the intermolecular interaction. Fractions of interest are collected and subjected to SDS PAGE. This method of pull down protein is time consuming and requires a large quantity of solid support with ligand immobilized.
- B. Comparison variant-In this procedure, inactive analogue of ligand (drug) is immobilized on the solid support and then the protein pattern eluted by solid phase elution is compared with that of the active immobilized ligand. This helps in identification of the nonspecific binding proteins.
- C. Competition variant-In this protocol, free bioactive ligand in buffer is used for elution of the protein bound to the immobilized ligand on solid matrix packed in the column. This method is effective only if the free ligand is soluble in the elution buffer.
- D. Serial affinity chromatography- According to this method, the cell lysate is incubated with the bioactive ligand immobilized on solid matrix. The supernatant obtained after first incubation is treated again with the fresh

batch of ligand immobilized on solid support. The binding proteins captured after sequential incubation of cell lysate or protein extract with fresh batch of affinity matrices (at least twice) are comparatively analyzed.³⁸

In this chapter, the effects of phenoxy propane diol derivatives related to guaifenesin, and its enantiomers on neuroaxonal growth as potential agents for the treatment of diabetic neuropathy are disclosed. Results of serial affinity chromatography approach adopted for identification of (*R*)-guaifenesin's (**9**) molecular targets are revealed here.

3.2 Objective

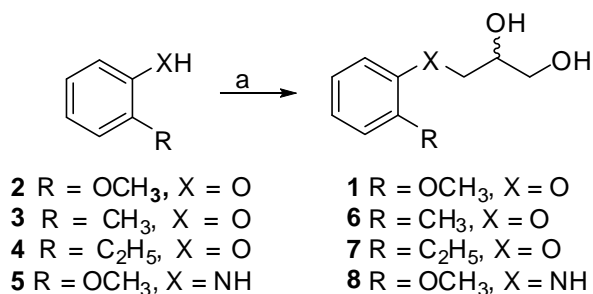
On discovery of guaifenesin as a promising candidate stimulating axonal regeneration in diabetic neuropathy, a systematic approach was adopted to study the importance of the functional moieties of guaifenesin. In the present study, synthesis and biological evaluation of the racemate guaifenesin analogs and guaifenesin enantiomers were accomplished. Further, prodrugs of potent (*R*)-guaifenesin (**9**) were synthesized to improve its pharmacokinetics. In-vitro plasma protein binding and permeability study for (*R*)-guaifenesin and its prodrugs were studied. Target deconvolution for (*R*)-guaifenesin was conducted. As described previously serial affinity chromatography is easy and quick as compared to other affinity chromatography techniques. Serial affinity chromatography strategy was adopted for to fish the (*R*)-guaifenesin binding druggable protein from sensory neuronal cell extract. Stages involved in the target deconvolution study included,

- a) Synthesis of (*R*)-guaifenesin ligand with hydrophilic linker.
- b) Immobilization of ligand on affinity resin.
- c) Isolation and identification of specific (*R*)-guaifenesin binding neuronal proteins.

3.3 Experimental Section

3.3.1 *Synthetic schemes and procedures*

General: All chemicals were purchased from commercial suppliers and used without further purification. DMF and triethylamine were dried over 4 Å molecular sieves. Microwave reactions were carried out in a Biotage Initiator microwave equipped with a robotic arm for four consecutive reactions. Reactions were monitored by thin layer chromatography (TLC) plates with silica gel 60 F₂₅₄ (Merck) coated on aluminum sheets. For column chromatography, silica gel (230-400 Å mesh) from EMD Chemicals was used. NMR spectra were recorded on a Joel spectrometer (500 MHz for ¹H, 125 MHz for ¹³C) or a Bruker (400 MHz for ¹H, 100 MHz for ¹³C). The chemical shifts are reported in ppm (δ) and the spectra were recorded using tetramethylsilane as a reference for ¹H NMR spectra. Mass spectra (ESI) were recorded on a Waters UPLC[®]/MS with Waters 3100 mass detector. Specific rotation of synthesized enantiomers and their prodrugs were obtained from Interscience AA-55 polarimeter in methanol at 23 °C. Elemental analysis and LC-MS were used to determine chemical purity of synthesized compounds.



Scheme 3.1. Preparation of guaifenesin and its derivatives. Reagents and conditions: a. NaOH, anhydrous DMF, μ W at 210 °C, 15 min, (\pm)-chloropropane-2,3-diol.

General procedures for synthesis of compounds **1** and **6-8**

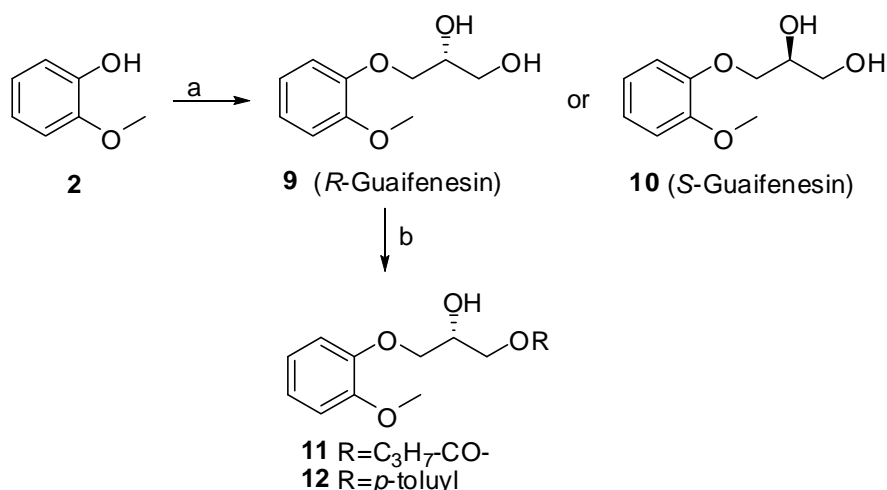
Appropriate *ortho* substituted phenol or aniline (1.0 equiv), NaOH (0.9-2.5 equiv), 3-chloropropane-1, 2-diol (0.9-2.5 equiv) and DMF (1 - 2 mL) were added to a reaction vessel containing a Teflon stir bar. The vessel was securely capped and the reaction mixture was transferred to the Biotage Initiator microwave and irradiated at 210 °C for 10 min to yield **1**, **6**, **7** phenol derivatives and at 150 °C for 5 min to get aniline derivative **8**. The reaction mixture was diluted with ethyl acetate (10 mL) and washed with water (10 mL). The organic phase was separated, the aqueous phase was extracted with ethyl acetate (3 x 50 mL), and the combined organic layers were washed with water (2 x 50 mL) followed by brine and dried over anhydrous Na₂SO₄. The solvents were removed under reduced pressure and the resulting crude was purified by silica gel flash chromatography using a gradient 1-5% MeOH/CHCl₃.

(±)-3-(2-Methoxyphenoxy)-1,2-propanediol (1). White solid (149 mg, 75%). m.p. 79-80 °C. ¹H NMR (CDCl₃) δ 2.60 (t, 1H), 3.39 (d, 1H), 3.75-3.84 (m, 2H), 3.86 (s, 3H), 4.04-4.12 (m, 2H), 4.13-4.20 (m, 1H), 6.88-6.95 (m, 3H), 6.96-7.01 (m, 1H). ¹³C NMR (CDCl₃) δ 55.97, 64.06, 70.11, 72.52, 111.89, 114.97, 121.25, 122.43, 148.07, 149.82. ESI (+ve) (M+Na⁺) calculated 221.19, found 221.

(±)-3-(2-Methylphenoxy)-1,2-propanediol (6). White solid (171 mg, 94%). m.p. 68 °C. ¹H NMR (CDCl₃) δ 2.15 (t, 1H), 2.23 (s, 3H), 2.66 (d, 1H) 3.76-3.82 (m, 1H), 3.84-3.91 (m, 1H), 4.06 (d, 2H), 4.11-4.17 (m, 1H), 6.83 (d, 1H), 6.89 (t, 1H), 7.16 (t, 2H). MS (ESI, +ve) (M+Na⁺) calculated 182.22, found 182.1.

(±)-3-(2-Ethylphenoxy)-1,2-propanediol (7). White solid (175 mg, 89%). m.p. 53 °C. ¹H NMR (CDCl₃) δ 1.20 (t, 3H), 2.08-2.18 (br, m, 1H), 2.64 (q, 2H), 3.76-3.83 (m, 1H), 3.85-3.91 (m, 1H), 4.06 (d, 2H), 4.11-4.18 (m, 1H), 6.84 (d, 1H), 6.91 (t, 1H), 7.14-7.21 (m, 2H). MS (ESI, +ve) (M+Na⁺) calculated 196.24, found 196.1.

(±)-3-(2-Methoxyphenylamino)-1,2-propanediol (8). Light brown solid (315 mg, 26%). ¹H NMR (CDCl₃) δ 3.24 (dd, 1H), 3.30 (dd, 1H), 3.66 (dd, 1H), 3.80 (dd, 1H), 3.896 (s, 3H), 3.98-4.02 (m, 1H), 6.67 (dd, 1H), 6.70-6.74 (m, 1H), 6.79 (dd, 1H), 6.86-6.89 (m, 1H). MS (ESI, +ve) (M+Na⁺) calculated 220.3, found 220.1.



Scheme 3.2. Preparation of guaifenesin enantiomers. Reagents and conditions: a. NaOH, anhydrous DMF, μ W at 210 °C, 15 min, (*R*)-chloropropane-2,3-diol, 64 % (for **9**) or (*S*)-Chloropropane-2,3-diol, 64 % (for **10**); b. Compound **9**, dry Et₃N, anhyd DMF, ClCOC₃H₇, 42% (for **11**) or toluyl chloride, 46% (for **12**).

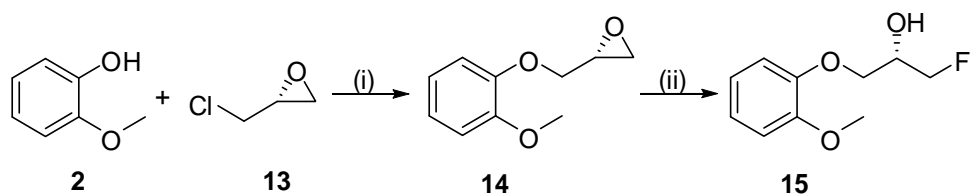
(2*R*)-3-(2-Methoxyphenoxy) propane-1, 2-diol (9). To a stirred suspension of NaOH (298 mg, 7.45 mmol) in anhyd DMF (2 mL), guaiacol (616 mg, 4.96 mmol) and (*R*)-(-)- α -monochlorohydrine (822 mg, 7.44 mmol) were added and the reaction was carried out at 210 °C for 15 min in a microwave. The reaction mixture was then diluted with EtOAc (30 mL), washed with H₂O (15 mL), brine (15 mL), and dried (Na₂SO₄). Evaporation of the solvent and purification of the crude by column chromatography (6 % MeOH in CH₂Cl₂) yielded compound **9** (630 mg, 64%) as a white powder which was further recrystallized from EtOAc. ¹H NMR (CDCl₃) δ 3.78-3.79 (m, 2H), 3.81 (s, 3H), 4.04-4.06 (m, 1H), 4.13 (d, 2H), 6.90-6.91 (m, 4H). ¹³C NMR (CDCl₃) δ 56.14, 64.21, 70.34, 72.59, 112.17, 115.22, 121.44, 122.58, 148.30, 150.02. MS (ESI, +ve) (M+Na⁺) calculated 221.32, found 221.0 [α]_D^{23.6} -7.14° (*c* 1.12, MeOH).

(2S)-3-(2-Methoxyphenoxy) propane-1, 2-diol (10). Compound **10** was synthesized using the same reaction conditions as for compound **9** in presence of (*S*)-(+)- α -monochlorohydrine, and the product was isolated as a white solid (630 mg, 64%). $^1\text{H NMR}$ (CDCl_3) δ 3.78-3.79 (m, 2H), 3.81 (s, 3H), 4.04-4.06 (m, 1H), 4.13 (d, 2H), 6.90-6.91 (m, 4H). MS (ESI, +ve) ($\text{M}+\text{Na}^+$) calculated 221.32, found 221. $[\alpha]_{\text{D}}^{23.6} +7.5^\circ$ (*c* 1.2, MeOH).

(2R)-2-Hydroxy-3-(2-methoxyphenoxy) propyl butanoate (11). Butyryl chloride (145 mg, 0.14 mL, 1.36 mmol) was added drop wise to a cold stirred solution of compound **9** (300 mg, 1.51 mmol) in anhydrous DCM (3 mL) and anhydrous Et_3N (153 mg, 0.2 mL, 1.51 mmol) at -12°C . The reaction was then stirred at the same temperature for 30 min, diluted with EtOAc (15 mL), and washed with H_2O (8 mL), brine (8 mL), and dried (Na_2SO_4). The combined organic layers was concentrated and purified by silica gel column chromatography (35% EtOAc/Hexanes) to yield compound **11** (169 mg, 42%) as a solid. $^1\text{H NMR}$ (CDCl_3) δ 0.91-0.94 (m, 3H), 1.61-1.66 (m, 2H), 2.28-2.32 (m, 2H), 3.85 (s, 3H), 3.98-4.07 (m, 2H), 4.22-4.28 (m, 3H), 6.86-6.96 (m, 4H). $^{13}\text{C NMR}$ (CDCl_3) δ 13.74, 18.50, 36.10, 55.96, 65.13, 68.50, 71.31, 112.27, 115.23, 121.14, 122.38, 148.20, 149.94, 173.83. MS (ESI, +ve) ($\text{M}+\text{Na}^+$) calculated 291.12, found 291.13. $[\alpha]_{\text{D}}^{23.6} +6.08^\circ$ (*c* 1.15, MeOH).

(2S)-2-Hydroxy-3-(2-methoxyphenoxy) propyl-4-methylbenzoate (12). Toluoyl chloride (350 mg, 0.3 mL, 2.27 mmol) was added drop wise to a cold stirred solution of compound **9** (500 mg, 2.52 mmol) in anhydrous dichloromethane (3 mL) and anhydrous Et_3N (257 mg, 0.35 mL, 2.52 mmol) at -12°C . The reaction was stirred at the same temperature for 1 h. The reaction mixture was then diluted with EtOAc (20 mL), washed with H_2O (10

mL), brine (10 mL), and dried (Na_2SO_4). The combined organic layers was concentrated and was purified by silica gel column chromatography (35% EtOAc in Hexanes) to give compound **12** (169 mg, 42 %) as a yellow syrup. ^1H NMR (CDCl_3) δ 2.40 (s, 3H), 3.85 (s, 3H), 4.07-4.20 (m, 2H), 4.34-4.39 (m, 1H), 4.49-4.51 (m, 2H), 6.88-7.00 (m, 4H), 7.22-7.26 (m, 2H), 7.93-7.99 (m, 2H). ^{13}C NMR (CDCl_3) δ 21.98, 56.17, 65.82, 68.98, 71.91, 112.46, 116.15, 122.88, 130.52, 144.22, 148.35, 150.42, 167.05. ESI (+ve) ($\text{M}+\text{Na}^+$) calculated 339.12, found 339.35. $[\alpha]_{\text{D}}^{23.6} +9.6^\circ$ (c 1.25, MeOH).



Scheme 3.3. Preparation of fluorinated derivative of guaifenesin. Reagents and conditions: (i) NaOH, K_2CO_3 , *tetra-n*-butylammonium bromide, MW, 110 $^\circ\text{C}$, 5 min, 33%, (for **14**) (ii) 1 M TBAF in THF, Toluene, 80 $^\circ\text{C}$, 3h, 41.4% (for **15**).

(R)-2-((2-methoxyphenoxy) methyl) oxirane (14). To a stirred mixture of NaOH (363 mg, 9.09mmol), K_2CO_3 (2.5 g, 18.28 mmol), guaiaacol (1.12 g, 9.09 mmol) and TBABr (295 mg, 0.91 mmol), (*R*)-(-)-epichlorohydrin (1.26g, 13.61 mmol) was added and the reaction was subjected to microwave at 110 $^\circ\text{C}$ for 5 min. After cooling the reaction mixture it was diluted with H_2O (15 mL). Aqueous layer was then extracted with EtOAc (60 mL) washed with brine (15 mL) and dried over Na_2SO_4 . Organic layer was concentrated and purified by silica gel chromatography (10% EtOAc in Hexanes) to yield compound **14** (430 mg, 80.6%). ^1H NMR (CDCl_3), δ 2.73-2.74 (dd, 1H), 2.88-

2.90 (dd, 1H), 3.80-3.90 (m, 1H), 3.86 (s, 3H), 4.02-4.06 (dd, 1H), 4.21-4.25 (dd, 1H), 6.89-6.95 (m, 4H). ^{13}C NMR (CDCl_3) δ 44.68, 49.92, 55.58, 69.94, 111.67, 113.99, 120.56, 121.66, 147.7, 149.36.

(S)-1-fluoro-3-(2-methoxyphenoxy) propan-2-ol (15). To a stirred solution of compound **15** (50 mg, 0.27 mmol) in toluene (1 mL), TBAF (1M, 1.66 mL) was added and heated to 80 °C for 3 h. The reaction mixture was diluted with H_2O (15 mL) and then extracted with EtOAc (60 mL). Organic layer was washed with brine (15 mL), dried over Na_2SO_4 and concentrated. It was further purified by silica gel chromatography (5% MeOH in CHCl_3) to give compound **15** (23 mg, 41%). ^1H NMR (CDCl_3), δ 3.86 (s, 3H), 4.06-4.14 (m, 2H), 4.21-4.27 (dd, 2H), 4.48-4.67 (dd, 2H), 6.89-7.01 (m 4H). ^{13}C NMR (CDCl_3) δ 55.94, 68.98 (d, $J_{\text{C-F}}$ 20.45 Hz, 1C), 70.56, (d, $J_{\text{C-F}}$ 6.59 Hz, 1C), 83.69 (d, $J_{\text{C-F}}$ 170.04 Hz, 1C). ESI (+ve) calculated ($\text{M}+\text{Na}^+$) 223.3, found 223. $[\alpha]_{\text{D}}^{23.6} +20.51^\circ$ (c 1.95, DCM).

Table 3.1: Purity data for guaifenesin derivatives

Compound No.	HPLC and microanalyses purity data		
1	Run time = 15 min; Column = C18, 4.6*150 mm (Xbridge, Waters), Flow rate = 1 mL/min, Solvents = A (Water with 0.05 % TFA) and B (MeOH with 0.05% TFA). <i>Condition 1:</i> 50% A & 50% B isocratic. Retention time = 2.83 min, Purity: 97.03%. <i>Condition 2:</i> 70 % A and 30 % B isocratic. Retention time = 7.62 min, Purity: 96.31%		
	Microanalyses		
	Calculated	Found	
6	C=65.91 H=7.74	C=65.84 H=8.10	
7	C=67.32 H=8.22	C=67.28 H=8.67	
8	C=60.90 H=7.67 N=7.10	C=60.50 H=7.47 N=6.90	
9	C=60.59 H=7.12	C=60.62 H=7.00	
10	C=60.59 H=7.12	C=60.65 H=7.25	
11	C=62.67 H=7.51	C=62.46 H=7.43	
12	C=68.34 H=6.37	C=68.30 H=6.62	
15	<i>Condition 1:</i> Run time = 40 min; Column = C18, 4.6*250 mm (Spherisorb, Waters), Flow rate = 1 mL/min, Solvents = A (Water with 0.05 % TFA) and B (MeOH with 0.05% TFA). Gradient: RT = 21.81 min Purity: 90.6%		
	Time (min)	A%	B%
	0	95	5
	15	60	40
	40	5	95
	<i>Condition 2:</i> Run time = 12 min; Column = Silica, 4.6*150 mm (Sunfire, Waters), Flow rate = 1 mL/min, Solvents = A (Hexanes) and B (Ethylacetate). Isocratic Method:60 % A and 40 % B. RT = 4.09 min, Purity 90.07%		

3.3. 2 *In vitro* screening assay

In vitro screening of compounds was carried out in Fernyhough laboratory. Guaifenesin and its analogs were screened in-vitro to assess their stimulatory effect on axon regeneration and outgrowth from adult sensory neurons by a cell based assay as previously described.^{13,14,26} In brief, DRG sensory neurons isolated from the STZ-diabetic rats were plated onto poly-D-*L*-ornithine hydrobromide and laminin coated multi-well plate. After which they were incubated with a known concentration of desired compound under sterile conditions at about 37 °C for at least 24 hours. After incubation, the neurons in each well were morphometrically (total neurite length and axon out growth) assessed to determine the extent of the axon regeneration and outgrowth that occurred. Axonal regeneration and outgrowth taking place by the drug treatment was then statistically analyzed after comparing with the control treatment.

3.3. 3 *Motor nerve conduction velocity measurement (MNCV)*

Sciatic motor NCV (MNVC) was carried out in Neigel A. Calcutt laboratory. MNCV studies were performed in STZ-diabetic (diabetes was induced by injecting streptozotocin 2 x 90 mg/kg on alternate days, i.p.) male C57 Bl/6J mice. In prevention study, treatment (guaifenesin or vehicle) began with onset of diabetes and continued for 4 weeks. Guaifenesin was delivered by oral gavage at three different doses (low (10 mg/Kg), medium (100 mg/Kg) and high (1000 mg/Kg)). Intervention study was carried on mice untreated for 4 weeks of diabetes. STZ-mice for intervention study were treated with guaifenesin by s.c. injection at two doses 1.0 and 10.0 mg/kg/day for 4 weeks.

MNCV was measured at 37 °C in isoflurane anesthetized mice using electrodes placed at the sciatic notch and Achilles tendon to deliver 5V for 0.05 ms single square wave stimuli and recording electrodes placed within the interosseus muscles of the ipsilateral paw, exactly described elsewhere.³⁹

3.3. 4 Thermal latency (*Thermal hypoalgesia*)

Hind paw thermal response latency experiments were carried out in Neigel A. Calcutt laboratory. Paw thermal response latency studies were performed in STZ-diabetic (diabetes was induced by injecting streptozotocin 2 x 90 mg/kg on alternate days, i.p.) male C57 Bl/6J mice. In prevention study, treatment (guaifenesin or vehicle) began with onset of diabetes and continued for 4 weeks. Guaifenesin was delivered by oral gavage at three different doses (low (10 mg/Kg), medium (100 mg/Kg) and high (1000 mg/Kg)). Intervention study was carried on mice untreated for 4 weeks of diabetes. STZ-mice for intervention study were treated with guaifenesin by s.c. injection at two doses 1.0 and 10.0 mg/kg/day for 4 weeks. Detailed procedure is described elsewhere.⁴⁰

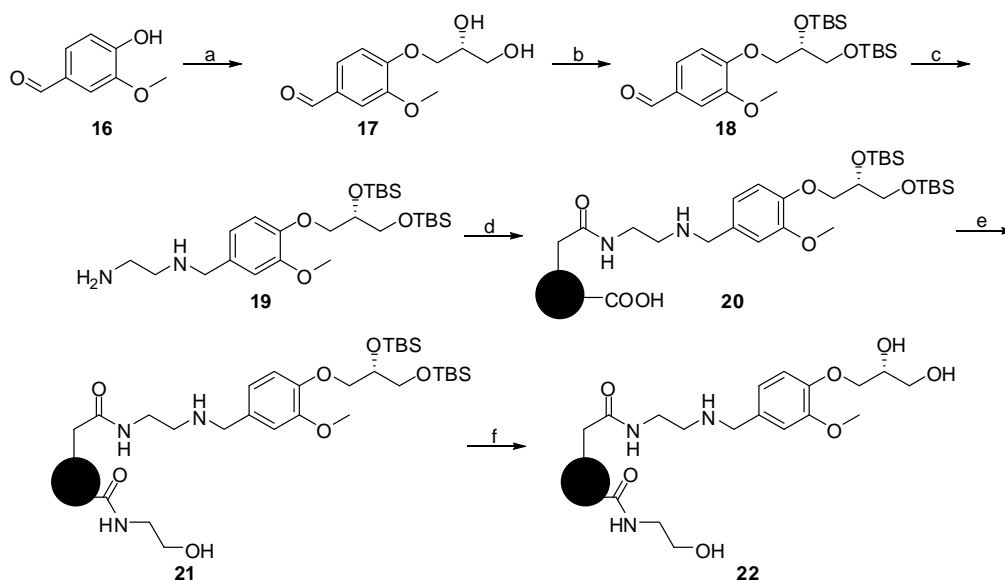
3.3. 5 Pharmacokinetics studies

Bioanalytical method for guaifenesin (**1**) (*R*)-guaifenesin (**9**) and was developed by Drumetix laboratories protocol.⁴¹ In brief, Internal standard solution: 50 µM (±)-3-(2-trifluoromethoxyphenoxy)-1,2-propanediol in water (IS response was variable and was not used in quantification). Working standard solution for either (*R*)-guaifenesin (**9**), (*R*)-guaifenesin toluyl ester (separate): 20, 50, 200, 500, 2000, 5000, 20000, 50000, 100000 nM in water. Mouse plasma was spiked with the drug working solution and the samples

were vortex mixed for 2 minutes, the analyte was further extracted from plasma with water immiscible organic solvent. The samples were then capped, vortex mixed for 2 minutes, centrifuged for 5 min at 3500 rpm and followed by freezing of the aqueous layer in dry ice-methanol bath. The organic layer was then transferred into 16x100 mm culture tubes and dried down under N₂ stream (10 psi) at room temperature for 30 minutes. The residue was then reconstituted with 100 μL 0.2% TFA in MeOH: Water (20:80) and transferred into 96-well plates for LC-MS/MS.

3.3. 6 Experimental section for target deconvolution

- Synthesis of (*R*)-guaiifenesin ligand with hydrophilic linker and immobilization of ligand on affinity resin



Scheme 3.4. Synthesis of ligand loaded resin **22**. Reagents and conditions: a. (*R*)-chloropropane-2,3-diol, NaOH, MW 210 °C, 10 min; b. TBDMSCl, DMAP, imidazole, anhydrous DCM, room temperature, overnight; c. Ethylene diamine, MgSO₄, NaBH₄; d. Toyopearl carboxy 650AF resin, EDAC, NHS, DCM, room temperature, 2 days; e. Ethanolamine, EDAC, NHS, DCM, room temperature, 2 days; f. 20% TFA in DCM, 15 min.

(*R*)-4-(2, 3-Dihydroxypropoxy)-3-methoxybenzaldehyde (17). To a stirred suspension of NaOH (158 mg, 3.94 mmol) in anhydrous DMF (2 mL), vanillin (500 mg, 3.28 mmol) and (*R*)-(-)- α -monochlorohydrine (545 mg, 4.92 mmol) were added and the reaction was carried out at 210 °C for 10 min in a microwave. The reaction mixture was then diluted with EtOAc (30 mL), washed with H₂O (15 mL), brine (15 mL), and dried (Na₂SO₄). Evaporation of the solvent and purification of the crude by column chromatography (10% EtOAc in Hexanes) yielded compound **17** (504.24 mg, 68%) as a white powder which was further recrystallized from EtOAc. ¹H NMR (CDCl₃) δ

3.77 - 3.87 (m, 2H), 3.92 (s, 3H), 4.09 - 4.30 (m, 3H), 6.99 (d, $J = 8.03$ Hz, 1H), 7.34 - 7.54 (m, 2H), 9.85 (s, 1H).

(S)-4-(2,3-Bis(*tert*-butyldimethylsilyloxy)propoxy)-3-

methoxybenzaldehyde (18). To a stirred suspension of compound **17** (909 mg, 4.01 mmol), dimethyl amino pyridine (1.07 g, 8.83 mmol), imidazole (820.6 mg, 12.05 mmol) in anhydrous DCM (5 mL), *tert*-butyl dimethylsilane chloride (1.3g, 8.83 mmol) was added at 0 °C. The reaction mixture was stirred overnight at room temperature. The reaction mixture was adsorbed on silica gel and purified by column chromatography (5% EtOAc-Hexanes) to yield yellow oil **18** (1.4 g, 78%). ^1H NMR (CDCl_3) δ 0.03 - 0.12 (m, 12H), 0.84 - 0.92 (m, 18H), 3.59 - 3.70 (m, 2H), 3.89 (s, 3H), 4.00 (dd, $J = 9.79, 7.03$ Hz, 1H), 4.09 - 4.17 (m, 1H), 4.25 (dd, $J = 9.79, 3.51$ Hz, 1H) 7.00 (d, $J = 8.03$ Hz, 1H) 7.37 - 7.45 (m, 2H), 9.84 (s, 1H).

(S)- N^1 -(4-(2,3-Bis(*tert*-butyldimethylsilyloxy)propoxy)-3-

methoxybenzyl)ethane-1,2-diamine (19). To a round bottom flask containing ethylene diamine (593.7 mg, 9.89 mmol) and MgSO_4 (1.41 g, 11.82 mmol) in anhydrous methanol (10 mL), compound **18** (900 mg, 1.97 mmol) dissolved in methanol was added dropwise at 0 °C. After stirring at room temperature for 2h a small aliquot of reaction mixture was used to record ^1H NMR to confirm imine formation. (Imine formation, crude NMR) ^1H NMR (CDCl_3) δ 0.06 - 0.12 (m, 12H), 0.88 (d, $J = 7.03$ Hz, 18H), 3.64 (br, s, 2H), 3.87 (s, 3H), 3.89 - 3.98 (m, 1H), 4.07 - 4.21 (m, 2H), 6.87 (d, $J = 8.03$ Hz, 1H), 7.07 (d, $J = 8.03$ Hz, 1H), 7.37 (s, 1H), 8.19 (s, 1H). The reaction mixture was cooled to 0 °C and NaBH_4 (74.5 mg, 1.97 mmol) was added in fractions. On complete addition of NaBH_4 the reaction mixture warmed to room temperature and

stirred for additional 1h. The reaction crude was purified by column chromatography (1-10% MeOH in DCM) to obtain product **19** (785.36 mg, 80%) as oil. $^1\text{H NMR}$ (CDCl_3) δ 0.03 - 0.11 (m, 12H), 0.88 (d, $J = 4.02$ Hz, 18H), 2.69 - 2.74 (m, 2H), 2.82 - 2.87 (m, 2H), 3.63 - 3.66 (m, 2H), 3.74 (s, 2H), 3.83 (s, 3H), 3.86 - 3.92 (m, 1H), 4.05 - 4.12 (m, 2H), 6.81 (d, $J = 1.76$ Hz, 1H), 6.83 (s, 1H), 6.89 (d, $J = 1.51$ Hz, 1H).

- Resin loaded (R)-guaifenesin (22).

Drying of resin-A 3mL of Toyopearl carboxy AF 650 resin (suspended in 20% v/v ethanol in water) was transferred to Watman filter paper and washed sequentially with water (3mL), ethanol (3mL), methanol (4 mL) and DCM (6 mL). Air dried resin was then transferred to a pre-weighed 20mL Biotage microwave vial, capped and dried over vacuum (through 27 gauge needle).

Loading of ligand -Vacuum dried Toyopearl carboxy 650 AF resin (308.3 mg, 0.15 mmol), EDAC (88.56 mg, 0.46 mmol) and NHS (53.17 mg, 0.46 mmol) were suspended in anhydrous DCM (6 mL). The reaction vial was shaken on bench shaker for 1h at 26-30 rpm at room temperature. Solution of compound **19** (246 mg, 0.49 mmol) in DCM (1 mL) was added to it and subjected to shaking for 48h. The reaction suspension was carefully filtered under gravity. The resin beads were washed thoroughly with organic solvents in sequence of DCM (3mL), methanol (3ml), water (3mL), methanol (6mL) and DCM (6mL). Air dried resin was then transferred to a pre-weighed vial and dried over vacuum to yield resin **20** (357.8 mg).

Capping of resin-Vacuum dried resin **20** (354.8 mg), EDAC (34 mg, 0.18 mmol) and NHS (20.5 mg, 0.18 mmol) were suspended in anhydrous DCM (6 mL). The reaction vial was subjected to shaking on bench-top shaker for 1h at

26-30 rpm at room temperature. Ethanolamine (11 mg, 0.18 mmol) was added to it and shaken for 48h. The reaction suspension was filtered and the resin was washed carefully with organic solvents in order of DCM (3mL), methanol (3ml), water (3mL), methanol (6mL) and DCM (6mL). Air dried resin was then transferred to a pre-weighed vial and dried over vacuum to obtain resin **21** (359.4 mg).

Removal of protecting groups-To a suspension of resin **21** (357 mg) in anhydrous DCM (4 mL), 20% v/v TFA in DCM (0.5mL) was added at 0°C. The reaction mixture was shaken at room temperature for 1h. The reaction suspension was filtered and the resin beads were washed cautiously with series of organic solvents DCM (3 mL), methanol (3 mL), water (3 mL), methanol (6 mL) and DCM (6 mL). Air dried resin was then transferred carefully to a pre-weighed vial and dried over vacuum to obtain desired resin **22**(332 mg).

- Isolation and identification of (R)-guaiifenesin binding neuronal proteins

Isolation of (R)-guaiifenesin binding neuronal proteins-Cell lysis, affinity chromatography and gel electrophoresis - Cell lysate of cultured adult sensory rat neurons was supplied by Dr. Fernyhough Paul laboratory. The protein content of the neuronal cell lysate determined by Bradford assay was 7 mg/mL. Stock solutions required for preparation of lysis buffers are described in Table 3.2. Lysis buffer-1 was prepared as per recipe described in Table 3.3. Final lysis buffer used for the target deconvolution experiments was freshly prepared as described in Table 3.4. To an eppendorf tube containing 15 mg of resin **22** and 50 μ L of final lysis buffer, 200 μ L of rat neuronal cell lysate was added and shaken at 4 °C for 4h. It was then centrifuged at 12000 rpm for 2 min. The resulting supernatant was pipette out and mixed with another 15 mg of resin **22** suspended in 50 μ L of lysis buffer for 4h at 4 °C. The above cycle of protein extraction was repeated thrice (Figure 3.2). The resulting resin with netted proteins was then gently washed three times with 250 μ L of lysis buffer, resuspended in 20 μ L of SDS sample buffer (Table 3.5), shaken at room temperature for 15 min, and then centrifuged at 12000 rpm for 1min. The supernatant was carefully pipetted out and subjected to SDS-polyacrylamide gel electrophoresis (PAGE) (Bio-Rad). The resulting protein bands were detected by silver staining using commercially available silver staining kit (Sigma-Aldrich). Similar procedure was reported with (a) neat Toyopearl AF carboxy 650M resin and (b) ethanolamine immobilized resin as positive controls.

Identification of (R)-guaifenesin binding neuronal proteins-LC/MS/MS, database search and human orthologs - After detailed comparison of protein bands present in the lanes of cell lysate, controls and treatments, individual bands of interest were manually excised and suspended in 200 μ L of lysis buffer. These protein bands were then submitted for LC/MS/MS analysis. Protein identification was completed by searching the peptide mass and the corresponding MS/MS fragmentation information from each sample against the database of rat. Human orthologs of rat neuronal proteins were searched through BLAST (DAVID).⁴²

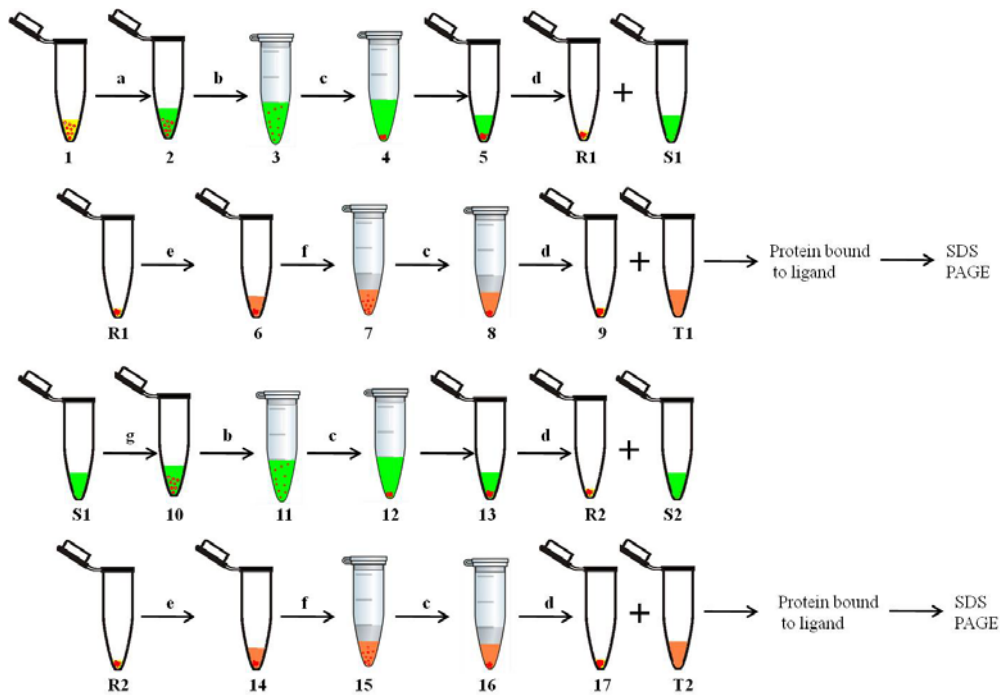


Figure 3.2: Schematic presentation of procedure to isolate the molecular proteins binding to ligand immobilised on the solid matrix. Step a. Addition of cell lysate to suspension of resin loaded ligand in buffer, step b. Incubation of the cell lysate with ligand in buffer, step b. Incubation of the cell lysate with ligand immobilised on resin at 4 °C, 4h, step c. Centrifugation 12000 rpm, 2 min, step d. Removal of the supernatant (S1) followed by gentle and thorough washing of the residual resin (R1), step e. Addition of surfactant (20 μ l), step f. Incubation of the surfactant solution with ligand immobilised resin (R1), rt, 15 min. Repetition of step c and d to isolate the proteins fished by the ligand immobilised on the solid matrix.

Table 3.2: Stock solutions preparation.

Ingredients	M.Wt	Wt (mg)	Volume (mL)	Solvent	Molarities
MgCl ₂ .6H ₂ O	203.31	508.27	5	water	0.5 M
EDTA	372.24	930.6	10	water	0.25 M
PMSF	174.19	850.95	5	dry DMSO	1 M
Na ₃ VO ₄	183.91	91.95	5	water	0.1M

Table 3.3: Lysis buffer-1 recipe.

Ingredients	Wt (mg) or Volume (mL)	Resultant M/mM/%
PIPES Na	3.35 g	0.01 M (10 mM)
0.5M MgCl ₂ (hexahydrate)	2 ml	5 mM
0.25M EDTA	2 ml	5 mM
Triton X-100	0.5 ml	0.5%
Glycerol	20 ml	20%
Sodium Fluoride	0.042 g	10 mM
Distilled Water	76.5 ml	
Total Volume	100 ml	

Table 3.4: Final lysis buffer recipe.

Ingredients	Volume	Resultant mM
1M PMSF	10 µl	1 mM
0.1M Sodium orthovanadate	200 µl	2 mM
Tablet protease inhibitor cocktail	1 tablet	
Total volume of lysis buffer-1	10 ml	

Table 3.5: SDS buffer recipe.

Ingredients	Amount taken	Final Conc.
1 M Tris HCl pH 6.8	2.4 ml	240 mM
SDS	0.8 g	8 %
Water	10 ml	

3.4 Chemistry discussion

Based on the structure of guaifenesin (**1**), phenoxy propane diol derivatives including the enantiomers of guaifenesin were synthesized. First, *o*-methoxy group in guaifenesin was replaced with a methyl and ethyl moieties (**6** and **7**, respectively) (Scheme 3.1). The ethereal oxygen in **1** was replaced by nitrogen leading to compound **8**. Compounds **6** and **7** were synthesized by Dr. Chandrasekhar Vanampally and compound **8** was prepared by Dr. Mallinath Hadimani. Two enantiomers of guaifenesin, (*R*)-guaifenesin (**9**) and (*S*)-guaifenesin (**10**) were synthesized to understand the effect of the chirality on the corresponding biological activity (Scheme 3.2). Two ester derivatives **11** and **12** and a fluorinated derivative **15** were synthesized (Scheme 3.2). These modifications reflect subtle changes to the structure of guaifenesin (**1**), to understand the changes to the resulting neuroaxonal growth.

Compounds **1** and **6-8** were synthesized by the addition of racemic chloropropane diol to *ortho*-substituted phenol derivatives **2-5** under alkaline conditions (Scheme 3.1). This reaction was carried out efficiently employing microwave irradiation at 210 °C for 15 min. The (*R*)- and (*S*)-enantiomers of guaifenesin, (**9**) and (**10**), respectively, were synthesized by coupling *o*-methoxyphenol to the appropriate (*R*)- or (*S*)-chloropropane-2,3-diol using conditions similar to that for the racemate synthesis (Scheme 3.2). Two ester prodrugs to the (*R*)-enantiomer **9** were synthesized to evaluate the pharmacokinetics effects of these molecules and bioavailability. Compounds **11** and **12** were synthesized by the esterification of the primary alcohol on compound **9** using propionyl chloride and *p*-toluyl sulfonyl chloride, respectively. The fluoro derivative of (*R*)-guaifenesin **15** was obtained via the

epoxide **14** using *tetra*-butyl ammonium fluoride (TBAF) (Scheme 3.3). All derivatives of guaifenesin were evaluated for the ability to enhance axonal growth. All synthesized compounds are studied in the in vitro and/or in vivo models for neuroaxonal growth.

Scheme 3.4 outlines the synthesis of (*R*)-guaifenesin loaded resin **22**. Coupling of vanillin (**16**) and (*R*) - chloropropane-2, 3-diol was carried out in the presence of NaOH under microwave irradiation to yield compound **17**. The vicinal 1,2-diols of the compound **17** were protected with *tert*-butyl dimethylsilyl (TBDMS) group to gain compound **18**. The imine intermediate formed on reaction of the reactive aldehyde **18** with ethylene diamine was reduced in-situ with sodium borohydride (NaBH₄) giving compound **19**. Imine reaction for compound **19** was successfully accomplished in methanol as solvent in the presence of magnesium sulfate (MgSO₄). Imine dimer formation in the reaction of compound **19** was avoided by adding compound **18** dropwise over excess of ethylene diamine.

Toyopearl carboxy AF 650 M resin beads are supplied in 20%v/v ethanol in water. 1mL wet volume of resin was approximately equivalent to 200 mg of dry resin. As per MSDS supplied with resin, 1mL of Toyopearl carboxy AF 650 M resin contains 100 μmoles of carboxy functional groups. Therefore, every 200 mg of dry resin would approximately correspond to 0.1 mmol of carboxy group was considered for calculation. Amine **19** was coupled to carboxy resin with EDAC and NHS in anhydrous DCM as solvent. The reaction was shaken instead of stirring with stir bar because stirring would cause attrition of beads. After the loading reaction the resin **20** was washed and dried. The weight of resin **20** (W₂) after loading of compound **19** was

noted and subtracted from the initial weight of resin (W1) used for the coupling. The increase in weight was then divided by the molecular weight of compound **19** (loss of water was compensated) to calculate the mmol of immobilized compound **19**. Percent loading of compound **19** was calculated by dividing mmol of immobilized **19** by initial mmol of carboxy groups on resin (M) used for the reaction (Equation 3.1). Approximately, 67% of the carboxy groups of resin **20** were coupled to compound **19** as per scheme 4. Unreacted carboxy groups of resin **20** were blocked with ethanolamine and the protecting groups were removed by 20% TFA in DCM to yield final resin **22**.

Equation 3.1: Equation to calculate percent loading of ligand 19

$$\% \text{ loading} = \left[\frac{W2 - W1}{\text{Mwt of ligand} - 18} + M \right] \times 100$$

Resin reactions in scheme 4 were monitored by infrared spectrometry (IR) (Figure 3.3). IR spectrum of neat Toyopearl carboxy AF 650M (Figure 3.3A) shows characteristic carboxylic acid OH stretch at 3406.54cm^{-1} and carbonyl at 1723.22 cm^{-1} . In the IR spectrum of ligand **19** (Figure 3.3B) aromatic symmetric and methyl CH stretches at $2929.36\text{-}2856.19\text{ cm}^{-1}$ and Si-O stretch at 831.63 cm^{-1} were selected to monitor the reactions. In the IR spectrum of resin **20** (Figure 3.3C), Si-O stretch at 839.37 cm^{-1} was observed. Subtraction of neat Toyopearl carboxy AF 650 IR spectra (Figure 3.3A) from resin **20** IR spectra (Figure 3.3C) furnished spectra Figure 3D, exhibiting the characteristic CH and Si-O stretches of ligand **19**. IR spectra of resin **21** (Figure 3.3E) acquired after capping with ethanolamine and the subtracted spectra of **21**(Figure 3.3F) obtained after subtraction with neat resin (Figure 3.3A) presented the OH, CH and Si-O stretches. On removal of the protective groups of vicinal diols the Si-O stretch around 839 cm^{-1} vanished from the

spectrum of resin **22** (Figure 3.3G) and the subtracted spectrum of resin **22** (Figure 3.3H) obtained after subtraction from neat Toyop pearl carboxy AF 650.

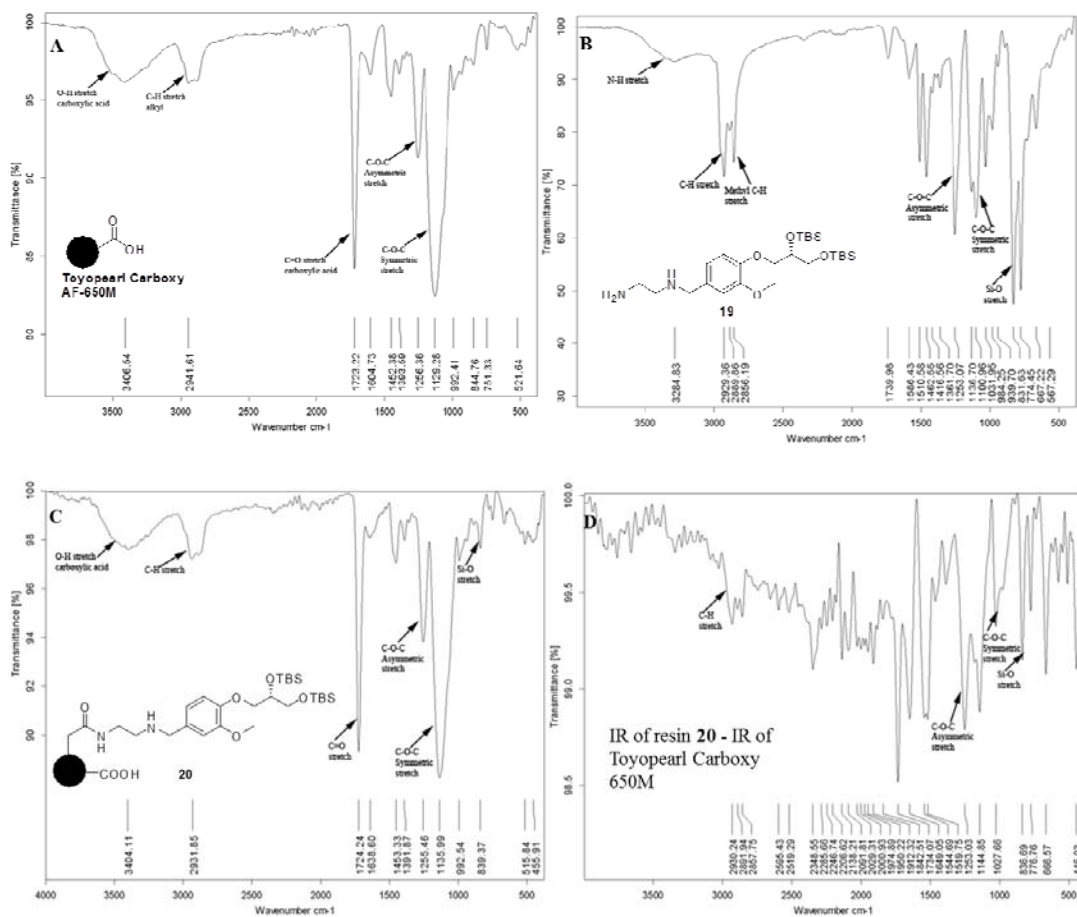


Figure 3.3: (A) IR spectra of Neat affinity resin-Toyopearl Carboxy AF 650M, (B) IR spectra of ligand **19**, (C) IR spectra of resin **20** after loading of ligand **19**, (D) IR spectra obtained after subtraction of resin **20** spectra from spectrum A

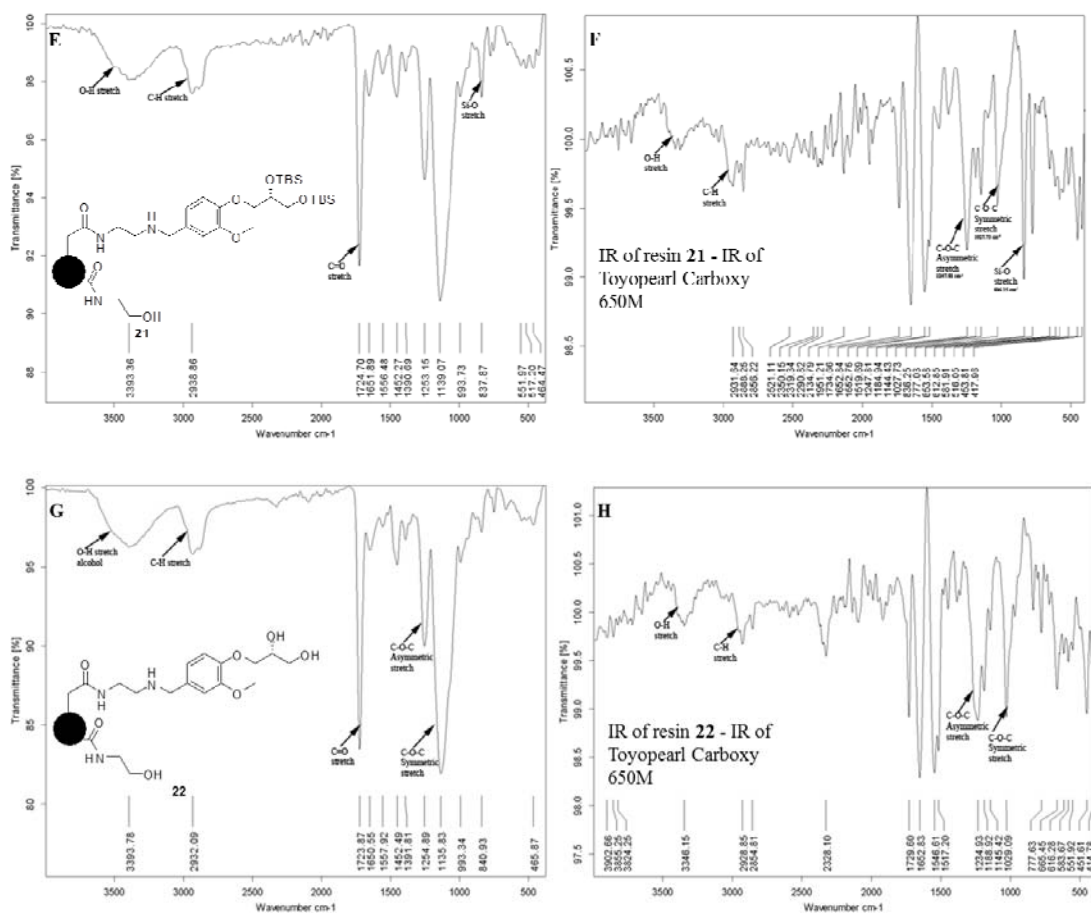


Figure 3.4: (E) IR spectra of resin **21** after capping with ethanolamine, (F) IR spectra acquired after subtraction of resin **21** spectra from spectrum A, (G) IR spectra of resin **22** after removal of protective groups of vicinal 1,2-diols and (H) IR spectra obtained after subtraction of resin **22** spectra from spectrum A.

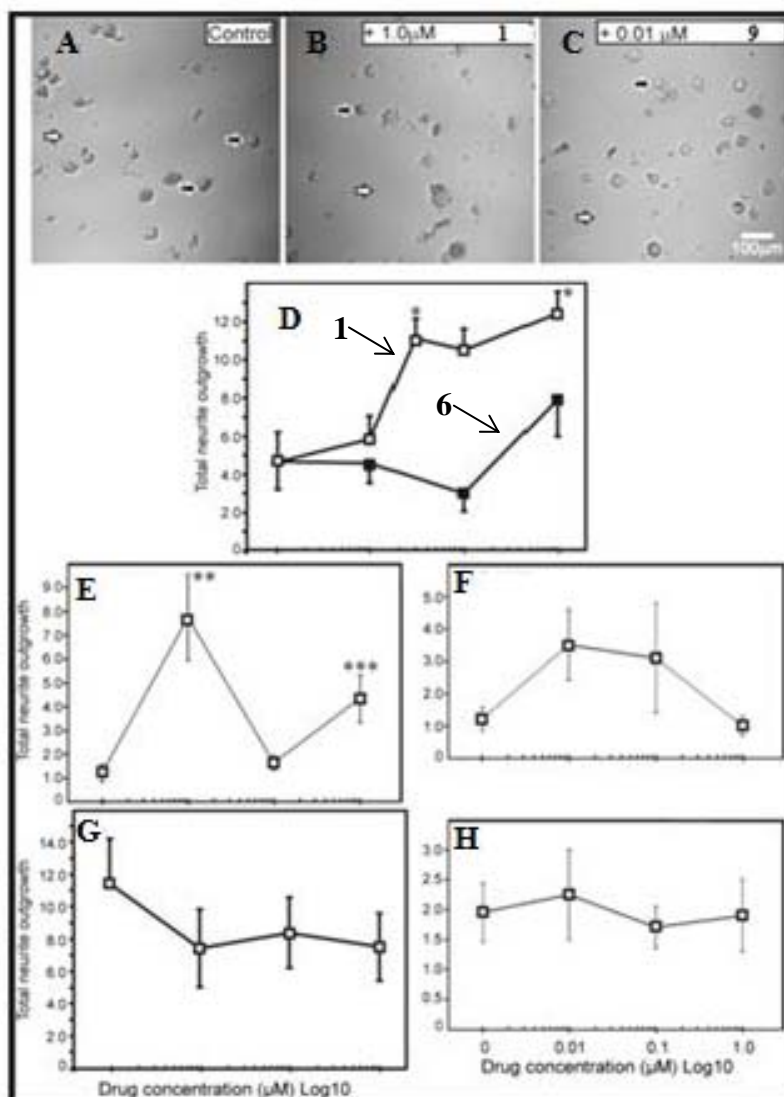


Figure 3.5: Rat sensory neuron cultures from the DRG of adult normal rats were grown for 1 day in the presence of a cocktail of growth factors, with 10 mM D-glucose and were exposed to a range of concentrations of compounds. Total neurite outgrowth was assessed by counting the neurite intersects with a Weibel grid. All data adjusted to number of cells (presented as number of intersects per cell). Values are means \pm SEM ($n = 6$ replicate cultures). * $P < 0.05$ vs control (oneway ANOVA with Tukeys); ** $P < 0.02$ vs control and 0.1 μ M (oneway ANOVA with Tukeys) and *** $P < 0.02$ vs control. Panel A is an image of 24h culture of adult rat STZ-diabetic sensory neurons. Panel B and C are images of 24h adult rat STZ diabetic sensory neurons incubated with compound **1** (1.0 μ M) and compound **9** (0.01 μ M) respectively. The graphs showing total axonal regeneration and outgrowth from adult rat STZ diabetic sensory neurons stimulated by compounds **1** and **6** are presented in Panel D, whereas compounds **9**, **10**, **7**, and **8** are presented in Panel E, F, G and H respectively. White arrows show swellings or dystrophic regions on axon and black arrow non-neurons.

3.5 Result, discussion and conclusion

In vitro evaluation of axon regeneration: The effect of each compound on enhancing the axonal growth in comparison to no drug treatment was assessed using adult rat sensory neurons as per the established procedure in our laboratories.^{26,27} Dose-response curves when the sensory neurons were treated with compounds **1**, **6** to **10**, are presented in Figure 3.4. Guaifenesin (**1**) has been known as an expectorant and is a common active ingredient in cough medicines. Identification of this drug as a potential candidate for neuroaxonal regeneration using adult rat sensory neuronal assay was intriguing and we undertook further experiments to investigate the structural features responsible for this activity. Guaifenesin racemate (**1**) exhibits neurite growth at higher than 10 nM concentration in vitro (Figure 3.4D). In vitro cell cultures clearly show the sprouting of the axons after the treatment with the compound at 1 μ M concentration (Figure 3.4B). As part of the structure-activity relationship, we undertook minor changes to the structure of guaifenesin on its propyl side chain as well as the ortho substitution, and these changes were introduced onto the guaifenesin racemate. *O*-Methyl and *O*-ethyl substitutions on the phenyl ring gave rise to compounds **6** and **7**. Substitution of the methoxy with the methyl group (**1** and **6**, respectively) compromised the activity at least by two orders of magnitude (Figure 3.4D). An ethyl substitution in place of methoxy (compound **1** vs **7**, Figures 3.4D and 3.4G) completely abrogated the activity. Thus, methyl ether at ortho position appears to be an essential group on guaifenesin.

Then changes to the propyl ether side chain were introduced. A

substitution of the ethereal oxygen of the propyl side chain with an amino moiety gave compound **8**. At physiological pH, including the pH used for the in vitro assays, this molecule would be protonated due to the secondary amine. Compound **8** was inactive at upto 1 mM concentration in the cell culture, confirming the importance of ethereal link to the propyl side chain.

Guaifenesin (**1**) was a racemate and it was of interest to explore if there is any role for the stereo center on the guaifenesin side chain. Thus enantiomerically pure *R*- and *S*-guaifenesin (**9** and **10**, respectively) were synthesized from chiral precursors (Scheme 3.2). Compound **9**, an (*R*)-enantiomer of **1**, exhibited very high efficacy at 0.01 μ M which was quite potent and unlike any other compound known to date affecting the axonal outgrowth. Compound **10**, the (*S*)-enantiomer of guaifenesin was found to be less efficacious in vitro when compared to the racemate and the corresponding (*R*)-enantiomer **9** (Figure 3.4F vs 3.4G); confirming that the chiral center has influence on the neurite outgrowth. The general trend of the dose-response curves (Figures 3.4E vs 3.4F) indicate that there is at least a two-fold difference in the activities of (*R*)- and (*S*)-guaifenesin, preferring the *R*-enantiomer. It was thus obvious from the dose-response curves that 1, 2-diol side chain with ether linkage and methoxy group on benzene ring are essential for the activity. Fluorinated analog **15** failed to stimulate axonal neurite outgrowth in sensory neurons in-vitro assay.

In-vivo evaluation of axon regeneration: Diabetic neuropathy leads to thermal hyperalgesia which then progresses to thermal hypoalgesia. Slowing of motor nerve conduction velocity (MNCV) is a characteristic feature of diabetic neuropathy.⁴³ Axonal degeneration, structural abnormality in diabetic neuropathy is one of the culprits for thermal latency and slowing of nerve conduction velocity. The guaifenesin racemate (**1**) was studied in-vivo in STZ-diabetic mice to see whether it can prevent the induction of diabetes induced slowing of MNCV and thermal latency. In-order to study the functionality of the regenerated neurons in-vivo, intervention and prevention studies of compound **1** was conducted. In a prevention study, compound **1** treatment was initiated with the onset of diabetes in mice and continued for 4 weeks. Whereas in the intervention study after 4 weeks of untreated diabetes, guaifenesin (**1**) treatment was started and continued for another 4 weeks. In prevention study, diabetes caused significant ($p < 0.05$ vs control) MNCV slowing that was attenuated only by the lowest dose of guaifenesin (**1**) (Figure 3.5A). There was no clear diabetes induced change in thermal latency (Figure 3.5B). Even successive treatments of guaifenesin (**1**) during intervention, study did not reverse statistically induced MNCV slowing and thermal hypoalgesia in STZ diabetic mice (Figure 3.5C and D).

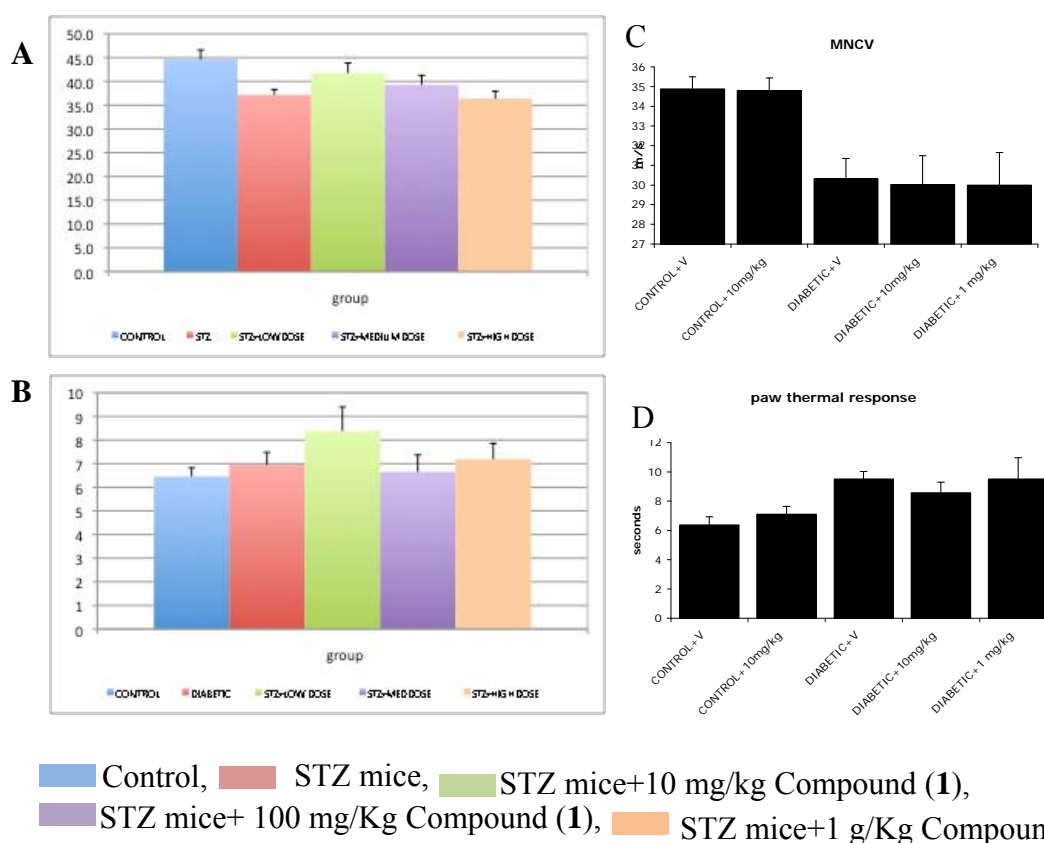


Figure 3.6. Prevention study of guaifenesin (**1**) investigating its effect on diabetes induced MNCV slowing (**A**) and thermal latency (**B**) in STZ-diabetic mice. Intervention study of guaifenesin (**1**) investigating its effect on diabetes induced MNCV slowing (**C**) and thermal latency (**D**) in STZ-diabetic mice.

Since the mode of action of racemate guaifenesin (**1**) on peripheral nerves is not known the only reason for the unexpected in-vivo results of guaifenesin may be due to its poor pharmacokinetic properties. (*R*)-guaifenesin (**9**) showed marginal efficacy in preventing MNCV slowing after 4 weeks of diabetes that was maintained to 8 weeks (Figure 3.6). To improve the pharmacokinetic properties and potency of compound **9**, fluorinated derivative **15** was synthesized but it had no in-vitro activity.

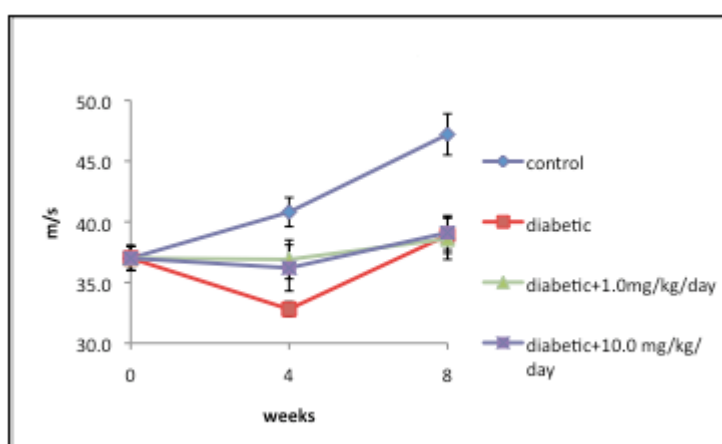


Figure 3.7. Effect of (*R*)-guaifenesin (**9**) on diabetes induced MNCV slowing in STZ-diabetic mice. MNCV was measured at weekly intervals. Data are group mean \pm SEM.

Pharmacokinetics study: Guaifenesin racemate (**1**) at a dose of 10 mg/kg failed to show any effect on well-established slowing on MNCV and thermal latency in STZ mice (Figure 3.6). Therefore it was worth studying the oral bioavailability of compound **1** in both diabetic and control mice. Pharmacokinetics of guaifenesin (**1**) in rats is well reported in literature.⁴⁴ Pharmacokinetic profiles of compound **1** in diabetic and control mice were almost same (Table 3.6) but compound (**1**) appeared to have slightly shorter half-life in diabetic mice.

Table 3.6: Pharmacokinetic parameters of racemate guaifenesin (**1**) and (*R*)-guaifenesin (**9**) in control and STZ- diabetic mice.

Parameters	1		9	
	Control	STZ-diabetic mice	Control	STZ-diabetic mice
Dose (mg/Kg PO)	10	10	10	10
T _{max} (mins)	4.98	4.98	10.02	10.02
C _{max} (nM)	5283	5267	440	741
AUC _{0-t} (hr * nM)	2725	1911	737	746

In vitro studies of (*R*)-enantiomer of guaifenesin (**9**) showed that it was more efficacious than the corresponding racemate **1**. Hence determining the oral bioavailability of (*R*)-guaifenesin in diabetic and control mice before its in-vivo study would be valuable. But the peak plasma concentration of compound **9** in both control and diabetic mice was 7 to 12 times lesser than that of the racemate **1**. Due to the poor pharmacokinetics of guaifenesin (*R*)-enantiomer **9** its ester prodrugs, toluyl **11** and *t*-butyl **12**, were synthesized. Ester prodrugs **11** and **12** of (*R*)-guaifenesin (**9**) were not as efficacious as compound **9** in the in-vitro axonal outgrowth cell based assay.

Target deconvolution: In drug discovery one of the most challenging aspects is to identify the molecular protein targeted by the chemical entities. The discovery of (R)-guaifenesin (**9**) stimulating axonal regeneration in diabetic neuropathy was very exciting but there was no clue about its molecular target. Therefore, an endeavour was made to deconvolute the druggable proteins corresponding to (R)-guaifenesin (**9**). (R)-guaifenesin derivative **19** with a five atom linker ortho to methoxy group was synthesized and immobilized on the affinity matrix (Toyopearl carboxy AF 650 M) to obtain resin **22**. Serial affinity chromatography as described in Figure 3.2 was used to capture the proteins binding to the immobilised ligand (**19**). Ethanolamine immobilised on the resin (Toyopearl carboxy AF 650 M) was used as a control. In the SDS-PAGE gel (Figure 3.8), lane 1, 2 and 3 corresponds to the molecular weight ladder, proteins captured by control and proteins binding to resin **22** after first treatment (or extraction) (T1) respectively. In all 11 bands were excised and submitted for mass analysis. Out of 11 bands 4 were from control lane and rest of 7 bands were from T1. Total proteins identified from 11 bands were 670. Both control and treated lanes contained keratin. Total numbers of keratin detected were 169. Total number of proteins detected in lanes of control (11, 10, 9 and 8 bands) and T1 (1 to 7) were 213 and 457 respectively. In T1 lane 3, overall proteins remained after excluding control, keratin and repeat proteins was 176 (Appendix). The 176 peptides identified in T1 comprised of proteins ranging from membrane to nuclear proteins. Hence, it was extremely difficult to nail down one target protein for compound **9**. The affinity chromatography experiment to deconvolute the (R)-guaifenesin (**9**) target was

not very conclusive. From this study it could be concluded that the (*R*)-guaifenesin (**9**) binds to several neuronal proteins with low affinity.

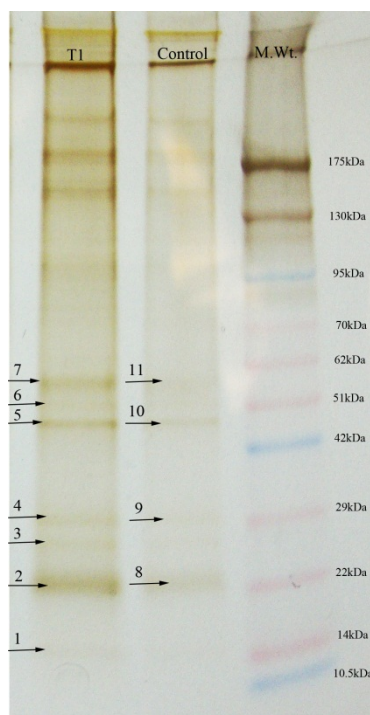


Figure 3.8: SDS PAGE for protein isolated by serial affinity chromatography. Lane T1 shows protein captured by resin **22**, lane of control shows protein captured by control resin and lane of MWt shows molecular weight ladder.

In summary, the (*R*)-enantiomer of guaifenesin (**9**) was the most efficacious molecule among the phenoxy propanediol derivatives to induce axonal outgrowth at the concentration of $0.01\mu\text{M}$. Lack of correlation between the in-vitro axonal enhancements activities of (*R*)-guaifenesin with the functionality of regenerated/outgrown neuron in-vivo could be due to the poor pharmacokinetics of (*R*)-guaifenesin (**9**). Additional chemical proteomics experiments should be conducted to deconvolute the target of (*R*)-guaifenesin (**9**).

3.6 References

- (1) Screening for Type 2 Diabetics. Report of a World Health Organization and International Diabetes Federation Meeting, 2003, World Health Organization, Geneva.
- (2) Centres for Disease Control and Prevention. National Data fact sheet: general information and national estimates on diabetes in the United States 2011. Atlanta, GA: US. Department of Health and Human Services, Centres for Disease Control and Prevention, **2011**. <http://www.cdc.gov/diabetes/pubs/references11.htm>. Date 7th June **2012**.
- (3) Sima, A. A. F.; Kamiya, H. Diabetic neuropathy differs in type I and type II diabetes. *Ann. N. Y. Acad. Sci.* **2006**, *1084*, 235-249.
- (4) Bohannon, N. J.; Zilbergeld, B.; Bullard DG; Stoklosa; J. M. Treatable impotence in diabetic patients. *West J Med.* **1982**, *136*, 6-10.
- (5) Tomlinson, D. R.; Gardiner, N. J. Glucose neurotoxicity. *Nat. Rev. Neurosci.* **2008**, *9*, 36-45.
- (6) Sima, A. A. F.; Sugimoto, K. Experimental diabetic neuropathy: updates. *Diabetologia* **1999**, *42*, 773-788.
- (7) Greene, D. A.; Sima, A. A. F. Diabetic neuropathy. *Annu. Rev. Med.* **1990**, *41*, 303-317.
- (8) Brownlee, M. Biochemistry and molecular cell biology of diabetic complications. *Nature* **2001**, *414*, 813-820.
- (9) Yin, Q.; Kemp, G. J.; Frostick, S. P. Neurotrophins, neurones and

- peripheral nerve regeneration. *J. Hand. Surg. Br.* **1998**, *23*, 433-437.
- (10) Lee, P. G.; Hohman, T. C.; Cai, F.; Regalia, J.; Helke, C. J. Streptozotocin-induced diabetes causes metabolic changes and alterations in neurotrophin content and retrograde transport in the cervical vagus nerve. *Exp. Neurol.* **2001**, *170*, 149-161.
- (11) Miele, C.; Paturzo, F.; Teperino, R.; Sakane, F.; Fiory, F.; Oriente, F.; Ungaro, P.; Valentino, R.; Beguinot, F.; Formisano, P. Glucose regulates diacylglycerol intracellular levels and protein kinase C activity by modulating diacylglycerol kinase subcellular localization. *J. Biol. Chem.* **2007**, *282*, 31835-31843.
- (12) Zhrebetskaya, E.; Akude, E.; Smith, D. R.; Fernyhough, P. Development of axonopathy in adult sensory neurons isolated from diabetic rats: role of glucose induced oxidative stress. *Diabetes* **2009**, *58*, 1356-1364.
- (13) Fernyhough, P.; Willars, G. B.; Lindsay, R. M.; Tomlinson, D. R. Insulin and insulin-like growth factor I enhance regeneration in cultured adult rat sensory neurones. *Brain Res.* **1993**, *607*, 117-124
- (14) Gardiner, N. J.; Fernyhough, P.; Tomlinson, D. R.; Mayer, U.; von der Mark, H.; Streuli, C. H. Alpha7 integrin mediates neurite outgrowth of distinct populations of adult sensory neurons. *Mol. Cell Neurosci.* **2005**, *28*, 229-240
- (15) Huang, T. J.; Verkhatsky, A.; Fernyhough, P. Insulin enhances mitochondrial inner membrane potential and increases ATP levels through phosphoinositide 3-kinase in adult sensory neurons. *Mol. Cell Neurosci.* **2005**, *28*, 42-54.

- (16) Mohiuddin, L.; Fernyhough, P.; Tomlinson, D. R. Reduced levels of mRNA encoding endoskeletal and growth-associated proteins in sensory ganglia in experimental diabetes. *Diabetes* **1995**, *44*, 25-30.
- (17) Mohiuddin, L.; Fernyhough, P.; Tomlinson, D. R. Acidic fibroblast growth factor enhances neurite outgrowth and stimulates expression of GAP-43 and T alpha 1 alpha-tubulin in cultured neurones from adult rat dorsal root ganglia. *Neurosci. Lett.* **1996**, *215*, 111-114.
- (18) Huang, T. J.; Sayers, N. M.; Fernyhough, P.; Verkhratsky, A. Diabetes-induced alterations in calcium homeostasis in sensory neurons of streptozotocin-diabetic rats are restricted to lumbar ganglia and are prevented by neurotrophin-3. *Diabetologia* **2002**, *45*, 560-570. rats are restricted to lumbar ganglia and are prevented by neurotrophin-3. *Diabetologia*, **2002**, *45*, 560-570.
- (19) Huang, T. J.; Price, S. A.; Chilton, L.; Calcutt, N. A.; Tomlinson, D. R.; Verkhratsky, A.; Fernyhough, P. Insulin prevents depolarization of the mitochondrial inner membrane in sensory neurons of type 1 diabetic rats in the presence of sustained hyperglycemia. *Diabetes* **2003**, *52*, 2129-2136.
- (20) Purves, T.; Middlemas, A.; Agthong, S.; Jude, E. B.; Boulton, A. J.; Fernyhough, P.; Tomlinson, D. R. A role for mitogen-activated protein kinases in the etiology of diabetic neuropathy. *Faseb. J.* **2001**, *15*, 2508-2514.
- (21) Fernyhough, P.; Smith, D. R.; Schapansky, J.; Van Der Ploeg R., Gardiner N. J., Tweed C. W., Kontos A., Freeman L., Purves-Tyson T. D. and Glazner G. W. Activation of nuclear factor-kappaB via

- endogenous tumor necrosis factor alpha regulates survival of axotomized adult sensory neurons. *Neurosci.* **2005**, *25*, 1682-1690.
- (22) Smith, D. S.; and Skene, J. H..A transcription-dependent switch controls competence of adult neurons for distinct modes of axon growth. *J Neurosci* , **1997**, *17*, 646-658.
- (23) Gavazzi, I.; Kumar, R. D.; McMahon, S. B.; Cohen, J. Growth responses of different subpopulations of adult sensory neurons to neurotrophic factors in vitro. *Eur. J. Neurosci.* **1999**,*11*, 3405-3414.
- (24) Navarro, X. Chapter 27. Neural plasticity after nerve injury and regeneration. *Int. Rev. Neurobiol.* **2009**, *87*, 483-505.
- (25) Bontioti, E.; Dahlin, L. B. Chapter 12: Mechanisms underlying the end-to-side nerve regeneration. *Int. Rev. Neurobiol.* **2009**, *87*, 251-268.
- (26) Paul Fernyhough, University of Manitoba, Canada. Axon regeneration from adult sensory neurons. US patent 2008/0255062 A1, October, 16, **2008**.
- (27) Holmes, M.; Maysinger, D.; Foerster, A.; Pertens, E.; Barlas, C.; Diamond, J. Neotrofin, a novel purine that induces NGF-dependent nociceptive nerve sprouting but not hyperalgesia in adult rat skin. *Mol. Cell. Neurosci.* **2003**, *24(3)*, 568-580.
- (28) Hudack, R. A. Jr; Barta, N.S; Guo, C.; Deal, J.; Dong, L.; Fay, L. K.; Caprathe, B.; Chatterjee, A.; Vanderpool, D.; Bigge, C.; Showalter, R.; Bender, S.; Augelli-Szafran, C. E.; Lunney, E.; Hou, X. Design, synthesis, and biological activity of novel polycyclic aza-amide FKBP12 ligands, *J. Med. Chem.* **2006**, *49*, 1202-1206.

-
- (29) Wu, X.; Wan, Y.; Mahalingam, A. K.; Murugaiah, A. M.; Plouffe, B.; Botros, M.; Karlén, A.; Hallberg, M.; Gallo-Payet, N.; Alterman, M. Selective angiotensin II AT2 receptor agonists: arylbenzylimidazole structure-activity relationships. *J. Med. Chem.* **2006**, *49*, 7160-7168.
- (30) Van Overmeire, I.; Boldin, S. A.; Dumont, F.; Van Calenbergh, S.; Slegers, G.; De Keukeleire, D.; Futerman, A. H.; Herdewijn, P. Effect of aromatic short-chain analogues of ceramide on axonal growth in hippocampal neurons. *J. Med. Chem.* **1999**, *42*, 2697-2705.
- (31) de Medina, P.; Paillasse, M. R.; Payré, B.; Silvente-Poirot, S.; Poirot, M. Synthesis of new alkylaminooxysterols with potent cell differentiating activities: identification of leads for the treatment of cancer and neurodegenerative diseases. *J. Med. Chem.* **2009**, *52*, 7765-7777.
- (32) Missner, E.; Bahr, I.; Badock, V.; Lücking, U.; Siemeister, G.; Donner, P. Off-target decoding of a multitarget kinase inhibitor by chemical proteomics. *Chembiochem.* **2009**, *10*(7), 1163-1174.
- (33) Bach, S.; Knockaert, M.; Reinhardt, J.; Lozach, O.; Schmitt, S.; Baratte, B.; Koken, M.; Coburn, S. P.; Tang, L.; Jiang, T.; Liang, D. C.; Galons, H.; Dierick, J. F.; Pinna, L. A.; Meggio, F.; Totzke, F.; Schächtele, C.; Lerman, A. S.; Carnero, A.; Wan, Y.; Gray, N.; Meijer, L. Roscovitine targets, protein kinases and pyridoxal kinase. *J. Biol. Chem.* **2005**, *280*(35), 31208-31219.

-
- (34) Terstappen, G. C.; Schlüpen, C.; Raggiaschi, R.; Gaviraghi, G. Target deconvolution strategies in drug discovery. *Nat. Rev. Drug Discov.* **2007**, *6*(11), 891-903.
- (35) Raida, M. Drug target deconvolution by chemical proteomics. *Curr. Opin. Chem. Biol.* **2011**, *15*(4), 570-575.
- (36) Wang, K.; Yang, T.; Wu, Q.; Zhao, X.; Nice, E. C.; Huang, C. Chemistry-based functional proteomics for drug target deconvolution. *Expert Rev. Proteomics.* **2012**, *9*(3), 293-310.
- (37) Inoue, K.; Hiratake, J.; Mizutani, M.; Takada, M.; Yamamoto, M.; Sakata, K. Beta-glycosylamidine as a ligand for affinity chromatography tailored to the glycon substrate specificity of beta-glycosidases. *Carbohydr. Res.* **2003**, *338*(14), 1477-1490.
- (38) Mori, T.; Kubo, T.; Kaya, K.; Hosoya, K. Importance of surface properties of affinity resin for capturing a target protein, cyclooxygenase-1. *Bioorg. Med. Chem.* **2009**, *17*(4), 1587-1589.
- (39) Mixcoatl-Zecuatl, T.; Jolival, C. G. A spinal mechanism of action for duloxetine in a rat model of painful diabetic neuropathy. *Br. J. Pharmacol.* **2011**, *164*(1), 159-169.
- (40) Calcutt, N. A.; Freshwater, J. D.; O'Brien, J. S. Protection of sensory function and antihyperalgesic properties of a prosaposin-derived peptide in diabetic rats. *Anesthesiology* **2000**, *93*, 1271-1278.

- (41) <http://www.drumetix.com/php/contact.php> Access Date 15th June **2012**.
- (42) <http://david.abcc.ncifcrf.gov/> Access Date: 12th March **2011**.
- (43) Brussee, V.; Guo, G., Dong Y.; Cheng, C., Martinez, J. A.; Smith, D.; Glazner, G. W.; Fernyhough, P.; Zochodne, D. W. Distal degenerative sensory neuropathy in long term type-2 diabetes rat model. *Diabetes* **2008**, *52*, 1664-1673.
- (44) Kagan, L.; Lavy, E.; Hoffman, A. Effect of guaifenesin pharmacokinetics and expectorant action in rat model. *Pulm. Pharmacol. Ther.* **2009**, *23*, 260-265.

Design and synthesis of novel
pyrazole derivatives inhibiting Fc γ
receptor mediated phagocytosis in
idiopathic-immune
thrombocytopenia (ITP)

4.1 Introduction and literature review

Thrombocytes, or platelets, are anucleate circulating blood cells involved in hemostasis. Normal platelet count for an adult is between 150,000 and 450,000 per μL of blood. A thrombocyte count less than 150,000 per μL of blood is defined as thrombocytopenia.¹ Degree of severity of the thrombocytopenia varies with the platelet counts (Table 4.1). Thrombocytopenia could be due to decreased platelet production (e.g. bone marrow failure), abnormal platelet distribution (splenomegaly), or increased platelet destruction or consumption.¹ Increased consumption or destruction of platelets in circulation as compared to their rate of production is a common pathophysiologic mechanism for thrombocytopenia. Decreased platelet count can result from either immune-mediated or non-immune-mediated destruction of thrombocytes.^{2, 3}

Table 4.1: Severity and clinical outcomes of thrombocytopenia^{1,4}

Severity	Platelet Counts (per μL)	Clinical outcome
Mild	> 50,000	Asymptomatic
Moderate	30,000-50,000	Longer bleeding time with major trauma
Severe	10,000-30,000	Bleeding with minor trauma
Life threatening	<10,000	Spontaneous, bleeding, petechiae and bruising. Risk of internal bleeding(mucosal, intracranial, gastrointestinal, and genitourinary bleeding)

Immunological destruction of platelets in response to unknown stimulus is known as “idiopathic thrombocytopenic purpura” or “primary immune thrombocytopenia” (ITP).⁵ This condition is caused by production of an autoantibody to autologous platelets. The antibodies are IgG against the platelet membrane glycoproteins, such as GP IIb/IIIa. These host antibodies then coats the platelet cells. The Fc receptors (FcRs) expressed on the macrophages recognize the opsonised platelets, engages with the Fc domains of the immunoglobulin and thereby clear them from circulation (Figure 4.1).

6,7

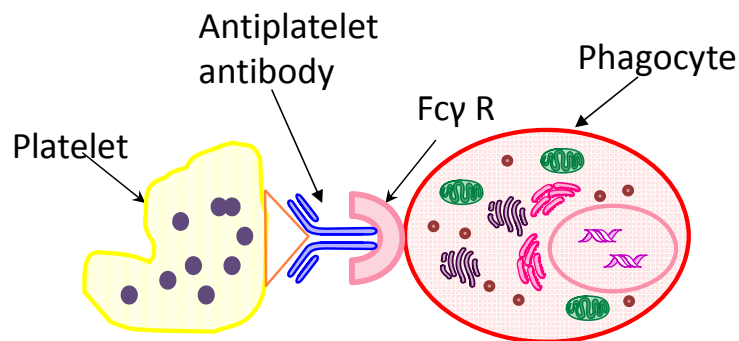


Figure 4.1: Fc γ mediated clearance of autoantibody sensitized platelets⁸

ITP can be treated either by reducing platelet destruction or by increasing platelet production. Current treatments for ITP include corticosteroids, rituximab (decreases anti-platelet autoantibody production), intravenous immunoglobulins (IVIg and anti-D) and splenectomy (surgical removal of spleen).⁹ Thrombopoietin (TPO) receptor agonists enhance platelet production by stimulating the TPO receptor expressed on pluripotent hematopoietic stem cells and in megakaryocytes.¹⁰

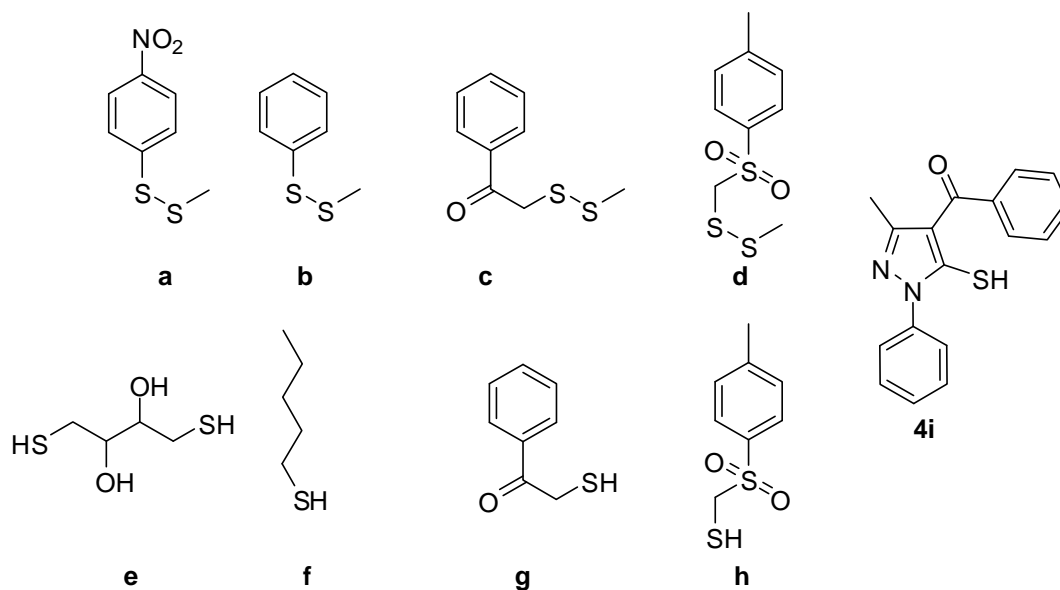
Based on the current American Society of Hematology guidelines, corticosteroids and IVIG and anti -D (in case of the Rh +ve patients) are the first line treatments for both children and adults. IVIG is produced from thousands of human plasma donors and, to date, no other source for this IgG therapeutic has been found, including cocktails of monoclonal antibodies. The recommended dose for IVIG is 0.8-1g/Kg and 1g/Kg for children and adults respectively. The base value for the IVIG is \$59.19 per gram¹¹; thus, therapy with IVIG is very expensive. Although a primary use of IVIG is for treatment of ITP, IVIG is also used in treatment of other autoimmune diseases and according to a report from Canadian Blood Services, the increase in average utilization of IVIG per year in Canada is 11.3%. Potential toxicities associated with immunosuppressants, increased chances of relapse on discontinuation of the TPO receptor agonists, limitations to an adequate IVIG supply and the possible exposure to blood borne infectious disease due to its human source requirement, limited options and especially the high cost of treatment for ITP has raised a need for new drug treatment.

Numerous possible mechanisms of action of IVIG and anti-D therapy have been proposed.^{12,13,14,15,16} Modulation or the competitive blockade of Fc γ receptor on macrophages is one of the most likely mechanisms of action for IVIG and anti-D therapy, but yet to be confirmed.¹⁷ Since the Fc γ receptor mediated phagocytosis of the opsonized platelets is the underlying pathogenesis of ITP, small molecules targeting Fc γ receptors expressed on mononuclear phagocytes could be an alternative treatment to ITP.

Several cell surface proteins of monocyte-macrophages expresses –SH and SS groups extracellular playing a crucial role in endocytic-phagocytic

function.^{18,19} Branch *et al*^{20,21} screened several small molecules having sulfhydryl and disulfide groups (Chart 4.1) which could interact with the –SH or SS groups on cell surface of human mononuclear phagocytes and inhibit the phagocytosis of antibody coated human RBC's with a classical and reliable in vitro monocyte monolayer assay (MMA) (Figure 4.2).^{22,23,24,25}

Chart 4.1: Preceding compounds inhibiting Fcγ receptor mediated phagocytosis of opsonized RBCs.^{20,21}



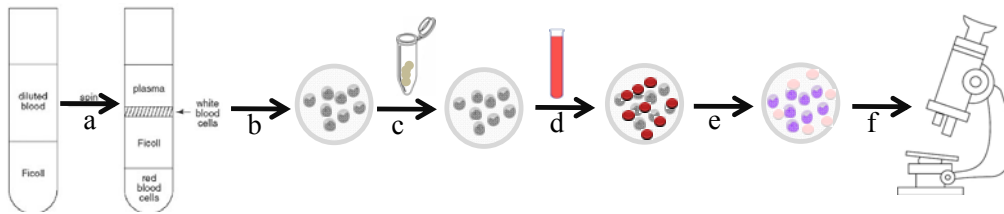
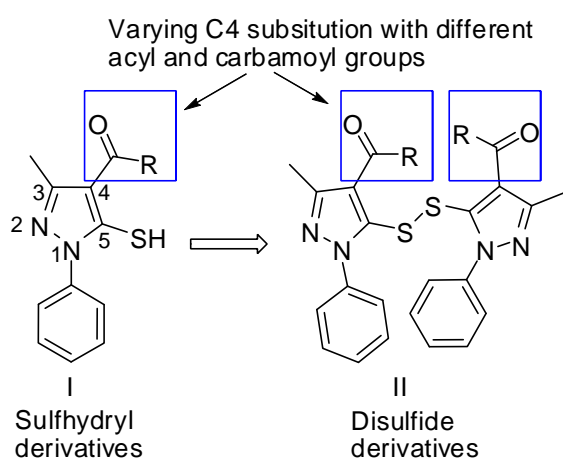
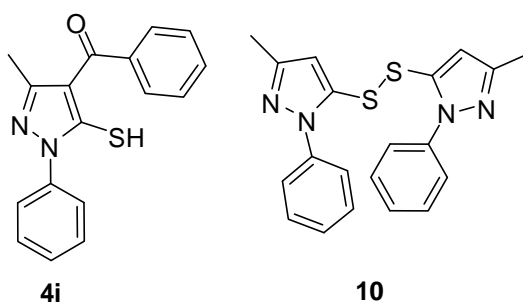
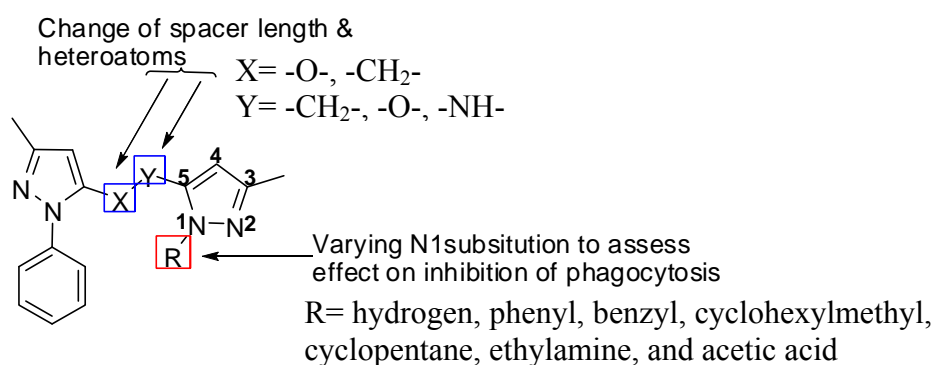


Figure 4.2: Monocyte monolayer assay (MMA) for screening drugs inhibiting phagocytosis. (MMA was carried out by Dr. Donald Branch laboratory²²) a. Isolation of peripheral blood mononuclear cells (PBMCs; containing monocytes) by density gradient centrifugation; b. After overnight incubation at 37°C, 5% CO₂, layering of PBMCs onto chamber slides followed by incubation at 37°C, 5% CO₂ for 1h; c. Incubation of the adhered monocytes with drug at 37°C, 5% CO₂ for 1h; d. Incubation of drug treated monocytes with anti-D opsonized RBCs at 37°C, 5% CO₂ for 2h; e. Fixing of slides and f. Read out of phagocytosis by microscopy with phase contrast.

4.2 Objective

In the present study, the synthesis, analysis and biological evaluation of a small set of sulfhydryl and disulfide compounds designed based on the lead candidate **4i** (Chart 4.2), as inhibitors of phagocytosis for potential use as therapeutics for ITP are described (Figure 4.3). From the biological screening results of the first generation sulfhydryl and disulfide derivatives, new design of the inhibitors inhibiting phagocytosis around the hit **10** (Chart 4.2) were investigated. Introductory structural changes considered around the scaffold **10** for second generation derivatives inhibiting Fc γ -receptor mediated phagocytosis of anti-D coated red blood cells to ameliorate idiopathic immune thrombocytopenia (ITP) are (Figure 4.4)

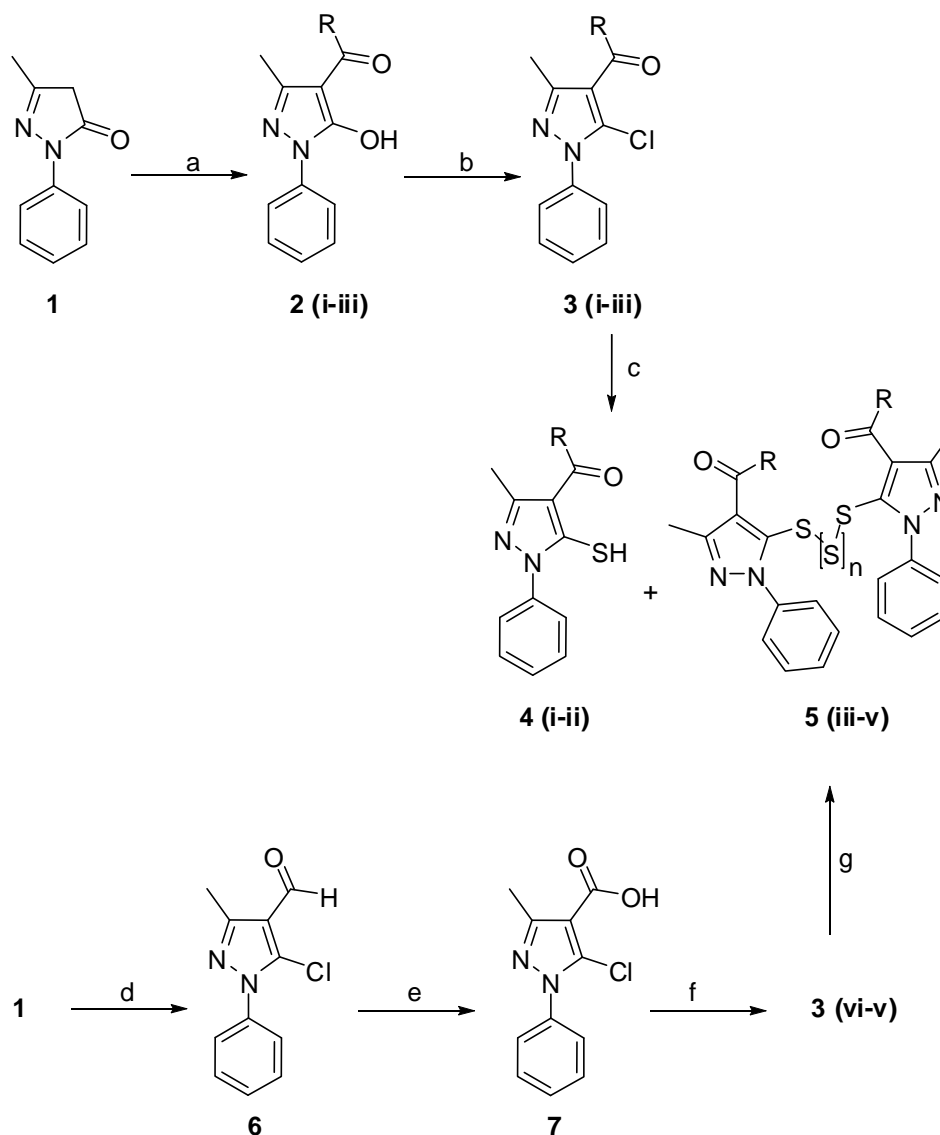
- a) Substitution of the disulfide bridge of the homodimer **10** to ethylene and ether (Scheme 4.5 and 4.6),
- b) Alteration of the chain length between the two pyrazole moieties (Scheme 4.7 and 4.8)
- c) Variation at the N1substitution of one of the pyrazole nucleus of heterodimers with ether spacer arm (Scheme 4.9-4.13).

Chart 4.2: Lead molecules chemical structures**Figure 4.3:** Template for first generation SH/SS pyrazole derivatives inhibiting phagocytosis**Figure 4.4:** Strategic structural modifications around the hit molecule **10**

4.3 Experimental Section

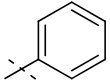
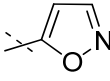
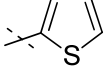
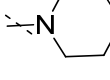
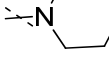
4.3.1 *Synthetic schemes and procedures*

General: All solvents and reagents were obtained from commercial sources. Column chromatography purifications were performed on Biotage flash chromatography system using normal silica gel (60 Å, 70-230 mesh) and reverse-phase (C18) cartridges. Reactions were monitored by thin layer chromatography Merck. NMR spectra were recorded on Bruker spectrometer (400 MHz for ^1H). Chemical shifts are reported in δ ppm using residual solvent peak as the reference for the ^1H NMR spectra. Purity of the synthesized compounds was determined by WatersTM LC-MS system (WatersTM 2545 binary gradient module) including eluting system. Mass spectra (ESI) were recorded on a WatersTM LC/MS system equipped with a WatersTM 3100 mass detector.



Scheme 4.1. Synthesis of compounds **4 (i-ii)** and **5 (i&iii-vi)**. Reagents and conditions: (a) Edaravone (1), Ca(OH)₂, acyl chloride, anhydrous 1,4-dioxane, reflux, 3-4h; (b) Phosphorous oxychloride (POCl₃), for R=phenyl (2i) reflux for 2 h, for R=5-isoxazolyl (2ii) heating at 80 °C for 50 min, for R=2-thienyl (2iii) heating at 50 °C for 30 min; (c) Sodium sulfide, anhydrous DMF, 60°C, 2-3 h; (d) A mixture of DMF and POCl₃ (1:3), microwave 100 °C, 4 min; (e) Potassium permanganate (KMnO₄), water, reflux, 20h; (f) HATU, DIPEA, anhydrous DMF, room temperature, 30 min; (g) Sodium sulfide, elemental sulfur, anhydrous DMF, 120°C, 3-6 h.

Table 4.2. Summary of the compounds synthesized in the Scheme 1

Substituent (R)	Series 2	Series 3	Series 4	Series 5	
				n=0	n=1,2,3,4,5
	2i	3i	4i	5i	-
	2ii	3ii	4ii	-	-
	2ii	3iii	-	5iii	-
	-	3iv	-	5iv	5iv
	-	3v	-	5v	5v

General procedure A for synthesis of C4-acylated pyrazolones 2i-2iii

The reaction was carried out in Mettler-Toledo Bohdan parallel synthesizer. A suspension of edaravone (500 mg, 2.87 mmol) and anhydrous calcium hydroxide (426 mg, 5.74mmol) in anhydrous 1, 4-dioxane (5 mL) was heated to 40 °C for 10 min. Acid chloride (2.87 mmol) was added to it dropwise. The reaction mixture was heated to reflux for 3-4 h, cooled to room temperature and poured into the ice-cold 2*N* HCl (10 mL). The acidic reaction mixture was allowed to stir at room temperature for 1 h. Then, it was diluted with 20 mL of ice-cold water. The precipitated C4 aryl methanone compound was filtered under vacuum and washed thoroughly with water. Without any further purification the crude C4 acylated edaravone derivatives **2i-2iii** were used for next reaction.

(5-Hydroxy-3-methyl-1-phenyl-1*H*-pyrazol-4-yl)(phenyl)methanone (2i):

The title compound was obtained by from edaravone (**1**) as described in general procedure A. Compound **2i** was gained as brown solid (790.19 mg, 99%). ¹H NMR (CDCl₃) δ 2.10 (s, 3H), 7.28 - 7.34 (m, 1H), 7.43 - 7.55 (m, 4H), 7.56 - 7.62 (m, 1H), 7.62 - 7.68 (m, 2H), 7.85 - 7.91 (m, 2H).

(5-Hydroxy-3-methyl-1-phenyl-1*H*-pyrazol-4-yl)(isoxazol-5-yl)methanone

(2ii): The title compound was obtained by from edaravone (**1**) as described in general procedure A. Compound **2ii** was obtained as light yellow solid (430 mg, 55%). ¹H NMR (CDCl₃) δ 2.81 (s, 3H), 7.01 (d, *J* = 1Hz, 1H), 7.49 - 7.58 (m, 1H), 7.69 (t, *J* = 7.91 Hz, 2 H), 8.07 (d, *J* = 8.03 Hz, 2 H), 8.65 (d, *J* = 1.00 Hz, 1 H), 12.92 (br, s, 1 H).

5-Chloro-3-methyl-1-phenyl-1*H*-pyrazole-4-carbaldehyde (6): Edaravone

(1) (1g, 5.74 mmol), DMF (839.26 mg, 11.48 mmol) and POCl₃ (5280.68 mg, 34.44 mmol) were added to a Biotage Initiator microwave reaction vial containing a Teflon stirrer bar. The vial was capped and the reaction mixture was transferred to the microwave and irradiated for 100 °C for 4 min at high absorption with cooling activated. The reaction crude was poured over crushed ice and neutralized with saturated Na₂HCO₃ solution. The aqueous layer was then extracted with EtOAc, combined organic layer was washed with brine and dried over dried over anhydrous Na₂SO₄. Organic layer was then evaporated under reduced pressure and the resulting crude was purified by flash chromatography using gradient 1-15 %EtOAc-Hexanes to afford compound **6** (460 mg, 36%). ¹H NMR (CDCl₃) δ 2.53 (s, 3H), 7.44-7.55 (m, 5H), 9.97 (s, 1H).

5-Chloro-3-methyl-1-phenyl-1H-pyrazole-4-carboxylic acid (7):

Compound **6** (780 mg, 3.53 mmol) was suspended in water. Potassium permanganate (870.18 mg, 5.50 mmol) was added in portion wise and refluxed for 20 h. The reaction was monitored by TLC and with carboxylic acid staining bromocresol green stain. On completion, the reaction mixture was cooled to room temperature and basified with 10% aq KOH. The reaction mixture was filtered under vacuum. The resulting filtrate was acidified to pH 1 with conc. HCl. The precipitated white solid was filtered off, washed with water and dried over vacuum to yield compound **7** (598 mg, 69%). ¹H NMR (CDCl₃) δ 2.56 (s, 3H), 7.45-7.55 (m, 5H).

General procedure B for synthesis of 3iv-v

A reaction mixture of acid **7** (150 mg, 0.63 mmol), HATU (241 mg, 0.63 mmol) and DIPEA (82 mg, 0.63 mmol) in anhydrous DMF was stirred at room temperature for 30 min. An appropriate secondary amine was added to it. Then, the reaction was stirred at room temperature for 30 min. The solvent was removed under vacuum and the resulting crude was purified by flash chromatography on silica gel using gradient 0-5% MeOH-DCM to afford the corresponding carbamoylated derivatives **3iv-v**.

(5-Chloro-3-methyl-1-phenyl-1H-pyrazol-4-yl)(morpholino)methanone

(3iv): The title compound was obtained from acid **7** by general procedure B. Compound **3iv** was yielded as white solid (163 mg, 85%). ¹H NMR (CDCl₃) δ 2.35 (s, 3H), 2.81 - 3.75 (m, 8H), 7.40 - 7.53 (m, 5H).

(5-Chloro-3-methyl-1-phenyl-1H-pyrazol-4-yl)(piperidin-1-yl)methanone

(3v): The title compound was obtained from acid **7** by general procedure B.

Compound **3v** was accomplished as clear liquid (182 mg, 95%). ^1H NMR (CDCl_3) δ 1.61-1.68 (m, 6H), 2.33 (s, 3H), 3.34 (br s, 2H), 3.73 (br s, 2H), 7.39-7.54 (m, 5H).

General procedure C for synthesis of compounds 3i-iii

A mixture of an appropriate C4 substituted aryl methanone **2i-iii** and POCl_3 (10-30 Eq) (POCl_3 more than 30 Eq resulted in poor yield) was heated at suited temperature until the reaction went to completion. Reaction was cooled to room temperature, poured over crushed-ice and neutralized by saturated solution of NaHCO_3 . The desired compound was extracted with EtOAc (10 \times 3 mL). Combined organic layer was washed with brine, dried over dried over anhydrous Na_2SO_4 and evaporated under reduced pressure to obtain the chlorinated derivatives.

(5-Chloro-3-methyl-1-phenyl-1H-pyrazol-4-yl) (phenyl)methanone (3i):

The title compound was obtained as described in the general procedure C, from (5-hydroxy-3-methyl-1-phenyl-1H-pyrazol-4-yl)(phenyl)methanone (**2i**) (2 g, 7.18 mmol) and phosphorus oxychloride (2.75 g, 17.95 mmol) heated to reflux for 2h. Compound **3i** was obtained as brown solid (1.99 g, 93%). ^1H NMR (CDCl_3) δ 2.37 (s, 3H), 7.42 - 7.63 (m, 8H), 7.78 - 7.88 (m, 2H).

(5-Chloro-3-methyl-1-phenyl-1H-pyrazol-4-yl)(isoxazol-5-yl)methanone

(3ii): The title compound was obtained as described in the general procedure C, from (5-hydroxy-3-methyl-1-phenyl-1H-pyrazol-4-yl)(isoxazol-5-yl)methanone (**2ii**) (250 mg, 0.92 mmol) and phosphorus oxychloride heated to 80 $^\circ\text{C}$ for 50 min. Reaction crude was purified by flash chromatography on silica gel using gradient 0-35% EtOAc-Hexanes to afford compound **3ii** as

white solid (160 mg, 60%). $^1\text{H NMR}$ (CDCl_3) δ 2.46 (s, 3H), 6.99 (d, $J = 2.01$ Hz, 1H), 7.45 - 7.59 (m, 5H), 8.42 (d, $J = 1.76$ Hz, 1H).

(5-Chloro-3-methyl-1-phenyl-1H-pyrazol-4-yl)(thiophen-2-yl) methanone (3iii): The title compound was obtained as described in the general procedure C, from (5-hydroxy-3-methyl-1-phenyl-1H-pyrazol-4-yl) (thiophen-2-yl) methanone (**3iii**) (180 mg, 0.63 mmol) and phosphorus oxychloride (289.79 mg, 1.89 mmol) heated to 50 °C for 30 min. The reaction crude was purified by flash chromatography on silica gel using gradient 0-35%EtOAc-Hexanes to obtain compound **3iii** as white solid (80 mg, 42%). $^1\text{H NMR}$ (CDCl_3) δ (s, 3H), 7.16 (dd, $J = 4.4, 8.8$ Hz, 1H), 7.43 -7.57 (m, 5H), 7.68 (d, $J = 3.2$ Hz, 1H), 7.74 (d, $J = 4.8$ Hz,1H).

General procedure D for synthesis of 4i-ii and 5iii-v

The reaction mixture of appropriate pyrazole derivative **3i-iii** and sodium sulfide ($\text{Na}_2\text{S}\cdot x\text{H}_2\text{O}$) (3Eq) in anhydrous DMF was heated to 60°C for suited time. For carbamolyated derivatives **3iv-v** in addition to $\text{Na}_2\text{S}\cdot x\text{H}_2\text{O}$ (3Eq), elemental sulfur (1Eq) was added to the reaction mixture and heated to 120 °C for suited time. On addition of the elemental sulfur the reaction color changes to green. Reaction was monitored by TLC. On completion of the reaction, it was cooled to room temperature, poured over cold water and acidified to pH 1 with 2N HCl. The precipitated solid was collected, dissolved in methanol, concentrated in vacuum and purified by flash chromatography on silica gel using gradient 10-90% EtOAc-Hexanes.

(5-Mercapto-3-methyl-1-phenyl-1H-pyrazol-4-yl)(phenyl)methanone (4i):

The title compound was obtained as described in the general procedure D,

from (5-chloro-3-methyl-1-phenyl-1H-pyrazol-4-yl)(phenyl)methanone (**3i**) (1.5 g, 5.05 mmol). Compound **4i** was gained as orange crystalline solid (1.10g, 74%). ¹H NMR (CDCl₃) δ, 2.01 (s, 3H), 7.43 - 7.62 (m, 8H), 7.64 - 7.72 (m, 2H). ESI (+ve) [M+H⁺] calculated 395.09, found 395.

Isoxazol-5-yl(5-mercapto-3-methyl-1-phenyl-1H-pyrazol-4-yl)methanone

(**4ii**): The title compound was obtained as described in the general procedure D, (5-chloro-3-methyl-1-phenyl-1H-pyrazol-4-yl) (isoxazol-5-yl) methanone (**3ii**) (70 mg, 0.24 mmol). Compound **4ii** was obtained as off-white solid (20 mg, 29%). ¹H NMR (CDCl₃) δ 2.35 (s, 3H), 2.95 - 3.32 (m, 2H), 5.90 (br, s, 1H), 7.32 - 7.39 (dd, *J* = 8.16 Hz, 1H) 7.46 (dd, *J* = 8.16 Hz, 2H), 7.52 (d, *J* = 8Hz, 2H). ESI (+ve) [M+H⁺] calculated 286.07, found 286.14.

(5,5'-Disulfanediylobis(3-methyl-1-phenyl-1H-pyrazole-5,4-

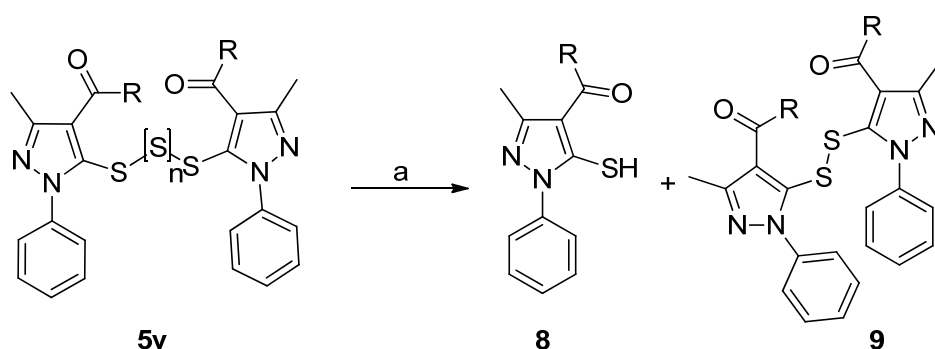
diyl))bis(phenylmethanone)(5i): A solution of compound **4i** (100 mg, 0.34 mmol) in DMF (2 mL) was refluxed for 3h and stirred at room temperature for 22h. The reaction mixture was then diluted with water. The aqueous layer was extracted with EtOAc, washed with brine, dried over Na₂SO₄ and concentrated under reduced pressure. The reaction crude was then passed through silica gel column using gradient 5-30% EtOAc-Hexanes to obtain compound **5i** (49.9 mg, 50%) as yellow solid. ¹H NMR (CDCl₃) δ 2.29 (s, 3H), 7.13-7.15 (m, 4H), 7.35-7.44 (m, 12H), 7.55 (d, 6H). ESI (+ve) [M+H⁺] calculated 587.18, found 589.26.

(5,5'-Disulfanediylobis(3-methyl-1-phenyl-1H-pyrazole-5,4-

diyl))bis(thiophen-2-ylmethanone) (5iii): The title compound was obtained as described in the general procedure D, from 5-chloro-3-methyl-1-phenyl-1H-pyrazol-4-yl)(thiophen-2-yl)methanone (**3iii**) (73 mg, 0.24 mmol).

Compound **5iii** was achieved as light yellow solid (22 mg, 31%). ^1H NMR (CDCl_3) δ 2.29 (s, 6H), 7.10 (dd, $J = 12.00$, 4Hz, 6H), 7.23 (m, 4H) 7.34 - 7.44 (m, 8H), 7.70 (d, $J = 4.00$ Hz, 2H). Since it has trace of polysulfides small peaks were seen near the major compound peaks. ESI (+ve) $[\text{M}+\text{H}^+]$ calculated 599.07, found 599.26.

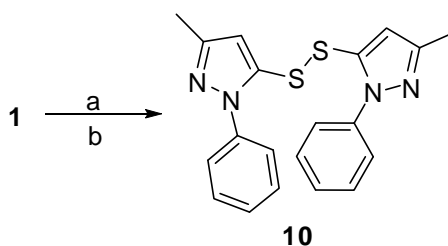
(5,5'-Disulfanediybis(3-methyl-1-phenyl-1H-pyrazole-5,4-diyl))bis(morpholinomethanone) (5iv): The title compound was obtained as described in the procedure D, from (5-chloro-3-methyl-1-phenyl-1H-pyrazol-4-yl)(morpholino)methanone (**3v**) (110 mg, 0.36 mmol). Compound **5iv** was obtained as light yellow solid (26 mg, 12%). But it was obtained as a mixture of polysulfide. ^1H NMR (CDCl_3) δ 2.27 (s, 3H), 2.29 (s, 0.6H), 2.31-2.34 (m, 0.8H), 3.26-3.71 (br, m, 12.6H), 7.21 (br, s, 2H), 7.36-7.46 (m, 5.6H). ESI (+ve) $[\text{M}+\text{H}^+]$ calculated 605.20, found 605.40.



Scheme 4.2. Reduction of compound **5v**. Reagents and conditions: (a) Polysulfide mixture **5v** (R= piperidin-1-yl) NaBH_4 , EtOH, room temperature, 1 h.

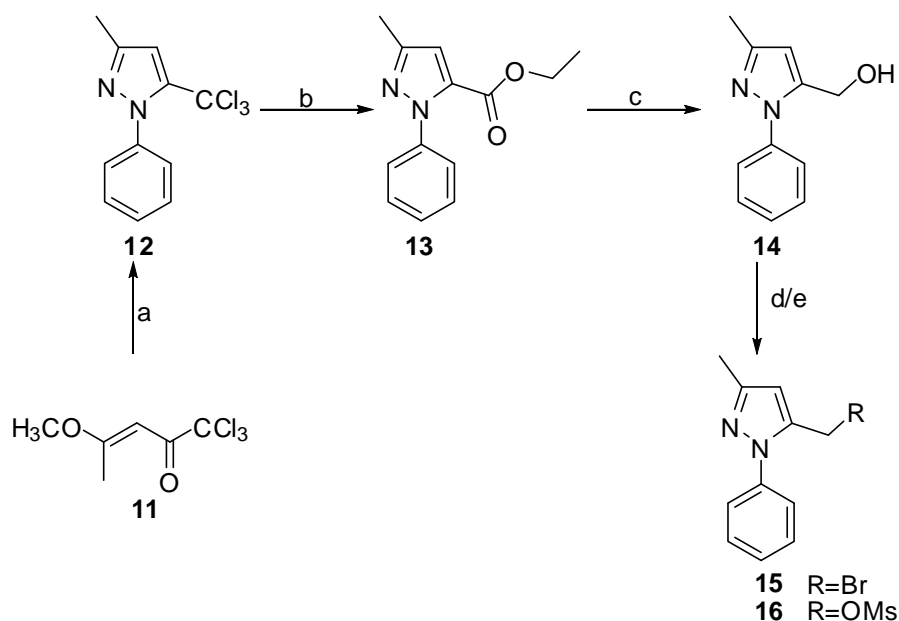
(5,5'-Disulfanediylbis(3-methyl-1-phenyl-1H-pyrazole-5,4-

diyl))bis(piperidin-1-ylmethanone) (9): The title compound was obtained as described in the procedure D, from, (5-chloro-3-methyl-1-phenyl-1H-pyrazol-4-yl)(piperidin-1-yl)methanone (**3vi**) (232 mg, 0.76 mmol). Light yellow colored mixture of poly sulfide was obtained (64 mg) (**5vi**). (CDCl_3) δ 1.43-1.62 (br, m, 8H), 2.26 (s, 3H), 3.18-3.42 (br, m, 2, 8H), 3.68 (br, s, 2.6H), 7.22 (br, s, 1.6H), 7.34-7.43 (m, 4.6H). It was then reduced with NaBH_4 (5 Eq) in ethanol at room temperature and the reaction was monitored by HPLC. The reaction was quenched with water. Solvent was evaporated and the resultant crude was purified over HPLC to obtain final compound **9** (10 mg, 2%). ^1H NMR (CDCl_3) δ 1.45-1.64 (br, m, 6H), 2.27 (s, 3H), 3.20 (br, s, 2H), 3.66 (br, s, 2H), 6.22 (br, s, 1H), 7.21 (br, s, 2H), 7.37 (m, 3H). ESI (+ve) $[\text{M}+\text{H}^+]$ calculated 601.24, found 601.48.



Scheme 4.3. Synthesis of 1,2-Bis(3-methyl-1-phenyl-1*H*-pyrazol-5-yl)disulfane (**10**). Reagents and conditions: (a) Lawesson's reagent, 1,4-dioxane, reflux, 2 h; (b) MeOH, room temperature, overnight.

1,2-Bis(3-methyl-1-phenyl-1*H*-pyrazol-5-yl)disulfane (10): To a flask containing solution of edaravone (**1**) (500 mg, 5.74 mmol) in anhydrous 1,4-dioxane, Lawesson's reagent was added (1.39 g, 3.44 mmol) and was refluxed for 2h. Then, the reaction mixture was cooled to room temperature and concentrated under vacuum. To the resultant crude, methanol was added and stirred at room temperature overnight. The methanolic solution was filtered off and the filtrate was concentrated under vacuum. The resulting residue was initially purified by column chromatography on neutral alumina using gradient 0-5%EtOAc-Hexanes. Fractions containing the compound of interest were combined together and the solvent was removed under vacuum. The obtained impure compound **10** was further subjected to column chromatography on silica gel using gradient 0-15%EtOAc-Hexanes to afford compound **10** (346 mg, 32%). ¹H NMR (CDCl₃) δ 2.30 (s, 3H), 6.06 (s, 2H), 7.31-7.41 (m, 10H). ESI (+ve) [M+H⁺] calculated 379.52, found 379.22.



Scheme 4.4. Synthesis of intermediates **15** and **16**. Reagents and conditions. a. Phenylhydrazine, toluene, MW-85 °C, 5 min; b. ethanol, pyridine, reflux, 2 h; c. LAH, anhydrous THF, 0°C to rt, 30 min; d. PBr₃, toluene, reflux, 2 h ; e. Methane sulfonyl chloride, Et₃N, anhydrous DCM, reflux, 2 h.

(E)-1,1,1-Trichloro-4-methoxyprop-2-ene-2-one (11): In a flame dried flask, a solution of 2-methoxy propene (1.29 g, 17.91 mmol) and pyridine (1.41 g, 17.91 mmol) was cooled to 0 °C. The ionic liquid, 1-butyl-3-methylimidazolium hexafluorophosphate (BMIM.PF6) (508 mg, 1.79 mmol) was added to it and allowed to stir at 0 °C for 5 min. The above reaction mixture of enol ether, pyridine and ionic fluid was added dropwise to trichloroacetyl chloride (3.26 g, 17.91 mmol) at 0 °C. After the addition, the reaction was warmed to room temperature and allowed to stir for additional 1h. Reaction mixture was then diluted with diethyl ether, washed with water, brine and dried over Na₂SO₄. Organic layer was evaporated under reduced pressure to afford brown oil **11** (3.66g, 94%). ¹H NMR (CDCl₃) δ 2.41 (s, 3H), 3.81 (s, 3H), 6.01 (s, 1H).

3-Methyl-1-phenyl-5-(trichloromethyl)-1H-pyrazole (12): In a microwave vial, β -methoxyvinyl trichloromethyl ketone **11** (442 mg, 2.03 mmol), phenyl hydrazine (220 mg, 2.03 mmol) and anhydrous toluene (5mL) were added. The vial was capped and the reaction mixture was transferred to the microwave and irradiated at 85 °C for 5 min with cooling activated. The reaction solvent was evaporated under reduced pressure. The resulting crude was then purified by flash chromatography on silica gel using gradient 0-4% EtOAc-Hexanes to afford white crystalline compound **12** (190.30 mg, 34%). ^1H NMR (CDCl_3) δ 2.32 (s, 3H), 6.69 (s, 1H), 7.44-7.47 (m, 3H), 7.51-7.54 (m, 2H).

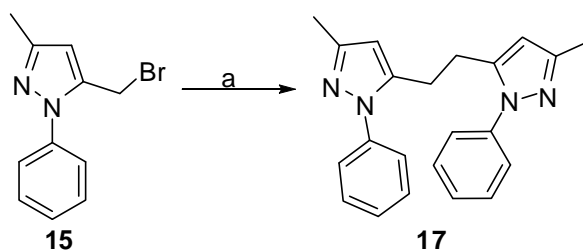
Ethyl 3-methyl-1-phenyl-1H-pyrazole-5-carboxylate (13): To a solution of compound **12** (750 mg, 2.72 mmol) in ethanol (5 mL) pyridine (647.18 mg, 8.18 mmol) was added and refluxed for 2h. Reaction was monitored by TLC. Reaction was cooled to room temperature and solvent was evaporated under reduced pressure. The reaction crude was then diluted with DCM (20 mL), washed with 10% HCl (5 mL) and dried over Na_2SO_4 . Organic layer was evaporated to obtain compound **13** (582.46 mg, 93%). ^1H NMR (CDCl_3) δ 1.27 (t, $J = 7.16$ Hz, 2H), 2.35 (s, 3H), 4.21 (q, $J = 7.16, 7.08$ Hz, 2H), 6.80 (d, $J = 4.00$ Hz, 1H), 7.39-7.44 (m, 5H).

(3-Methyl-1-phenyl-1H-pyrazol-5-yl)methanol (14): To a suspension of LAH (229.97 mg, 6.06 mmol) in anhydrous tetrahydrofuran (THF), a THF solution of compound **13** (696 mg, 3.03 mmol) was added dropwise at 0 °C. After the addition, the reaction was warmed to room temperature and allowed to stir for additional 30 min. Reaction was then cooled to 0 °C and quenched with saturated solution of Na_2SO_4 . The resultant precipitate was filtered off

under vacuum and the filtrate was evaporated to dryness to obtain white amorphous solid **14** (515 mg, 90%). ^1H NMR (CDCl_3) δ 2.34 (s, 3H), 4.65 (d, $J = 5.52$ Hz, 2H), 6.26 (s, 1H), 7.36 (dd, $J = 16.00, 8.00$ Hz, 1H), 7.46 (dd, $J = 16.00, 8.00$ Hz, 2H), 7.58 (d, $J = 7.53$ Hz, 1H).

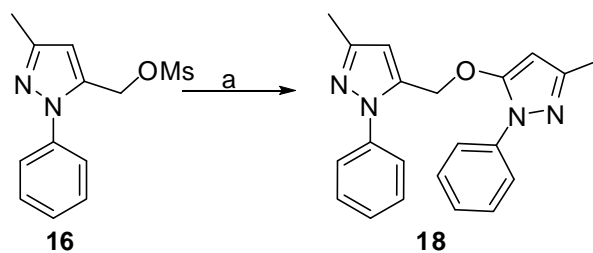
5-(Bromomethyl)-3-methyl-1-phenyl-1H-pyrazole (15): To a solution of compound **14** (92 mg, 0.49 mmol) in toluene, phosphorus tribromide (66.15 mg, 0.25 mmol) was added at room temperature. Reaction was then refluxed for 2 h, cooled to room temperature and neutralized with saturated NaHCO_3 solution. Aqueous layer was extracted with DCM. Organic layer was dried over Na_2SO_4 and evaporated to yield compound **15** (104 mg, 85%). ^1H NMR (CDCl_3) δ : 2.32 (s, 3H), 4.44 (s, 2H), 6.32 (s, 1H), 7.39-7.43 (m, 1H), 7.47-7.51 (m, 2H), 7.55 (d, $J = 7.76$ Hz, 1H).

(3-Methyl-1-phenyl-1H-pyrazol-5-yl)methyl methanesulfonate (16). To a solution of compound **14** (50 mg, 0.26 mmol), triethylamine (80.59 mg, 0.79 mmol) in anhydrous DCM (3 mL) methanesulfonyl chloride (45.7 mg, 0.40 mmol) was added drop wise at 0°C . After the addition, reaction mixture was refluxed for 2 h. The reaction was then cooled to room temperature, diluted with DCM (12 mL), washed with saturated NaHCO_3 solution and dried over Na_2SO_4 . Organic layer was evaporated to dryness to give compound **16** (65.4mg, 95%). Intermediate **18** was used right way for the next step.



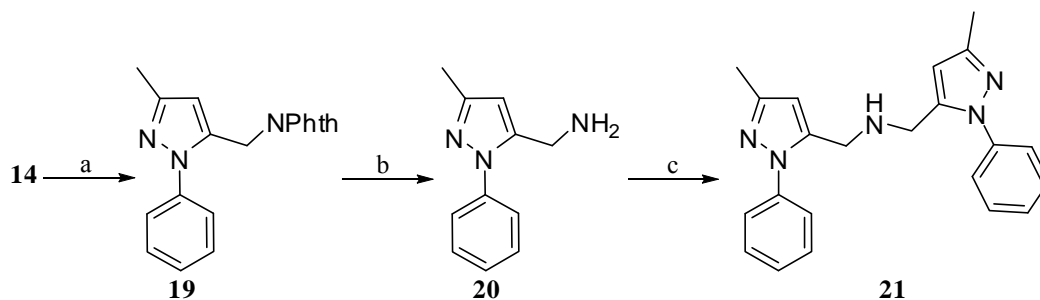
Scheme 4.5. Synthesis of compound **17**. Reagents and conditions: a. Mg turnings, anhydrous THF, MW 100 °C, 1h, additional stirring at room temperature 42 h.

1,2-Bis(3-methyl-1-phenyl-1H-pyrazol-5-yl)ethane (17): To an oven dried Biotage Initiator microwave reaction vial containing a Teflon stirrer bar magnesium (Mg) turnings (10.5 mg, 0.43 mmol) were added, vial was capped and purged with nitrogen. Anhydrous THF (2 mL) was added to the reaction vial. A solution of compound **15** (104 mg, 0.43 mmol) in anhydrous THF (1 mL) was added to above suspension. The reaction mixture was transferred to the microwave and irradiated at 100 with cooling activated. The reaction was then allowed to stir at room temperature for 42 h. The progress of reaction was monitored by TLC. On completion, the reaction was quenched with saturated solution of ammonium chloride at 0 °C. Aqueous layer was then extracted with EtOAc. Organic layer was then washed with brine, dried over Na₂SO₄ and evaporated under reduced pressure. The resulting crude was then purified by flash chromatography on silica gel using gradient 0-30% EtOAc-Hexanes to afford compound **7** (33 mg, 45%). ¹H NMR (CDCl₃) δ: 2.27 (s, 6H), 2.86 (s, 4H), 5.91 (s, 2H), 7.35-7.42 (m, 10 H). ESI (+ve) (M+H⁺) calculated 343.30, found 343.32.



Scheme 4.6. Synthesis of compound **18**. Reagents and conditions: a. Edaravone (**1**), Cs_2CO_3 , anhydrous ACN, 60 °C, 2 h.

3-Methyl-5-((3-methyl-1-phenyl-1H-pyrazol-5-yl)methoxy)-1-phenyl-1H-pyrazole (18): A suspension of edaravone (**1**) (41.6 mg, 0.24 mmol) and cesium carbonate (260 mg, 0.79 mmol) in anhydrous ACN (3 mL) was allowed to stir at room temperature for 5 min. Compound **16** synthesized from **14** (50 mg, 0.26 mmol) was dissolved in 2 mL of anhydrous ACN. The solution of **16** was added to the above reaction suspension and heated to 60 °C for 2h. On completion, reaction mixture was cooled and filtered off. The resultant filtrate was adsorbed over silica and purified by flash chromatography on silica gel using gradient 0-30% EtOAc-Hexanes to obtain yellow oily compound **18** (12 mg, 15%). ^1H NMR (CDCl_3) δ 2.26 (s, 3H), 2.35 (s, 3H), 5.03 (s, 2H), 5.50 (s, 1H), 6.33 (s, 1H), 7.20 (m, 1H), 7.32-7.45 (m, 7H), 7.50-7.53 (m, 2H). ESI (+ve) ($\text{M}+\text{H}^+$) calculated 345.17, found 345.30.



Scheme 4.7. Synthesis of compound **21**. Reagents and conditions: a. PPh_3 , DEAD, anhydrous THF, 0°C to room temperature, 48 h; b. $\text{NH}_2\text{NH}_2\cdot\text{H}_2\text{O}$, methanol, 0°C to room temperature, overnight; c. compound **5**, K_2CO_3 , ACN, 60°C , 2 h.

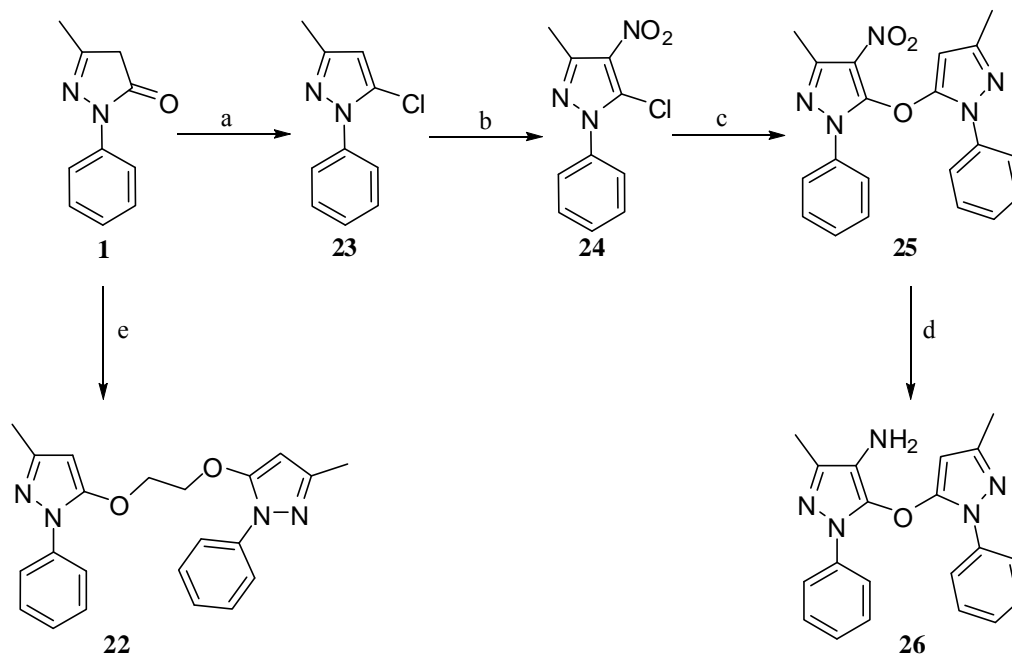
2-((3-Methyl-1-phenyl-1H-pyrazol-5-yl)methyl)isoindoline-1,3-dione (19):

To a reaction mixture of compound **14** (100 mg, 0.53 mmol), triphenylphosphine (167 mg, 0.64 mmol) and phthalimide (78.12 mg, 0.53 mmol) in anhydrous THF (5 mL) was added diethyl azodicarboxylate (138.62 mg, 0.64 mmol) at 0°C . After stirring the reaction at room temperature for 48 h, the solvent was evaporated under vacuum and the resultant crude was purified by flash chromatography using gradient 1-30%EtOAc-Hexanes to give compound **19** (158 mg, 94%). ^1H NMR (CDCl_3) δ 2.22 (s, 3H), 4.83 (s, 2H), 6.08 (s, 1H), 7.34-7.38 (m, 1H), 7.42-7.50 (m, 4H), 7.67-7.71 (m, 2H), 7.78-7.81 (m, 2H).

(3-Methyl-1-phenyl-1H-pyrazol-5-yl)methanamine (20): To a solution of compound **19** (158 mg, 0.50 mmol) in methanol (2 mL) was added hydrazine hydrate (125 mg, 2.5 mmol) at 0°C . The reaction mixture was then warmed up to room temperature and stirred overnight. The reaction solvent was evaporated under vacuum and the resultant crude was suspended in the methanol (2 mL). The white insoluble precipitate was filtered off and the filtrate was evaporated to afford compound **20** (79 mg, 84%) as oil. ^1H NMR

(CDCl₃) δ 2.28 (s, 3H), 3.83 (s, 2H), 6.13 (s, 1H), 7.30-7.33 (s, 1H), 7.38-7.43 (m, 4H).

Bis((3-methyl-1-phenyl-1H-pyrazol-5-yl)methyl)amine (21). To a flask containing suspension of compound **20** (58 mg, 0.26 mmol) and potassium carbonate (112 mg, 0.79 mmol) in anhydrous ACN (2 mL) was added a solution of compound **15**, synthesized from precursor **16** (50 mg, 0.26 mmol), in ACN (1 mL) at room temperature. The reaction mixture was then heated to 60°C for 2h. On cooling the reaction mixture was concentrated under vacuum and purified by flash chromatography using gradient 10-80% EtOAc-Hexanes to obtain compound **21** (41 mg, 43%) as oil. ¹H NMR (CDCl₃) δ 2.15 (s, 3H), 2.33 (s, 3H), 2.95 (br t, 2H), 3.82 (t, J = 6 Hz, 2H), 4.96 (s, 2H), 5.31 (s, 1H), 6.32 (s, 1H), 7.34-7.48 (m, 5H).



Scheme 4.8. Synthesis of compound **22** and **26**. Reagents and conditions: a. POCl₃, reflux 2h; b. Acetic anhydride, conc. HNO₃, 0 °C to room temperature, 4h; c. Edaravone (**1**), K₂CO₃, DMF, MW, 80 °C, 12 min; d. SnCl₂·2H₂O, conc. HCl, 0 °C to room temperature, 1h; e. Cs₂CO₃, ACN, 1,2-dibromoethane, 60 °C, overnight.

1,2-Bis(3-methyl-1-phenyl-1H-pyrazol-5-yloxy)ethane (22): To a suspension of edaravone (402 mg, 2.31 mmol) and cesium carbonate (1800 mg, 5.52 mmol) in anhydrous ACN (5 mL) 1,2-dibromoethane (217 mg, 1.15 mmol) was added. The reaction mixture was heated to 60°C for overnight. The reaction was filtered and the filtrate was concentrated under vacuum. The resultant crude was purified by flash chromatography using gradient 10%-100%EtOAc-Hexanes to obtain product **22** (221 mg, 54%). ¹H NMR (CDCl₃) δ 2.26 (s, 6H), 4.32 (s, 4H), 5.50 (s, 2H), 7.17-7.22 (m, 2H), 7.27-7.32 (m, 4H), 7.60-7.63 (m, 4H). ESI (+ve) (M+H⁺) calculated 375.18, found 375.30.

5-Chloro-3-methyl-1-phenyl-1H-pyrazole (23): To a flask containing edaravone (2.0g, 11.48 mmol) phosphorus oxychloride (3mL) was added and refluxed for 2h. On cooling the reaction mixture was poured over crushed ice.

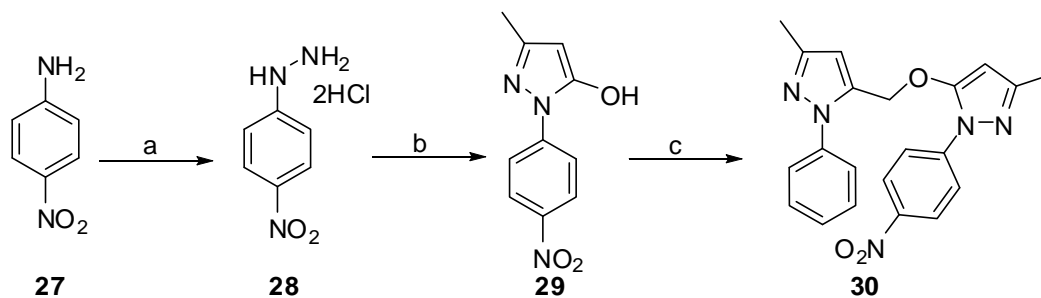
The aqueous layer was extracted with EtOAc which was then washed with brine, dried over Na₂SO₄ and concentrated under vacuum. The resultant crude was purified on a short column of silica gel using gradient 2-5% EtOAc-Hexanes to give compound **23** (1.8 g, 81%) as yellow oil. ¹H NMR (CDCl₃) δ 2.32 (s, 3H), 6.19 (s, 1H), 7.35 - 7.42 (m, 1H), 7.43 - 7.50 (m, 2H), 7.51 - 7.57 (m, 2H).

5-Chloro-3-methyl-4-nitro-1-phenyl-1H-pyrazole (24): To a round bottom flask containing compound **23** (110 mg, 0.57mmol) was added acetic anhydride (1.5 mL) and cooled to 0°C. Concentrated nitric acid (1mL) was then added dropwise. The reaction mixture was warmed up to room temperature and stirred for 4h. The reaction solution was then poured over crushed ice. The water insoluble yellow precipitate was collected and purified by flash chromatography using gradient 1-5% EtOAc-Hexanes to obtain compound **24** (126 mg, 92%). ¹H NMR (CDCl₃) δ 2.64 (s, 3H), 7.21-7.55 (m, 5H).

3-Methyl-5-(3-methyl-1-phenyl-1H-pyrazol-5-yloxy)-4-nitro-1-phenyl-1H-pyrazole (25): In a Biotage Initiator microwave reaction vial containing a Teflon stirrer bar compound **24** (50 mg, 0.21 mmol), edaravone (36.6 mg, 0.21 mmol) and potassium carbonate (87mg, 0.63 mmol) were added, vial was capped and purged with nitrogen. To this reaction vial anhydrous DMF (0.5 mL) was added and subjected to microwave irradiation at 80°C high absorption for 12 min with cooling activated. The reaction crude was then purified by flash chromatography using gradient 1-20% EtOAc-Hexanes to afford compound **25** (65 mg, 82%). ¹H NMR (CDCl₃) δ 2.22 (s, 3H), 2.64 (s,

3H), 5.47 (s, 1H), 7.30-7.34 (m, 1H), 7.40-7.45 (m, 5H), 7.51-7.54 (m, 2H), 7.62-7.66 (m, 2H).

3-Methyl-5-(3-methyl-1-phenyl-1H-pyrazol-5-yloxy)-1-phenyl-1H-pyrazol-4-amine (26): To a solution of compound **25** (20 mg, 0.05 mmol) in concentrated HCl (1ml) tin (II) chloride dihydrate (60.10 mg, 0.26 mmol) dissolved in conc. HCl (1mL) was added to it at 0°C. The reaction was warmed up to room temperature and stirred for 1h. On completion, the reaction mixture was poured over crushed ice and neutralized with saturated solution of NaHCO₃. The organic product was extracted with EtOAc which was then washed with brine, dried over Na₂SO₄ and concentrated under vacuum. The resultant crude was purified by flash chromatography using gradient 20-100% EtOAc-Hexanes to obtain product **26** (8.3 mg, 45%). ¹H NMR (CDCl₃) δ 2.26 (s, 3H), 2.27 (s, 3H), 2.63 9 s, br, 2H), 5.50 (s, 1H), 7.20-7.23 (m, 1H), 7.28-7.34 (m, 3H), 7.40-7.44 (m, 2H), 7.47 (d, *J* = 7.84 Hz, 2H), 7.64 (d, *J* = 7.60 Hz, 2H). ESI (+ve) (M+H⁺) calculated 346.16, found 346.27.



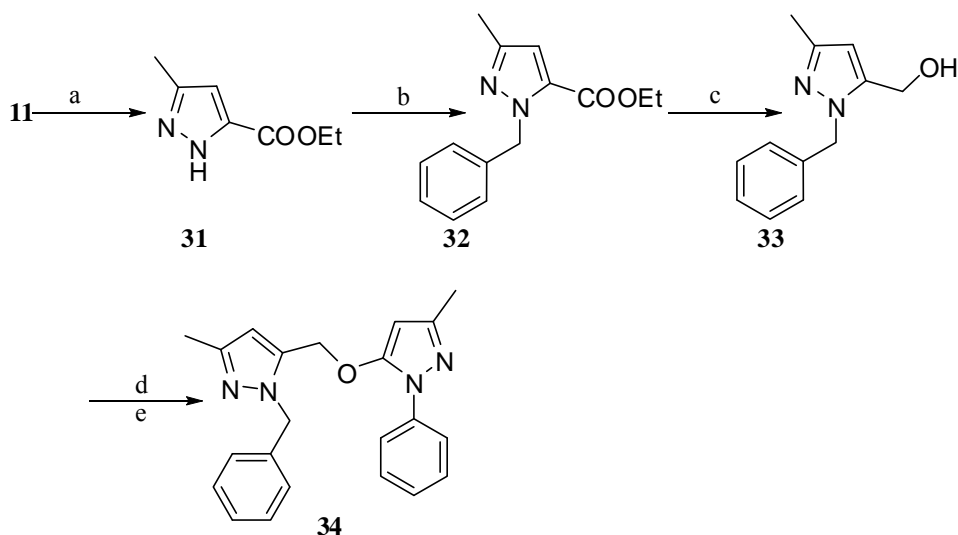
Scheme 4.9. Synthesis of compound **30**. Reagents and conditions: a. NaNO_2 , $\text{SnCl}_2 \cdot 2\text{H}_2\text{O}$, Conc.HCl, 0°C ; b. ethylacetoacetate, glacial acetic acid, reflux, 4 h; c. compound 6, Cs_2CO_3 , anhydrous ACN, 60°C , overnight.

(4-Nitrophenyl)hydrazine dihydrochloride salt (28): p-Nitroaniline (1437 mg, 10.40 mmol) was dissolved in conc. HCl (2 mL) and cooled to 0°C . A solution of sodium nitrite (717.77 mg, 10.40 mmol) in ice-cooled water (4 mL) was added dropwise to above acidic reaction mixture and stirred for 1h at 0°C . Ice-cooled solution of stannous chloride (4.69 g, 20.80 mmol) in conc. HCl (2 mL) was added slowly to above diazonium reaction mixture. The reaction was stirred at 0°C for 2h. The yellow-orange precipitate was collected and washed thoroughly with ice-cold water until the filtrate pH was neutral. Collected precipitate was dried overnight on high vacuum to give dihydrochloride salt of compound **28** (640 mg, 27%). ^1H NMR (DMSO- d_6) δ 4.49 (s, 2 H), 6.78 (d, $J = 8.78$ Hz, 2 H), 7.98 (d, $J = 9.29$ Hz, 2 H), 8.41 (s, 1 H).

3-Methyl-1-(4-nitrophenyl)-1H-pyrazol-5(4H)-one (29): To a solution of compound **28** (219 mg, 0.97 mmol) in glacial acetic acid (2mL) ethyl-3-oxobutanoate (167 mg, 1.28 mmol) was added and refluxed for 3h. The reaction mixture was cooled to 0°C and diethyl ether (5 mL) was added to it. After stirring for 1h at 0°C , the reaction mixture was filtered and the collected yellow-brown precipitate was washed with diethyl ether. The precipitate was

then purified by flash chromatography on silica gel using gradient 10-80% EtOAc-Hexanes to afford compound **29** (95 mg, 45%). ^1H NMR (CDCl_3) δ 2.24 (s, 3H), 3.50 (s, 2H), 8.13 (d, $J = 7.78$ Hz, 2H), 8.26 (d, $J = 8.53$ Hz, 2H).

3-Methyl-5-([3-methyl-1-(4-nitrophenyl)-1H-pyrazol-5-yl]oxy)methyl)-1-phenyl-1H-pyrazole (30): Compound **29** (113 mg, 1.02 mmol) and cesium carbonate (334.20 mg, 0.61 mmol) were suspended in anhydrous ACN (2mL). Compound **15** synthesized from compound **14** (100 mg, 0.51 mmol) was dissolved in 2mL of anhydrous ACN and added drop wise to above reaction suspension. The reaction was then heated to 60°C for overnight. The reaction solvent was removed by rotary evaporation and the resulting crude was purified by flash chromatography on silica gel using gradient 0-50% EtOAc-Hexanes to afford product **30** (25 mg, 12%). ^1H NMR (CDCl_3) δ 2.26 (s, 3H), 2.37 (s, 3H), 5.13 (s, 2H), 5.54 (s, 1H), 6.38 (s, 1H), 7.39 - 7.52 (m, 5H), 7.76 (d, $J = 9.29$ Hz, 2H), 8.19 (d, $J = 9.29$ Hz, 2H). ESI (+ve) ($\text{M}+\text{H}^+$) calculated 390.41, found 390.31.



Scheme 4.10. Synthesis of compound **34**. Reagents and conditions: a. Compound **11**, ethanol, $\text{NH}_2\text{NH}_2\cdot\text{HCl}$, reflux, 4 h; b. potassium carbonate, benzyl bromide and ACN, 0°C to room temperature, overnight; c. LAH, THF, 0°C to room temperature, 30 min; d. methanesulfonyl chloride, Et_3N , DCM, reflux 2 h; e. edaravone, Cs_2CO_3 , ACN, 60°C , 4 h.

Ethyl 3-methyl-1H-pyrazole-5-carboxylate (31): To a stirred suspension of hydrazine mono hydrochloride (642 mg, 9.38 mmol) in ethanol (5 mL) was added β -methoxy vinyl trichloromethylketone **11** (1700 mg, 7.80 mmol) at room temperature. After refluxing for 4h, the reaction mixture was filtered, solvent was removed under vacuum and the resultant crude was recrystallized in a mixture of EtOAc:Hexanes (1:1) to obtain product **31** (900 mg, 75%). ^1H NMR (CDCl_3) δ 1.34 (t, $J = 7.16$ Hz, 3H), 2.36 (s, 3H), 4.35 (q, $J = 7.08, 7.16$ Hz, 2H), 6.57 (s, 1H), 9.88 (br, s, 1H).

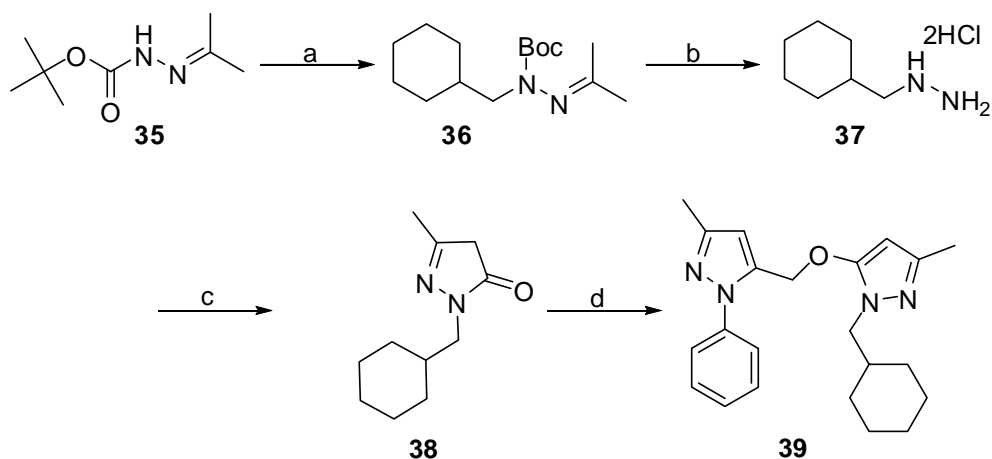
Ethyl 1-benzyl-3-methyl-1H-pyrazole-5-carboxylate (32): To a flask containing suspension of compound **31** (313 mg, 2.03 mmol) and potassium carbonate (842 mg, 6.09 mmol) in anhydrous ACN (4 mL) benzyl bromide (347.19 mg, 2.03 mmol) was added to it at 0°C . The reaction mixture was then stirred at room temperature for overnight. The reaction solvent was removed under vacuum and the resultant residue was purified by flash chromatography

using gradient 1%-40% EtOAc/Hexanes to afford compound **32** (114 mg, 23%) as clear liquid. ^1H NMR (CDCl_3) δ 1.31 (t, $J = 7.08$ Hz, 3H), 2.29 (s, 3H), 4.27 (q, $J = 7.16, 7.12$ Hz, 2H), 5.70 (s, 2H), 6.65 (s, 1H), 7.20-7.25 (m, 3H), 7.26-7.30 (m, 2H).

(1-Benzyl-3-methyl-1H-pyrazol-5-yl)methanol (33): To a suspension of LAH (53.12 mg, 1.39 mmol) in anhydrous THF (3 mL) at 0°C , a THF solution of compound **32** (112 mg, 0.45 mmol) was added dropwise. Followed by stirring the reaction at room temperature for 30 min, it was cooled to 0°C and quenched with saturated solution of Na_2SO_4 . The quenched reaction was filtered and filtrate was evaporated under vacuum to yield compound **33** (89 mg, 98%). ^1H NMR (CDCl_3) δ 2.27 (s, 3H), 4.51 (s, 2H), 5.34 (s, 2H), 6.04 (s, 1H), 7.12-7.15 (m, 2H), 7.26-7.33 (s, 3H).

1-Benzyl-3-methyl-5-((3-methyl-1-phenyl-1H-pyrazol-5-yloxy) methyl)-1H-pyrazole (34). To a solution of compound **33** (64 mg, 0.31 mmol), triethylamine (95.84 mg, 0.94 mmol) in anhydrous DCM (3 mL) methanesulfonyl chloride (54.29 mg, 0.47 mmol) was added drop wise at 0°C . After the addition, reaction mixture was refluxed for 2h. The reaction was then cooled to room temperature, diluted with DCM (12 mL), washed with saturated NaHCO_3 solution and dried over Na_2SO_4 . Organic layer was evaporated to dryness to give mesylated derivative of **33**. Crude mesylated derivative of **33** was dissolved in anhydrous ACN (2 mL) and added to the flask containing suspension of edaravone (55 mg, 0.31 mmol) and cesium carbonate (309 mg, 0.94 mmol) in anhydrous ACN (3 mL). After heating the reaction at 60°C for 4h, it was cooled, solvent was removed under vacuum and the resultant crude was purified by flash chromatography using gradient 1-

35%EtOAc-Hexanes to afford product **34** (40 mg, 36%). ^1H NMR (CDCl_3) δ 2.26 (s, 3H), 2.29 (s, 3H), 4.90 (s, 2H), 5.25 (s, 2H), 5.47 (s, 1H), 6.15 (s, 1H), 7.00-7.02 (m, 2H), 7.21-7.24 (m, 4H), 7.33-7.37 (m, 2H), 7.52-7.54 (m, 2H). ESI (+ve) ($\text{M}+\text{H}^+$) calculated 359.18, found 359.28.



Scheme 4.11. Synthesis of compound **39**. Reagents and conditions: a. KOH, Bu₄NHSO₄, toluene, (bromomethyl) cyclohexane, 80 °C, 2 h; b. 2N HCl, THF, reflux, 2 h; c. ethylacetoacetate, ethanol, reflux, 2 h; d. compound **5**, Cs₂CO₃, ACN, 60 °C, overnight.

1-(Pivaloyloxy)-2-(propan-2-ylidene) hydrazine (35): A suspension of *t*-butyl carbazate (1.00g, 7.56 mmol) and magnesium sulfate (182 mg, 1.51 mmol) in anhydrous acetone (7.5 mL) with catalytic amount of acetic acid (18.4 mg, 0.36 mmol) was refluxed for 1h. The reaction mixture was then cooled to room temperature and filtered off. Organic filtrate was evaporated under reduced pressure to afford white crystalline solid **35** (1.23 g, 94%). ¹H NMR (CDCl₃) δ 1.41 (s, 9H), 1.74 (s, 3H), 1.93 (s, 3H), 7.51 (br, s, 1H).

tert-Butyl-1-(cyclohexylmethyl)-2-(propan-2-ylidene)hydrazinecarboxylate (36): A suspension of compound **35** (496 mg, 2.88 mmol), potassium hydroxide (182 mg, 3.24) and *tetra* butyl ammonium hydrogen sulfate (11.38 mg, 0.29 mmol) in toluene (4 mL) was heated to 50 °C for 2h with vigorous stirring. To above reaction mixture (bromomethyl) cyclohexane (639.5 mg, 3.61 mmol) was added dropwise and heated to 80°C. After 2h, the reaction mixture was cooled to room temperature and diluted with EtOAc, washed with water, brine and dried over Na₂SO₄. The solvent was removed by rotary

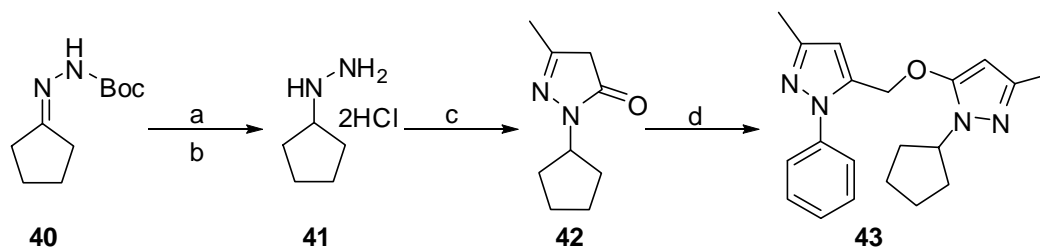
evaporation to give product **36** as yellow oil (720 mg, 95%). (Mixture of rotamers) ^1H NMR (CDCl_3) δ 0.84 - 1.07 (m, 2H), 1.08 - 1.32 (m, 4H), 1.44 and 1.50 (s, 9H), 1.57 - 1.77 (m, 5 H), 1.80 and 1.86 (s, 3 H), 2.03 and 2.06 (s, 3 H), 3.31 (d, $J = 8.00$ Hz, 2H).

(Cyclohexylmethyl) hydrazine dihydrochloride salt (37): To a flask containing compound **36** (800 mg, 2.98 mmol) was added 2N HCl in THF (217.54 mg, 5.96 mmol) at room temperature. The reaction mixture was then refluxed for 2h and after cooling the reaction solvent was evaporated under vacuum. The crude residue was dissolved in ethanol (3 mL) and cooled to 8°C (cooled water). Diethyl ether was then added slowly to precipitate dihydrochloride salt **37** as white solid (303 mg, 51%). ^1H NMR (DMSO-d_6) δ 0.84-0.93 (m, 2H), 1.04-1.22 (m, 3H), 1.58-1.74 (m, 6H), 2.72 (d, $J = 6.72$ Hz, 1H), 6.90 (br, s, 7H).

1-(Cyclohexylmethyl)-3-methyl-1H-pyrazol-5(4H)-one (38): To a solution compound **37** (150 mg, 0.74 mmol) in ethanol (3 mL), ethylacetoacetate (116.46 mg, 0.89 mmol) was added and refluxed for 2h. The solvent was removed by rotary evaporation and the resulting crude was purified by flash chromatography on silica gel using gradient 0-15% MeOH-DCM to afford compound **38** (42 mg, 29%). ^1H NMR (CDCl_3) δ 0.90-1.00 (m, 2H), 1.12-1.23 (m, 3H), 1.64-1.75 (m, 6H), 2.08 (s, 3H), 3.19 (s, 2H), 3.44 (d, $J = 7.08$ Hz, 2H).

1-(Cyclohexylmethyl)-3-methyl-5-((3-methyl-1-phenyl-1H-pyrazol-5-yl) methoxy)-1H-pyrazole (39): Compound **38** (40 mg, 0.20 mmol) and cesium carbonate (201.25mg, 0.61 mmol) were suspended in anhydrous ACN (2mL). Compound **15** synthesized from compound **14** (50 mg, 0.26 mmol) was

dissolved in 2mL of anhydrous ACN and added dropwise to above reaction suspension. The reaction was then heated to 60°C for overnight. The reaction solvent was removed by rotary evaporation and the resulting crude was purified by flash chromatography on silica gel using gradient 0-40% EtOAc-Hexanes to give yellow waxy product **39** (20 mg, 27%). ¹H NMR (CDCl₃) δ 0.80 - 0.98 (m, 2H) 1.05 - 1.29 (m, 5H) 1.58 - 1.87 (m, 5H) 2.18 (s, 3H) 2.37 (s, 3H) 3.62 (d, *J* = 7.28 Hz, 2H) 4.94 (s, 2H) 5.30 (s, 1H) 6.34 (s, 1H) 7.33 - 7.56 (m, 5H). ESI (+ve) (M+H⁺) calculated 365.23, found 365.36.



Scheme 4.12. Synthesis of compound **43**. Reagents and conditions: a. LAH, anhydrous THF, 0°C to room temperature, 30 min; b. 50%TFA in DCM, room temperature, 20 min c. ethylacetoacetate, ethanol, reflux; d. compound **15**, Cs₂CO₃, ACN, 45°C, 2 h.

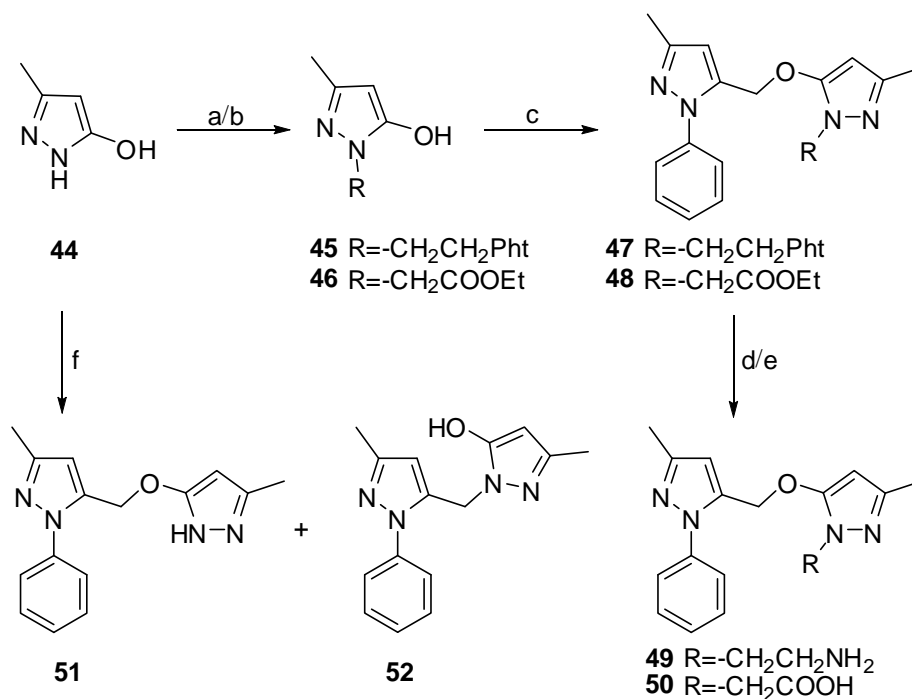
tert - Butyl 2-cyclopentylidenehydrazinecarboxylate (40): A suspension of *tert*-butyl carbazate (4.46 g, 33.77 mmol) and cyclopentanone (2.84 g, 33.77 mmol) in hexane (35 mL) was refluxed for 30 min. On completion, the reaction mixture was cooled and filtered. The white precipitate was collected and dried over vacuum to afford product **40** (6.4 g, 95%). ¹H NMR (CDCl₃) δ: 1.49 (s, 9H), 1.69-1.76 (m, 2H), 1.80-1.87 (m, 2H), 2.15 (t, *J* = 7.15 Hz, 2H), 2.45 (t, *J* = 7.28 Hz, 2H), 7.19 (br, s, 1H).

Cyclopentylhydrazine ditrifluoroacetate salt (41): To a suspension of LAH (268 mg, 7.06 mmol) in anhydrous THF (2 mL) at 0 °C, a THF (2 mL) solution of compound **40** (700 mg, 3.53 mmol) was added dropwise. After the addition, the reaction was warmed to room temperature and allowed to stir for additional 30 min. Reaction was then cooled to 0°C and quenched with saturated solution of Na₂SO₄. The resultant precipitate was filtered off under vacuum and the filtrate was evaporated to dryness and the resulting residue was carried to next step without any purification and characterization. The resulting residue was then dissolved in DCM (4 mL) and cooled to 0°C. A mixture of TFA and DCM (1:1) (1 mL) was added to it and stirred at room temperature for 20 min. On completion, the reaction solvent was removed

under vacuum to yield **41** (932 mg, crude yield 80%) and it was used in the next step without any purification.

1-Cyclopentyl-3-methyl-1H-pyrazol-5(4H)-one (42): To a solution of compound **41** (932 mg, 2.83 mmol) in ethanol (5 mL) ethylacetoacetate (49.74 mg, 3.11 mmol) was added. The reaction mixture was then refluxed overnight. The reaction solvent was removed under vacuum and the resulting residue was purified by flash chromatography on silica gel using gradient 0-50% EtOAc-Hexanes to give product **42** (60 mg, 13%). ¹H NMR (CDCl₃) δ 1.58-1.59 (m, 2H), 1.79-1.90 (m, 6H), 2.09 (s, 3H), 3.19 (s, 2H), 4.53-4.57 (m, 1H).

1-Cyclopentyl-3-methyl-5-((3-methyl-1-phenyl-1H-pyrazol-5-yl)methoxy)-1H-pyrazole (43): Compound **42** (60 mg, 0.36mmol) and potassium carbonate (54.19mg, 0.39 mmol) were suspended in anhydrous DMF (1 mL). The reactant **16** synthesized from compound **14** (50 mg, 0.26 mmol) was dissolved in 1mL of anhydrous DMF and added dropwise to above reaction suspension. The reaction was then heated to 45°C for 2h. The reaction solvent was removed by rotary evaporation and the resulting crude was purified by flash chromatography on silica gel using gradient 0-40% EtOAc-Hexanes to give yellow waxy product **43** (42 mg, 35%). ¹H NMR (CDCl₃) δ 1.47 - 1.65 (m, 2H), 1.77 - 1.98 (m, 6H), 2.13 - 2.22 (m, 3H), 2.29 - 2.43 (m, 3H), 4.35 - 4.51 (m, 1H), 4.95 (s, 2H), 5.25 - 5.36 (m, 1H), 6.35 (s, 1H), 7.34 - 7.56 (m, 5H). ESI (+ve) (M+H⁺) calculated 337.20, found, 337.34.



Scheme 4.13. Synthesis of compounds **49-52**. Reagents and conditions: a. *N*-(2-bromo ethyl) phthalimide, 1,4-dioxane, MW 180 °C, 60 min; b. ethylbromoacetate, reflux, 4 h; c. Compound 15, Cs₂CO₃, ACN, 60°C, overnight; d. NH₂NH₂.H₂O, methanol, 0°C to room temperature, overnight; e. LiOH, THF:MeOH (1:1), 0°C to room temperature, overnight; f. compound 16, Cs₂CO₃, ACN, 60°C, 2 h.

3-Methyl-1H-pyrazol-5-ol (44): To a suspension of hydrazine hydrate (2601 mg, 20 mmol) in methanol (5 mL) ethyl-3-oxobutanoate (1.00 g, 20 mmol) was added. The reaction mixture was then refluxed for 2h. The reaction solvent was evaporated under vacuum to afford white solid product **44** (1.92 g, 98%). ¹H NMR (CDCl₃) δ 2.08 (s, 3H), 5.20 (s, 1H), 10.07 (br, s, 1H).

2-(2-(5-hydroxy-3-methyl-1H-pyrazol-1-yl)ethyl)isoindoline-1,3-dione

(45): Compound **44** (500 mg, 5.10 mmol) and *N*-(2-bromo ethyl)-phthalimide (1.29 g, 5.58 mmol) were suspended in 1,4-dioxane (3mL) in a Biotage Initiator microwave reaction vial containing a Teflon stirrer bar. The vial was capped and the reaction mixture was transferred to the microwave and irradiated at 180°C for 60 min at normal absorption with cooling activated.

The reaction solvent was evaporated and the resulting crude was purified by flash chromatography on silica gel using gradient 0-10% MeOH-DCM to afford product **45** (335 mg, 24%). ^1H NMR (CDCl_3) δ 1.98 (s, 3H), 3.10 (s, 2H), 3.94 (s, 4H), 7.68-7.70 (m, 2H), 7.80-7.82 (m, 2H).

Ethyl 2-(3-methyl-5-oxo-4,5-dihydro-1H-pyrazol-1-yl)acetate (46): To a flask containing compound **44** (547 mg, 5.58 mmol) was added ethylbromoacetate (932.18 mg, 5.58 mmol) and refluxed for 4h. Then, the reaction was cooled, diluted with ice-cooled water (2 mL), neutralized with cold saturated solution of NaHCO_3 and stirred for 15 min at room temperature. Aqueous reaction mixture was extracted with EtOAc. Organic layer was washed with brine, dried over Na_2SO_4 and removed by rotary evaporation. The resultant crude was then purified by flash chromatography on silica gel using gradient 0-10% MeOH-DCM to yield compound **46** as white solid (138 mg, 13%). ^1H NMR (CDCl_3) δ 1.28 (t, $J = 1.00$ Hz, 8H), 2.15 (s, 3H), 3.26 (br, s, 1H), 3.73 (br, s, 1H), 4.22 (q, $J = 8.00$ Hz, 2H), 4.45 (s, 2H).

2-(2-(3-methyl-5-((3-methyl-1-phenyl-1H-pyrazol-5-yl)methoxy)-1H-pyrazol-1-yl)ethyl)isoindoline-1,3-dione (47): Compound **45** (144 mg, 0.53 mmol) and cesium carbonate (519.03 mg, 1.59 mmol) were suspended in anhydrous ACN (2mL). Compound **15** synthesized from compound **14** (100 mg, 0.51 mmol) was dissolved in 2mL of anhydrous ACN and added dropwise to above reaction suspension. The reaction was then heated to 60°C for overnight. The reaction solvent was removed by rotary evaporation and the resulting crude was purified by flash chromatography on silica gel using gradient 0-50% EtOAc-Hexanes to afford product **47** (40.61 mg, 17%). ^1H NMR (CDCl_3) δ 1.99 (s, 3H), 2.28 (s, 3H), 3.88-3.91 (t, $J = 5.7$ Hz, 2H), 4.09-

4.12 (t, $J = 5.2$ Hz, 2H), 4.79 (s, 2H), 5.24 (s, 1H), 6.12 (s, 1H), 7.31-7.35 (m, 1H), 7.38-7.45 (m, 4H), 7.61-7.63 (m, 2H), 7.70-7.72 (m, 2H).

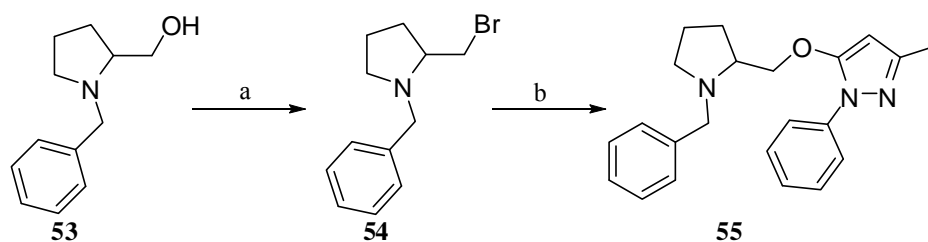
Ethyl-2-(3-methyl-5-((3-methyl-1-phenyl-1*H*-pyrazol-5-yl)methoxy)-1*H*-pyrazol-1-yl)acetate (48): Compound **46** (40mg, 0.21 mmol) and cesium carbonate (212.10 mg, 0.65 mmol) were suspended in anhydrous ACN (2mL). Compound **15** synthesized from compound **14** (41 mg, 0.21 mmol) was dissolved in 2mL of anhydrous ACN and added dropwise to above reaction suspension. The reaction was then heated to 60°C for 2h. The reaction solvent was removed by rotary evaporation and the resulting crude was purified by flash chromatography on silica gel using gradient 0-50% EtOAc-Hexanes to give product **48** (24.1 mg, 31%). ¹H NMR (CDCl₃) δ 1.21-1.25 (t, $J = 7.12$ Hz, 3H), 2.18 (s, 3H), 2.34(s, 3H), 4.15-4.20 (q, $J = 7.12, 7.16$ Hz, 2H), 4.58 (s, 2H), 4.96 (s, 2H), 5.35 (s, 1H), 6.33 (s, 1H), 7.34-7.38 (m, 1H), 7.42-7.48 (m, 4H).

2-(3-Methyl-5-((3-methyl-1-phenyl-1*H*-pyrazol-5-yl)methoxy)-1*H*-pyrazol-1-yl) ethanamine (49). To a cold solution of compound **47** (40.61 mg, 0.09 mmol) in methanol (2 mL) hydrazine hydrate (102.10 mg, 3.18 mmol) was added. The reaction was warmed to room temperature and stirred overnight. The reaction solvent was evaporated to dryness and the resulting crude was purified by flash chromatography on silica gel using gradient 0-10% MeOH-DCM to give oily product **49** (23 mg, 80%). ¹H NMR (CDCl₃) δ 2.15 (s, 3H), 2.33 (s, 3H), 2.95 (br, m, 2H), 3.81-3.84 (t, $J = 5.88$ Hz, 2H), 4.96 (s, 2H), 5.31 (s, 1H), 6.32 (s, 1H), 7.34-7.37 (m, 1H), 7.41-7.48 (m, 4H).

2-(3-Methyl-5-((3-methyl-1-phenyl-1*H*-pyrazol-5-yl)methoxy)-1*H*-pyrazol-1-yl)acetic acid (50): Compound **48** (24.1 mg, 0.07 mmol) was dissolved in a mixture of MeOH:THF (1:1) (2 mL). Lithium hydroxide (29 mg, 1.62 mmol) was added to the above reaction mixture at 0°C. The reaction was then warmed up to room temperature and stirred overnight. The solvent was removed under vacuum; water (1 mL) was added and neutralized with 10% HCl at 0°C. Aqueous layer was extracted with EtOAc. Organic layer was removed and the resultant crude was purified by short column chromatography on silica gel using gradient 1-10% MeOH-DCM to obtain compound **50** (21 mg, 95%) as yellow solid. ¹H NMR (CDCl₃) δ 2.16 (s, 3H), 2.34 (s, 3H), 4.63 (s, 2H), 4.96 (s, 2H), 5.34 (s, 1H), 6.33 (s, 1H), 7.34-7.35 (m, 1H), 7.40-7.44 (m, 4H).

3-Methyl-5-((3-methyl-1*H*-pyrazol-5-yloxy)methyl)-1-phenyl-1*H*-pyrazole (51) and **3-methyl-1-((3-methyl-1-phenyl-1*H*-pyrazol-5-yl)methyl)-1*H*-pyrazol-5-ol (52)**: Compound **44** (104.07mg, 1.06 mmol) and cesium carbonate (346 mg, 1.06 mmol) were suspended in anhydrous ACN (2mL). Compound **16** synthesized from compound **14** (200 mg, 1.06 mmol) was dissolved in 2mL of anhydrous ACN and added dropwise to above reaction suspension. The reaction was then heated to 80°C for 2h. The reaction solvent was removed by rotary evaporation and the resulting crude was purified by column chromatography on silica gel using gradient 0-3% MeOH-DCM to give products **51** (19 mg, 7%) and **52** (8 mg, 3%), as white solid. Compound **51**, ¹H NMR (CDCl₃) δ 2.23 (s, 3H), 2.34 (s, 3H), 5.11 (s, 2H), 5.52 (s, 1H), 6.37 (s, 1H), 7.30 - 7.36 (m, 1H), 7.42 (t, *J* = 7.91 Hz, 2H), 7.55 (d, *J* = 7.53 Hz, 2H). Compound **52**; ¹H NMR (CDCl₃) δ 1.92 (s, 3H), 2.28 (s, 3H), 5.00

(s, 2H), 5.40 (s, 1H), 5.97 (s, 1H), 7.32 - 7.58 (m, 5H). Compound **51**, ESI (+ve) ($M+H^+$) calculated 312.18, found 312.28. Compound **52**, ESI (+ve) ($M+H^+$) calculated 327.14, found 327.26.



Scheme 4.14. Synthesis of compound **55**. Reagents and conditions: a. CBr_4 , PPh_3 , anhydrous THF, 0°C to room temperature, overnight; b. edaravone, K_2CO_3 , DMF, 50°C , overnight.

1-Benzyl-2-(bromomethyl)pyrrolidine (54): In a flask containing carbon tetrabromide (1.69 g, 5.12 mmol) and triphenylphosphine (1.43 g, 5.49 mmol) in anhydrous THF (5 mL) (1-benzylpyrrolidin-2-yl)methanol (700 mg, 3.66 mmol) was added at 0°C . The reaction was allowed to stir at room temperature for overnight. The reaction mixture was purified by column chromatography 1-10% EtOAc-Hexanes to yield compound **54** (735 mg, 79%). ^1H NMR (CDCl_3) δ 1.55 - 1.84 (m, 3H), 2.13 (t, $J = 10.04$ Hz, 1H), 2.20 - 2.30 (m, 1H), 2.36 (t, $J = 10.42$ Hz, 1H), 2.75 (d, $J = 11.04$ Hz, 1H), 3.10 (d, $J = 8.78$ Hz, 1H), 3.54 (s, 2H), 4.06 - 4.19 (m, 1H), 7.19 - 7.39 (m, 5H).

5-((1-Benzylpyrrolidin-2-yl)methoxy)-3-methyl-1-phenyl-1H-pyrazole

(55): To a suspension of edaravone (34.32 mg, 0.19 mmol) and potassium carbonate (81.50 mg, 0.59 mmol) in anhydrous DMF (1 mL), compound **54** (50 mg, 0.19 mmol) dissolved in DMF (1 mL) was added. The reaction was heated overnight at 50°C . On completion, the reaction was cooled to the room temperature and diluted with 5 mL of water. The aqueous layer was extracted with EtOAc which was further washed with brine, dried over Na_2SO_4 and evaporated under vacuum. The resulting crude was then purified by column chromatography 1-25% EtOAc-Hexanes to afford compound **55** (26.50 mg, 39%). NMR (CDCl_3) δ 1.24-1.74 (m, 3H), 1.96-2.01 (m, 1H), 2.24 and 2.26

(s, 3H), 2.30-2.38 (m, 2H), 2.90-3.00 and 3.49 (m, 2H), 3.53 and 3.99 (s, 2H), 3.90-4.29 (m, 1H), 5.37 and 5.44 (s, 1H), 7.17-7.47 (m, 8H), 7.66-7.75 (m, 2H). ESI (+ve) (M+H⁺) calculated 348.20, found 348.34.

Semi - preparatory purification method for compound 9.

Column = Spherisorb C18-20*250 mm, Flow rate 8ml/min. Solvent I = water + 0.05%TFA and Solvent II = ACN+0.05%TFA.

Table 4.3: Semi - preparatory purification method for compound 9

<i>Time (min)</i>	<i>I</i>	<i>II</i>
0	70%	30%
30	15%	85%
45	15%	85%

Purity of the synthesized compounds:

Purity was evaluated on Water LC-MS system (Waters™ 2545 binary gradient module) with a photodiode array detector using a X-Bridge C18 column (4.6 x 150 mm, 5µm). Solvent **I** Water with 0.05% TFA and Solvent **II** Acetonitrile with 0.05% TFA. All HPLC solvents were filtered through the membrane filters (47 mm GHP 0.45µm, Pall Corporation). Injection samples were filtered using Pall Acrodisc ® Syringe filters 4 mm PTFE (0.2 µm). The HPLC methods used for the purity assessment are as follow as:

Table 4.4: HPLC methods used for the purity assessment of synthesized compounds

Method	Method Type	Method Detail		
		<i>Time(min)</i>	<i>I</i>	<i>II</i>
A	Gradient	0	75%	25%
		8	5%	95%
		10	5%	95%
F	Isocratic	35% I + 65% II		
H	Isocratic	45% I + 55% II		
I	Gradient	<i>Time(min)</i>	<i>I</i>	<i>II</i>
		0	55%	45%
		10	5%	95%
J	Gradient	<i>Time(min)</i>	<i>I</i>	<i>II</i>
		0	70%	30%
		10	5%	95%
K	Isocratic	60% I + 40% II		
L	Gradient	<i>Time(min)</i>	<i>I</i>	<i>II</i>
		0	80%	20%
		10	5%	95%
P	Gradient	<i>Time(min)</i>	<i>I</i>	<i>II</i>
		0	50%	50%
		8	2%	98%
		10	2%	98%
R	Isocratic	50% I + 50% II		
S	Gradient	<i>Time(min)</i>	<i>I</i>	<i>II</i>
		0	90%	10%
		10	5%	95%
T	Isocratic	40% I + 60% II		
U	Gradient	<i>Time(min)</i>	<i>I</i>	<i>II</i>
		0	40%	60%
		8	2%	98%
		10	2%	98%

Table 4.5: Purity data for the first generation synthesized compounds

Compound No.	Method	Rt (min)	Purity
4i	A	8.33	84%
	L	9.67	81%
4ii	K	5.11	>99.99%
	R	2.98	>99.99%
5i	A	9.62	96%
	L	11.17	95.21%
5iii	F	7.17	92%
	T	8.26	92%
5iv (Mix of polysulfides)	E	2.96	59% (disulfide)
	R	3.04	60% (disulfide)
9	E	5.66	>99.99%
	R	9.93	>99.99%
10	E	7.39	96.36%
	U	5.62	95.32%

Table 4.6: Purity data for the second generation synthesized compounds

Compound No.	Method	Rt (min)	Purity
17	R	4.88	96.41%
	P	4.06	95.88%
18	R	6.91	>99.99%
	P	4.89	>96.37%
11	J	3.19	91.24%
	L	5.30	90.06%
22	R	6.33	>99.99%
	P	4.65	>99.99%
25	J	7.99	95.91%
	F	3.91	>99.99%
26	J	4.92	>99.99%
	K	3.95	>99.99%
30	R	11.11	93.50
	P	5.80	92.82
34	H	5.21	>99.99%
	I	6.49	>99.99%
39	R	6.28	>99.99%
	P	4.57	>99.99%
43	R	4.37	>99.99%
	P	3.79	>99.99%
39	J	2.87	85.44%
	S	5.42	84.81%
50	J	4.21	97.91%
	S	6.47	96.01%
51	A	5.15	97.89%
	R	2.76	>99.99%
52	A	3.67	93.38%
	F	2.94	91.72%
55 (Mix of rotamers)	A	4.12	96.26%
	F	3.08	>99.99%

4.3.2 *Monocyte monolayer assay*

The monocyte monolayer assay (MMA) was performed by Donald Branch laboratory, as previously described¹⁸⁻²¹ with slight modification. Briefly, peripheral blood mononuclear cells (PBMC) containing monocytes were isolated by ficoll-paque density gradient centrifugation and incubated overnight at 37 °C under 5% CO₂ atmosphere. PBMCs were then layered onto chamber slides (Labtek, Thermo Scientific) and incubated at 37 °C, 5% CO₂ for 1 hr to allow the monocytes to adhere. Following an aspiration of non-adherent cells, compounds were added at various concentrations to the adhered cells and further incubated for an additional hour. The compounds were aspirated and the monocytes treated with anti-D opsonized RBCs at the aforementioned incubation conditions for an additional 2 hrs. The slides were analyzed under phase microscopy for phagocytosis. A minimum of 100 monocytes were counted per sample and the number of observed RBCs that were phagocytized were counted and normalized to a positive control to generate a phagocytosis index. Percent inhibition of phagocytosis was calculated as the percentage of control phagocytosis (phagocytosis of opsonized RBCs with compound diluent only).

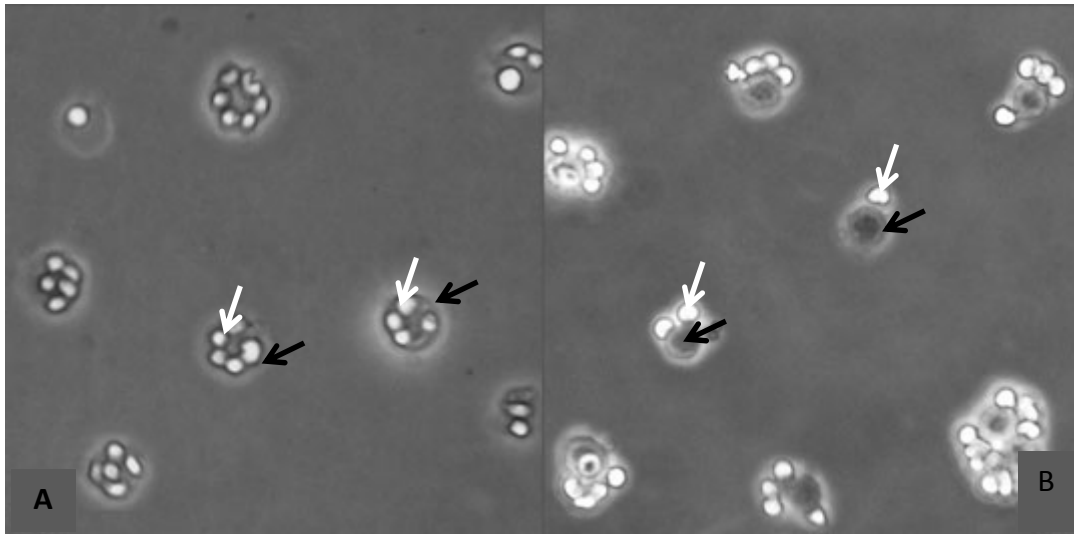


Figure 4.5. MMA slide under microscope. (A) Opsonised RBCs (white arrows) phagocytised by Mφ (black arrows); (B) Opsonised RBCs (white arrows) attached on Mφ (black arrows)²⁰

4.4. Chemistry Discussion

A series of 4-acyl substituted analogues of 1-phenyl-3-methyl-5-pyrazolones (Edaravone) (**1**) were synthesized in parallel using Mettler-Toledo Bohdan synthesizer. (5-hydroxy-3-methyl-1-phenyl-1*H*-pyrazol-4-yl) aryl methanone derivatives were synthesized using Jensen method by heating aryl chlorides with edaravone (**1**) in the presence of Ca(OH)₂ in high yields (Scheme 4.1 Scheme 4.1).²⁶ Reaction of Edaravone (**1**) with various carbamoyl chlorides under Jensen conditions afforded O-5 carbamates instead of C-carbamoylated desired product. Therefore, an alternative route was approached to synthesis C4-carbamoylated compounds **5iv** and **5v**. An in-situ reaction was performed to formylate and chlorinate the electron rich pyrazol-5-one (**1**) at C4 and C5 position respectively using Vilsmeier-Hacck reaction conditions (DMF-POCl₃).²⁷ The resultant aldehyde **5** was then oxidized by heating with KMnO₄ under aqueous conditions to obtain **6**.²⁸ Subsequent reaction of the carboxylic acid **6** and the secondary amines (morpholine and piperidine) with HATU and DIPEA at ambient temperature yielded 80-85% of compounds **3iv** and **3v**. Alternatively, aryl methanone derivatives **3i-iii** was chlorinated with phosphorous oxychloride to achieve the corresponding (5-chloro-3-methyl-1-phenyl-1*H*-pyrazo-4-yl) aryl methanone derivatives (**3i-iii**).²⁹ The temperature and the time required for chlorination varied based on the aromaticity and the acid stability of the heteroaryl groups at C4 position of pyrazole derivatives **2i-iii**. Due to the poor yields in chlorination reaction, it was decided to change the leaving group at C-5 position of the 4-acylated pyrazole compounds **2i-iii**. Compound **2iii** was tosylated in quantitative yields

but it did not work in the subsequent thiolation reaction. Several brominating conditions such as PBr_3 , CBr_4 and PPh_3 were tried to halogenate the C5 position of **2iii** but none gave positive results. Therefore it was decided to follow chlorination using POCl_3 method. 4-Acyl-5-chloro-pyrazole derivatives **3i-iii** was then treated with sodium sulfide to furnish thiolated pyrazole **4i-ii** and **5iii**. For C4-carbamoylated pyrazole derivatives **3iv-v** a combination of sodium sulfide with elemental sulfur was used for substitution of chloride.^{30,31} The hindrance in the nucleophilic displacement of the chloride by the sulfide anion in the compounds **3v-vi** could be due to the weaker activating nature of the carbamoyl group at C4. Due to the enhanced negative charge distribution polysulfide ions are more nucleophilic than the sulfide. Iso-oxazole as an acyl group at C4 of compound **3ii** was isolated as free sulfide **4ii**. Whereas the compounds **5i** and **5iii** were obtained as mixture of sulfhydryl and disulfide, confirmed by LCMS (Table 4.2) (Figure 4.6 and 4.7). TLC and NMR as initial characterization tools were insufficient to distinguish between the mono and polysulfide. Polysulfide mixture of compound **5v** was reduced using sodium borohydride in ethanol (Scheme 4.2). Resultant free sulfide **8** and disulfide **9** from **5v** were separated by semi-preparatory column on HPLC. Compound **8** was dimerized to **9** during the solvent evaporation step. Disulfide **5i** of the prototype compound **4i** was synthesized by heating it in DMF at 100 °C. The oxidation reaction of **4i** was monitored by the HPLC (Figure 4.8). Compound **10** was prepared as shown in Scheme 4.3. Edaravone (**1**) was thionated with Lawesson's reagent in 1,4-Dioxane at 101 °C, followed by overnight stirring in methanol gave compound **10**. Product **10** was purified initially on alumina column followed by silica gel column.

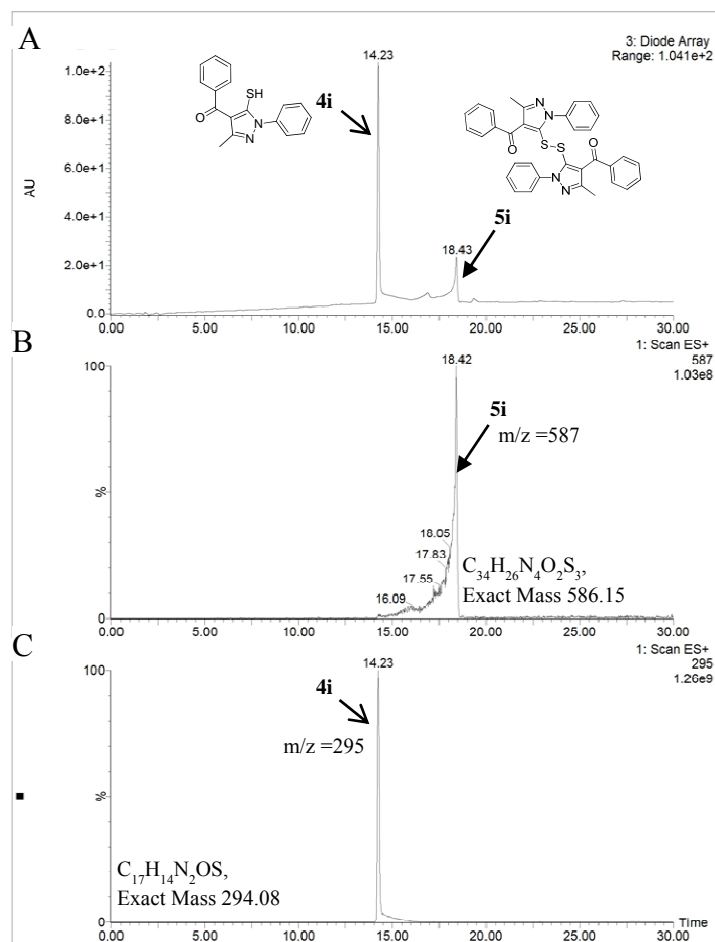


Figure 4.6: (A) Chromatogram of purchased **4i** found to be a mixture of sulfide **4i** and disulfide **5i** (B) Mass Spectrum of peak 18.43 min **5i**, (C) Mass Spectrum of peak 14.23 min **4i**.

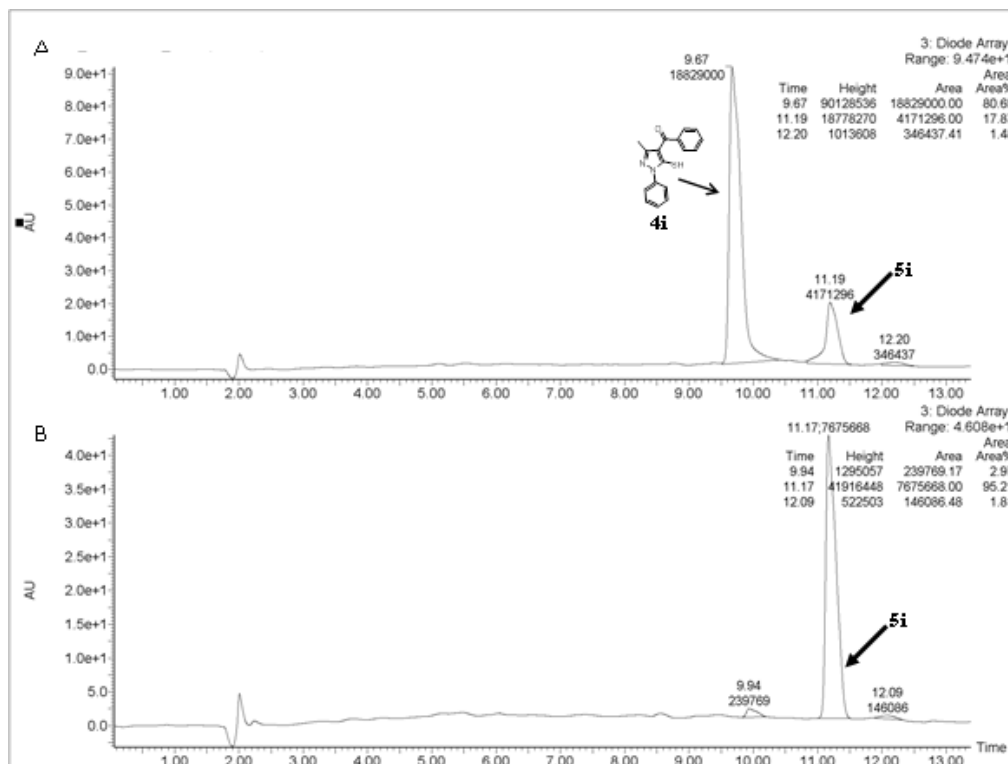


Figure 4.7: Chromatograph of compounds (A) **4i** and (B) **5ii**.

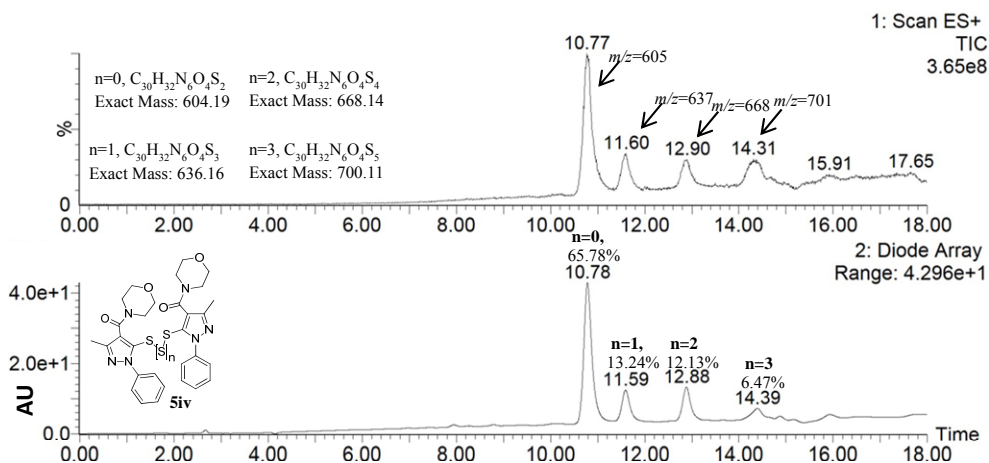


Figure 4.8: Chromatograph of compound **5iv** as polysulfide mixture.

From the first generation of library of derivatives designed based on the 4-benzoyl-5-mercapto-3-methyl-1-phenyl pyrazole (**4i**), as a lead candidate inhibiting Fc γ -receptor mediated phagocytosis, directed that it was the homodimer **5i** with disulfide bridge capable of inhibiting the phagocytosis of opsonized RBCs by monocytes and not the free thiol compound **4i**. As compared to compound **5i** its analogue **10**, devoid of C4 substitution, exhibited high efficacy in inhibiting Fc γ -receptor mediated phagocytosis. Therefore, it was decided to build a library of compounds based on the dimer scaffold **10** and identify structure activity relationships for the synthesized analogues that could enhance the inhibition of Fc γ -receptor mediated phagocytosis to ameliorate idiopathic immune thrombocytopenia (ITP). Introductory pharmaco-modulation considered around the scaffold **10** are (a) substituting the disulfide bridge of the homodimer **10** to ethylene and ether (Scheme 4.5 and 4.6), (b) altering the chain length between the two pyrazole moieties (Scheme 4.7 and 4.8) (c) varying the N1 substitution of one of the pyrazole nucleus of heterodimers with ether spacer arm (Scheme 4.9-4.13) and

(d) changing one of the pyrazole nucleus of heterodimers with ether spacer arm (Scheme 4.14) (Figure 4.4).

Scheme 4.4 illustrates the synthesis of the common intermediates **15** and **16** for building the library of compounds inhibiting Fcγ-receptor mediated phagocytosis. The β-methoxy vinyl trichloromethyl ketone (**11**) was synthesized by acylation of the 2-methoxy propene with trichloroacetyl chloride.^{32,33} Microwave assisted cyclocondensation of the 1,3-dielectrophilic building block **11** with ethylacetoacetate yielded compound **12**. The trichloromethyl pyrazole derivative **12** on refluxing with ethanol gave compound **13** in high yields.³⁴ On reduction of ethoxycarbonyl group of compound **13** by lithium aluminium hydride (LAH) yielded intermediate **14**. Treatment of compound **14** with phosphorus tribromide or methanesulfonyl chloride gave compound **15** and **16** respectively. Scheme 4.5 outlines the synthesis of homodimer **17** with ethylene bridge. Intermediate **15** on treating with magnesium turnings led to the formation of in-situ Grignard reagent. The homocoupling of the resultant Grignard reagent was accelerated by microwave heating followed by stirring at room temperature for 42 h to afford target compound **17**. Alkylation of edaravone (**1**) with the intermediate **16** in the presence of Cs₂CO₃ at 60 °C in anhydrous acetonitrile (ACN) gave product **18** (Scheme 6).

To substantiate the role of the spacer arm, compounds with spacer length 3 atoms (**21**), 4 atoms (**22**) and 1 atom (**26**), were synthesized. As shown in the Scheme 4.7, compound **19** was obtained after the Mitsunobu reaction of compound **14** and phthalimide.³⁵ Treatment of **19** with hydrazine hydrate resulted in amino compound **20**. N-alkylation of **20** with intermediate **15** in the

presence of inorganic base K_2CO_3 gave compound **21** with a small percentage of trisubstituted side-product. Edaravone (**1**) on refluxing with phosphorus oxychloride resulted in compound **23** as yellow oil.³⁶ Facile nitration of compound **23** was achieved by nitrating mixture of conc. HNO_3 and acetic anhydride.³⁷ The electron-withdrawing nature of C4 nitro moiety of compound **24** facilitated the nucleophilic substitution at C5 by phenolic OH of edaravone under microwave heating to afford compound **25**. Tin (II) chloride reduction of nitropyrazole **25** provided heterodimer **26** with one atom as spacer arm. Compound **22** with four atom spacer was synthesized by refluxing 1,2-dibromoethane with edaravone under alkaline condition (Scheme 4.8). Hydrazine **28** was synthesized by conventional route of diazotization of p-nitroaniline (**27**) followed by tin (II) chloride reduction (Scheme 4.9).³⁸ Pyrazole **29** was prepared by Knorr reaction of hydrazine **28** and ethylacetoacetate.³⁹ Alkylation of p-nitrophenyl N1-substituted pyrazole **29** with mesylated intermediate **16** afforded the final compound **30**.

Scheme 4.10 portrays the synthetic strategy for compound **34**. Cyclocondensation of hydrazine hydrochloride with β -methoxy vinyl trichloromethyl ketone (**11**) in ethanol yielded compound **31**, as previously reported literature.³⁴ N1-benylation of compound **31** with benzyl bromide in the presence of K_2CO_3 gave product **32**. The ethoxycarbonyl group of **32** was reduced with LAH to obtain compound **33**. Mesylation of N1-benzyl substituted pyrazole **33** followed by alkylation with edaravone provided final compound **34**. Synthesis of compound **39** (Scheme 4.11) began with the preparation of hydrazone **35** by protecting the amino functional group of *tert*-butyl carbazate with isopropylidene, as previously reported in the literature.⁴⁰

Alkylation of hydrazone **35** with (bromomethyl)cyclohexane was accomplished in the presence potassium hydroxide, *tetra*-butylammonium hydrogen sulfate (Bu_4NHSO_4), at 80°C in anhydrous toluene to afford **36**. The catalyst Bu_4NHSO_4 was used to enhance the solubility and the reaction rate.⁴¹ After the initial aqueous work up of compound **36** the boc and isopropylidene groups were removed by refluxing in $2N$ HCl in THF.⁴⁰ (Cyclohexylmethyl) hydrazine dihydrochloride salt (**37**) obtained after acidic deprotection was subjected to cyclocondensation with ethylacetoacetate in ethanol to give compound **38**. N1-cyclohexylmethyl substituted pyrazolone **38** was then alkylated with intermediate **15** under basic condition to give the target product **39**. Scheme 4.12 depicts the synthesis of the heterodimer compound **43** with ether spacer. The desired imine **40** was obtained by nucleophilic addition of *tert*-butyl carbazate with cyclopentanone followed by dehydration.⁴² Imine **40** reduction with LAH followed by trifluoroacetic acid boc deprotection gave dihydrochloride salt of cyclopentane hydrazine (**41**). Compound **41** obtained after cyclocondensation of **42** with ethylacetoacetate, was alkylated under basic condition with intermediate **15** to furnish product **43**.

3-Methyl-1*H*-pyrazol-5-ol (**44**) was obtained by Knorr reaction of hydrazine hydrochloride salt with ethylacetoacetate in high yield (Scheme 4.13).⁴³ The key intermediate **44** was used for the synthesis of novel N1-substituted pyrazole derivatives **45**. *N*-(2-bromo ethyl) phthalimide on microwave heating at 180°C for 60 min with pyrazole **44** in 1,4-dioxane yielded compound **45**. The TLC profile for the reaction of **45** without base was simple and clean. Compound **46** was obtained by refluxing neat ethylbromoacetate with pyrazole **44**, as white solid. N1-alkyl substituted

pyrazole derivatives **45** and **46** were alkylated with compound **15** in the presence of Cs_2CO_3 in anhydrous ACN at 60 °C to yield compounds **47** and **48** respectively. Strict anhydrous conditions were maintained for synthesis of compound **47** because traces of moisture in the presence of base lead to the partial hydrolysis of the phthalimide ring leading to acidic side product positive to bromocresol green stain on TLC. Formation of the partial hydrolyzed phthalimide side product of **47** was unequivocally confirmed by mass spectrometry. The amino group of compound **47** was unmasked on treatment with hydrazine hydrate in methanol procuring compound **49**. Alkaline hydrolysis of **48** followed by neutralization with 10% HCl yielded target compound **50**. Alkylation of compound **44** with intermediate **16** yielded a mixture of two major regio isomers **51** and **52**. O-alkylated isomer **51** and N1-alkylated isomer **52** were unambiguously characterized by the ^1H NMR. To evaluate the importance of the pyrazole nucleus, one of the pyrazole rings was substituted to pyrrolidine as shown in Scheme 14. Commercially available (1-benzylpyrrolidin-2-yl)methanol **53** was brominated by classical Appel reaction conditions, i.e. carbon tetrabromide (CBr_4) and triphenylphosphine (PPh_3), and intermediate **54** was used for alkylation of edaravone to furnish compound **55**.⁴⁴

4.5. Result, discussion and conclusion

Table 4.7: Biological activity for first generation compounds **4i-4ii**, **5i**, **5iii-iv**, **9** and **10** at 5 μ M concentration, in comparison to the positive control IVIG. Results represent the mean percentage phagocytosis inhibition \pm SEM of three independent experiments.

Compound	%Inhibition Phagocytosis	SEM
IVIG	94	
4i	0	10%
5i	22	7%
5iii	19	4%
5iv	20	13%
9	34	7%
10	43	4%

Table 4.8: Biological activity for second generation inhibitors at 5 μ M concentration, in comparison to the positive control IVIG. Results represent the mean percentage phagocytosis inhibition \pm SEM of three independent experiments.

Compound	%Inhibition of Phagocytosis	SEM
IVIG	94	
17	16	11%
18	14	8%
21	20	14%
32	4	3%
25	12	8%
26	2	4%
30	16	3%
34	0	17%
39	45	5%
43	17	2%
39	33	2%
50	10	5%
51	6	4%
52	58	4%
55	15	14%

The action of the described derivatives to inhibit Fc γ receptor-mediated phagocytosis was evaluated by MMA assay and is shown in Table 4.7. The lead molecule **4i**, entirely lacked activity at 5 μ M. But **4i** showed a significant activity at 1mM concentration (Transfusion, 2005). A thorough chromatographic analysis of **4i** revealed that the compound was a mixture of thiol **4i** and disulfide **5i** (18%) (Figure 4.6). Prior work done by Branch et al proved that disulfides (**a-d**, Chart 4.1) were able to inhibit the Fc γ receptor mediated phagocytosis using the in-vitro MMA. Since **4i** was active only at a high concentration, the observed activity was thought due to the disulfide **5i** present in the preparation. Therefore, disulfide **5i** was synthesized and tested in the MMA for its potential to inhibit phagocytosis of anti-D opsonized human RBCs. Compound **5i** effectively inhibited Fc γ receptor-mediated phagocytosis of opsonized RBCs at 5 μ M concentration (Table 4.7). Analogue **4ii** of the lead compound with iso-oxazole at C4 failed to show activity at 5 μ M concentration. Compound **5iii** with 2-thienyl acyl group at C4 was found to inhibit phagocytosis similar to **5i** at 5 μ M concentration. This further gave assurance that the compounds with disulfide functional groups are those able to inhibit the Fc γ receptor-mediated phagocytosis. If one assumes that the thiol/disulfide exchange between the disulfide compounds and the cell surface protein thiol was the mode of action of the above compounds (**5i** and **5iii**) then compounds with trisulfides, tetrasulfides, etc. should be active too. The S-S bond in polysulfides ($n \geq 1$, Scheme 4.1) is longer and weaker than in disulfides. Polysulfides are more reactive towards protein thiol as the dissociation energy of S-S bond in polysulfide (138-151kJ mol⁻¹)⁴⁵ is lower than in disulfide (272-293 kJmol⁻¹).⁴⁵ Therefore, it was decided to test a

polysulfide for its ability to inhibit phagocytosis in the in-vitro MMA. Carbamoylated derivative **5iv** with morpholine at C4, a mixture of polysulfide, was able to inhibit 20% of phagocytosis at 5 μ M. Compared with **5iv**, carbamoylated analogue **9** with piperidine at C4 was purely disulfide and inhibited 34% phagocytosis of anti-D opsonized RBCs. One of the reasons for the low activity of compound **5iv** (with 65% active disulfide) could be that the disulfide might be involved in more than one mechanism along with thiol/disulfide exchange in inhibiting Fc γ receptor-dependent phagocytosis. Intriguingly, compound **10** devoid of any C4 substitution was found to be the most active inhibitor of Fc γ receptor-mediated phagocytosis of human RBCs with IC₅₀ of 100 nM.

The preliminary study in search of small molecule probes inhibiting Fc γ receptor-mediated phagocytosis of anti-D opsonized human RBCs in-vitro, indicated that the substitution at C4 of the pyrazole moiety in the disulfide dimers influenced the potency in the increasing order of **5i** < **5iii** < **9** < **10**. Due to robust analytical chromatography methods and screening assay it was possible to discover a novel scaffold **10** with IC₅₀ 100 nM inhibiting Fc γ receptor-mediated phagocytosis, as an a potential candidate for further study as an alternative therapeutic for ITP. Second step in this search was aimed at exploring the structure-activity relationship around the lead molecule **10** and develop a potential drug candidate for ITP.

Establishment of the pharmacophore: On analysis of the first generation sulfhydryl (**4i-ii**) and disulfide (**5i**, **5iii**, **9** and **10**) derivatives, it was understood that the homodimers with disulfide spacer was the basic scaffold for the molecules inhibiting Fc γ receptor dependent phagocytosis of opsonized

RBCs. Substitution at C4 of the pyrazole moiety in the disulfide dimers influenced the potency in the increasing order of **5i** < **5iii** < **9** < **10**. After establishing the importance of the disulfide dimer over sulfhydryl compounds, it was then decided to explore the effect of different spacer groups of varying length and N1 substitution of one of the pyrazole of homodimer on their ability to inhibit phagocytosis.

In an attempt to better understand the role of the disulfide bridge in the lead molecule **10**, the sulfur atoms were replaced with their bivalent bioisosteres⁴⁶ -CH₂- and -O- in the analogs **17** and **18** respectively. The screening results of analogs **17** and **18** were unanticipated, the bioisosteric replacement of the sulfur atoms in the disulfide bridge resulted in compromised activity (Table 4.8). Compounds **21**, **22** and **26** were prepared with varying spacer nature and length of 3, 4 and 1 atom respectively. Compound **21** with 3 atom spacer arm inhibited 20% of phagocytosis at 5 μM concentration. Analogs **22** and **26** comprising of 4 and 1 atom spacer arm displayed dramatic decrease in activity at 5 μM concentration in MMA (Table 4.8). Change of the nature and the length of the spacer arm between the two pyrazole moieties of lead **10** gave an understanding that the 2-3 atoms spacer arm was appropriate for minimum inhibition (10-20%) of the phagocytosis in MMA. The weak performance of these analogs (**17**, **18**, **21**, **22** and **26**) could be attributed to the varying resultant bond lengths and the torsional angles of different spacer arm affecting the conformation of the ligand at its unknown active site. Regardless of the compromised activity, compound **18** was selected for further structural modification study. It was envisioned that the

inhibition potential of the bivalent compound **18** could be improved with suitable N1 substitution at one of the pyrazole moiety (Figure 4.4).

Previously Branch et al reported that the disulfide with aromatic nitro group efficiently inhibited in-vitro Fcγ receptor mediated phagocytosis of opsonized RBCs.^{47,48} In an endeavor to comprehend the influence of the strong electron withdrawing group nitro on the activity of the bivalent scaffold **18**, analog **30** with *p*-nitro phenyl at N1 position of one of the pyrazole was synthesized and evaluated. There was insignificant difference between the phagocytosis inhibition profile of the unsymmetrical ligand **30** and symmetrical ligand **18** (Table 4.8). Compound **34** with N1-benzyl pyrazole failed to inhibit Fcγ receptor dependent phagocytosis of anti-D coated RBCs. Compounds **39** and **43** with 6 and 5 membered saturated carbocyclic rings at N1 position of pyrazole respectively were prepared and tested in-vitro MMA. Compound **39** with methyl cyclohexyl as N1 substitution inhibited 45% phagocytosis of opsonized RBCs. In contrast, the compound **43** with cyclopentane at N1 was able to inhibit 17% of in-vitro phagocytosis of sensitized RBCs. Further modifications considered at N1 position of the pyrazole in bivalent scaffold **18**, included ethyl amino and methyl carboxylic acid. Ethyl amino derivative **49** suppressed 33% of anti-D coated RBC's phagocytosis. However, methyl carboxylic acid derivative **50** exhibited poor inhibition of phagocytosis at 5 μM concentration. Before considering other substituents at N1 position of one of the pyrazole of analog **18**, it was worth assessing the activity of the compound devoid of mono N1 substitution. Hence, compound **51** was designed and synthesized. Phagocytosis of opsonized RBCs by compound **51** treated monocytes was reduced to 6 %.

During synthesis of compound **51**, its expected regio-isomer **52** was formed which was isolated and tested in MMA. It was interesting to observe a remarkable 58% decrease in phagocytosis of sensitized erythrocytes by monocytes treated with isomer **52** (Table 4.8). In order to explore the scope of substitutes for pyrazole, heterodimer **55** with *N*-benzyl pyrrolidine as nucleus was made and tested for its potential to inhibit in-vitro phagocytosis. Phagocytosis by compound **55** treated monocytes decreased to 15%. Compound **55** performed better than the *N*-benzyl substituted pyrazole derivative **34**.

The preliminary results of search for a novel small molecules inhibiting Fcγ dependent phagocytosis of sensitized RBCs has suggested three potential candidates **10**, **39** and **52**. The current study has revealed importance of certain functional features such as 2-atom spacer arm, alkyl substitution at one of the N1 position of bivalent pyrazole core nucleus, may be useful for phagocytosis inhibition. In future, efforts will be taken to translate the in-vitro activity of the potential candidates into a pertinent in-vivo mouse model of ITP developed in our laboratory.⁴⁹

4.6. References

- (1) Gauer, R. L.; Braun, M. M. Thrombocytopenia. *Am. Fam. Physician* **2012**, *85* (6), 612-622.
- (2) Veneri, D.; Franchini, M.; Randon, F.; Nichele, I.; Pizzolo, G.; Ambrosetti, A. Thrombocytopenias: a clinical point of view. *Blood Transfus.* **2009**, *7* (2), 75-85.
- (3) Cines, D. B.; Bussel, J. B.; Liebman, H. A.; Luning Prak, E. T. The ITP syndrome: pathogenic and clinical diversity. *Blood.* **2009**, *113* (26), 6511-6521.
- (4) Buckley, M. F.; James, J. W.; Brown, D. E.; Whyte, G. S.; Dean, M. G.; Chesterman, C. N.; Donald, J. A. A novel approach to the assessment of variations in the human platelet count. *Thromb. Haemost.* **2000**, *83* (3), 480-484.
- (5) Neunert, C.; Lim, W.; Crowther, M.; Cohen, A.; Solberg, L. Jr.; Crowther, M. A. The American Society of Hematology 2011 evidence-based practice guideline for immune thrombocytopenia. *Blood* **2011**, *117* (16), 4190-41207.
- (6) Handin, R. I.; Stossel, T. P. Phagocytosis of antibody-coated platelets by human granulocytes. *N. Engl. J. Med.* **1974**, *290* (18), 989-993.
- (7) Kuwana, M.; Okazaki, Y.; Ikeda, Y. Splenic macrophages maintain the anti-platelet autoimmune response via uptake of opsonized platelets in patients with immune thrombocytopenic purpura. *J. Thromb. Haemost.* **2009**, *7* (2), 322-329.

- (8) Crow, A. R.; Lazarus, A. H. Role of Fcγ receptors in the pathogenesis and treatment of idiopathic thrombocytopenic purpura. *J. Pediatr. Hematol. Oncol.* **2003**, *25*, S14-18.
- (9) George, J. N. Sequence of treatments for adults with primary immune thrombocytopenia. *Am. J. Hematol.* **2012**, *87*, Suppl 1, S12-15.
- (10) Kuter, D. J. New drugs for familiar therapeutic targets: thrombopoietin receptor agonists and immune thrombocytopenic purpura. *Eur. J. Haematol. Suppl.* **2008**, *69*, 9-18.
- (11) Blackhouse, G.; Xie, F.; Levine, M.A.; Campbell, K.; Assasi, N.; Gaebel, K.; O'Reilly, D.; Tarride, J.; Goeree, R. Canadian cost- utility analysis of intravenous immunoglobulin for acute childhood idiopathic thrombocytopenic purpura. *J. Popul. Ther. Clin. Pharmacol.* **2012**, *19* (2), e166-e178.
- (12) Baerenwaldt, A.; Biburger, M.; Nimmerjahn, F. Mechanisms of action of intravenous immunoglobulins. *Expert Rev Clin Immunol.* **2010**, *6* (3), 425-434.
- (13) Crow, A. R.; Lazarus, A. H. The mechanisms of action of intravenous immunoglobulin and polyclonal anti-d immunoglobulin in the amelioration of immune thrombocytopenic purpura: what do we really know? *Transfus. Med. Rev.* **2008**, *22* (2), 103-116.
- (14) Stangel, M.; Pul, R. Basic principles of intravenous immunoglobulin (IVIg) treatment. *J. Neurol.* **2006**, *253*, V18-24.
- (15) Hansen, R. J.; Balthasar, J. P. Mechanisms of IVIG action in immune thrombocytopenic purpura. *Clin Lab.* **2004**, *50* (3-4), 133-140.

-
- (16) Lazarus, A. H. Mechanism of action of IVIG in ITP. *Vox Sang.* **2002**, 83 (1), 53-55.
- (17) Crow, A. R.; Song, S.; Semple, J. W.; Freedman, J.; Lazarus, A. H. IVIg inhibits reticuloendothelial system function and ameliorates murine passive-immune thrombocytopenia independent of anti-idiotypic reactivity. *Br. J. Haematol.* **2001**, 115, 679–686.
- (18) Carpenter, R. R.; Barsales, P. B. Uptake by mononuclear phagocytes of protein-coated bentonite particles stabilized with a carbodiimide. *J. Immunol.* **1967**, 98 (4), 844-853.
- (19) Sahaf, B.; Heydari, K.; Herzenberg, L. A.; Herzenberg, L. A. Lymphocyte surface thiol levels. *Proc. Natl. Acad. Sci.* **2003**, 100 (7), 4001-4005.
- (20) Rampersad, G. C.; Suck, G.; Sakac, D.; Fahim, S.; Foo, A.; Denomme, G. A.; Langler, R. F.; Branch, D. R. Chemical compounds that target thiol-disulfide groups on mononuclear phagocytes inhibit immune mediated phagocytosis of red blood cells. *Transfusion.* **2005**, 45 (3), 384-393.
- (21) Foo, A. H.; Fletcher, S. P.; Langler, R. F.; Porter, C. H.; Branch, D. R. Structure-function studies for in vitro chemical inhibition of Fc gamma receptor-mediated phagocytosis. *Transfusion.* **2007**, 47 (2), 290-298.
- (22) Branch, D. R.; Gallagher, M. T.; Mison, A. P.; Sy Siok Hian, A. L.; Petz, L. D. In vitro determination of red cell alloantibody significance using an assay of monocyte-macrophage interaction with sensitized erythrocytes. *Br. J. Haematol.* **1984**, 56 (1), 19-29.

-
- (23) Gallagher, M. T.; Branch, D. R.; Mison A.; Petz, L. D. Evaluation of reticuloendothelial function in autoimmune hemolytic anemia using an in vitro assay of monocyte-macrophage interaction with erythrocytes. *Exp. Hematol.* **1983**, *11* (1), 82-89.
- (24) Hadley, A. G. Laboratory assays for predicting the severity of haemolytic disease of the fetus and newborn. *Transpl. Immunol.* **2002**, *10* (2-3), 191-198.
- (25) Arndt, P. A.; Garratty G. A retrospective analysis of the value of monocyte monolayer assay results for predicting the clinical significance of blood group alloantibodies. *Transfusion* **2004**, *44* (9), 1273-1281.
- (26) Jensen, B. S. The synthesis of 1-phenyl-3-methyl-4-acyl-pyrazolones-5. *Acta. Chemica. Scandinavica* **1959**, *13*, 1668-1670.
- (27) Barreiro, E. J.; Camara, C. A. Verli, H. Brazil-Más, L.; Castro, N. G.; Cintra, W. M.; Aracava, Y.; Rodrigues, C. R.; Fraga, C. A. Design, synthesis, and pharmacological profile of novel fused pyrazolo[4,3-d]pyridine and pyrazolo[3,4-b][1,8]naphthyridine isosteres: a new class of potent and selective acetylcholinesterase inhibitors. *J. Med. Chem.* **2003**, *46* (7), 1144-1152.
- (28) Datterl, B.; Tröstner, N.; Kucharski, D.; Holzer, W. Heterocyclic analogues of xanthone and xanthione. 1H-pyrano[2,3-c:6,5-c]dipyrazol-4(7H)-ones and thiones: synthesis and NMR Data. *Molecules* **2010**, *15*, 6106-6126.

-
- (29) Holzer, W., Hahn, K. Synthesis of substituted 3-phenyl-6H-pyrazolo[4,3-d]isoxazoles from corresponding 4-benzoyl-5-hydroxypyrazoles. *J. Heterocycl. Chem.* **2003**, *40* (2), 303-308.
- (30) David, A.; Edyta, M.; Brzostowska, A. M.; Alexander, G. Regioselective (biomimetic) synthesis of a pentasulfane from ortho-benzoquinone. *J. Org. Chem.* **2007**, *72* (8), 2951-2955.
- (31) Ilari, F.; Anderson, G.; Abdul, H.; Lucian, A. L.; Dimitris, S. A. Spectral monitoring of the formation and degradation of polysulfide ions in alkaline conditions. *Ind. Eng. Chem. Res.* **2006**, *45* (22), 7388-7392.
- (32) Martins, M. A. P.; Bastos, G. P.; Bonacorso, H. G.; Zanatta, N.; Flores, A. F. C.; Siqueira, G. M. Regiospecific Acylation of Acetals. A convenient method to obtain β -methoxyvinyl trichloromethyl ketones. *Tetrahedron Lett.* **1999**, *40* (23), 4309-4312.
- (33) Martins, M. A. P.; Guarda, E. A.; Frizzo, C. P.; Scapin, E.; Beck, P.; Costa, A. C.; Zanatta, N.; Bonacorso, H. G. Synthesis of 1,1,1-trichloro[fluoro]-3-alken-2-ones using ionic liquids, *J. Mol. Catal. A: Chem.* **2007**, *266* (1-2), 100-103.
- (34) Martins, M. A. P.; Freitag, R. A.; Da Rosa, A.; Flores, A. F. C.; Zanatta, N.; Bonacorso, H. G. Haloacetylated enol ethers. 11. Synthesis of 1-methyl- and 1-phenyl pyrazole-3(5)-ethyl esters. A one-pot procedure. *J. Heterocyclic Chem.* **1999**, *36*, 217-220.
- (35) Więcek, M.; Kottke, T.; Ligneau, X.; Schunack, W.; Seifert, R.; Stark, H.; Handzlik, J.; Kieć-Kononowicz, K. N-Alkenyl and cycloalkyl

- carbamates as dual acting histamine H3 and H4 receptor ligands. *Bioorg Med Chem.* **2011**, *19* (9), 2850-2858.
- (36) Michaelis, A.; Behn, H. Ueber das 1-phenyl-3-methyl-5-chlor- und -5-brom-pyrazol. *Ber. dtsh. Chem. Ges.* **1900**, *33* (2), 2595-2607
- (37) Barreiro, E. J.; Camara, C. A.; Verli, H.; Brazil-Más, L.; Castro, N. G.; Cintra, W. M.; Aracava, Y.; Rodrigues, C. R.; Fraga, C. A. Design, synthesis, and pharmacological profile of novel fused pyrazolo[4,3-d]pyridine and pyrazolo[3,4-b][1,8]naphthyridine isosteres: a new class of potent and selective acetylcholinesterase inhibitors. *J. Med. Chem.* **2003**, *46* (7), 1144-1152.
- (38) Gu, W.; Wang, S. Synthesis and antimicrobial activities of novel 1H-dibenzo[a,c]carbazoles from dehydroabiatic acid. *Eur. J. Med. Chem.* **2010**, *45* (10), 4692-4696.
- (39) Tagawa, Y.; Minami, S.; Yoshida, T.; Tanaka, K.; Sato, S.; Goto, Y.; Yamagata, K. Preparation and antibacterial activity of 3-methyl-1-p-substituted phenylpyrazole-5-thiol. *Arch Pharm (Weinheim)*. **2002**, *335* (2-3), 99-103.
- (40) Meyer, K. G.; Simple preparation of monoalkylhydrazines (IV) *Synlett* **2004**, *13*, 2355-2356.
- (41) Freedman, H. H. Industrial applications of phase-transfer catalysis (Ptc): past, present and future. *Pure Appl. Chem.* **1986**, *58*, 857-868.
- (42) Krishnamurthy, M.; Li, W.; Moore, B. M. 2nd. Synthesis, biological evaluation, and structural studies on N1 and C5 substituted cycloalkyl analogues of the pyrazole class of CB1 and CB2 ligands. *Bioorg. Med. Chem.* **2004**, *12* (2), 393-404.

-
- (43) Mojtahedi, M. M.; Jalali, M. R.; Abaee, M. S.; Bolourtchian, M. Microwave-assisted synthesis of substituted pyrazolones under solvent-free conditions. *Heterocycl. Commun.* **2006**, *12* (3-4), 225–228.
- (44) Appel, R. Tertiary phosphane/tetrachloromethane, a versatile reagent for chlorination, dehydration, and p-n linkage. *Angew. Chem. Int. Ed. Engl.* **1975**, *14*, 801–811.
- (45) Argyropoulos, D. S.; Hou, Y.; Ganesaratnam, R.; Harpp, D. N.; Koda, K. Quantitative ¹H NMR analysis of alkaline polysulfide solutions. *Holzforschung* **2005**, *59*, 124-131.
- (46) Lima, L. M.; Barreiro, E.J. Bioisosterism: a useful strategy for molecular modification and drug design. *Curr. Med. Chem.* **2005**, *12* (1), 23-49.
- (47) Rampersad, G. C.; Suck, G.; Sakac, D.; Fahim, S.; Foo, A.; Denomme, G. A.; Langler, R. F.; Branch, D. R. Chemical compounds that target thiol-disulfide groups on mononuclear phagocytes inhibit immune mediated phagocytosis of red blood cells. *Transfusion.* **2005**, *45* (3), 384-393.
- (48) Foo, A. H.; Fletcher, S. P.; Langler, R. F.; Porter, C. H.; Branch, D. R. Structure-function studies for in vitro chemical inhibition of Fc gamma receptor-mediated phagocytosis. *Transfusion* **2007**, *47* (2), 290-298.
- (49) Katsman, Y.; Foo, A.H.; Leontyev, D.; Branch, D.R. Improved mouse models for the study of treatment modalities for immune-mediated platelet destruction. *Transfusion* **2010**, *50* (6), 1285-1294.

Appendix

List of publications

1. Bello, A. M.; **Purohit, M. K.**; Cui, Y. J. T.; Stead, B. S.; Kotra, L. P. Immunological targets in inflammation from the small molecule prespective. *Anti-Inflamm. Anti-Allergy Agents Med. Chem.* **2011**, *10*, 121-131.
2. **Purohit, M. K.**; Poduch, E.; Wei, L. W.; Crandall, I. E.; To, T.; Kain, K. C.; Pai, E. F.; Kotra, L. P. Novel cytidine-based orotidine-5'-monophosphate decarboxylase inhibitors with an unusual twist. *J. Med. Chem.* **2012**, *55* (22), 9988-9997.
3. Hadimani, M.; **Purohit, M. K.**; Vanampally, C.; Pleog, R.; Abrallo, V.; Morrow, D.; Frizzi, K.; Calcutt, N.; Fernyhough, P.; Kotra, L. P. Guaifenesin derivatives promote neurite outgrowth and protect diabetic mice from neuropathy. *J. Med. Chem.* **2013**, *56*(12), 5071-5078.
4. **Purohit, M. K.**; Scovell, I.; Neschadim, A.; Katsman, Y.; Branch, R. D.; Kotra, L. P. Disulfide Linked Pyrazole Derivatives Inhibit Fc γ Receptor Mediated Phagocytosis. *Bioorg. Med Chem Lett.* **2013**, *23*(8), 2324-2327.
5. **Purohit, M. K.**; Chakka, K. S.; Scovell, I.; Neschadim, A.; Katsman, Y.; Branch, R. D.; Kotra, L. P. Discovery and synthesis of novel pyrazole derivatives inhibiting in-vitro fc γ receptor mediated phagocytosis II. (Manuscript)
6. Wei, L.; **Purohit, M. K.**; Bello, A. M.; Lewis, M. M.; BeataMajchrzak-Kita, Fish, N. L.; Kotra, L. P. Discovery of small molecules mimicking protein-protein interactions at the interface of interferon- α 2a and type I interferon receptor. (Manuscript)

Work presented in conferences

1. **Purohit, M. K.**; Poduch, P.; Pai, E.; Kotra, L. P. Unconventional derivatives of CMP as inhibitors of Orotidine-5'-monophosphate decarboxylase-an antimalarial target. Indian Pharmaceutical Congress (IPC), **2010**, Manipal, India. (Best Paper Award)
2. **Purohit, M. K.**; Poduch, E.; Wei, L.; Crandall, I.; Kain, C. K.; Pai, E.; Kotra, L. P. N^3 - and N^4 -CMP derivatives as orotidine -5-monophosphate decarboxylase inhibitors. Canadian Society for Pharmaceutical Sciences (CSPS), **2012**, Toronto, Canada. (Poster Presentation).
3. **Purohit, M. K.**; Calcutt, A. N.; Fernyhough, P.; Kotra, L. P. Effect of chirality on neurite outgrowth of sensory neurons using phenoxy propanediol derivatives. Canadian Society for Pharmaceutical Sciences (CSPS), **2012**, Toronto, Canada. (Poster Presentation).
4. Branch, R. D.; **Purohit, M. K.**; Scovell, I.; Neschadim, A.; Katsman, Y.; Kotra, L. P. Small Molecule Inhibitors of Phagocytosis for Treatment of Immune Cytopenias. ISEH – Society for Hematology and Stem Cells, 42nd Annual Scientific Meeting, **2013**, Vienna, Austria. (Poster Presentation).

Biography of Lakshmi P. Kotra, B. Pharm.(Hons), Ph.D.

Dr. Kotra is the Director at the Center for Molecular Design and Preformulations (CMDP) a joint Center at University Health Network and the Leslie Dan Faculty of Pharmacy at the University of Toronto (<http://cmdp.uhnres.utoronto.ca>), a Scientist and Principal Investigator at University Health Network, an Associate Professor of Medicinal Chemistry at the University of Toronto (<http://www.uhnresearch.ca/kotralab>), and is a McLaughlin Scholar at the R. Samuel McLaughlin Center for Molecular Medicine. Dr. Kotra holds an adjunct professorship at Birla Institute of Tech & Sci, Pilani (India).

Dr. Kotra was born and completed his schooling in the state of Andhra Pradesh, followed by an undergraduate degree from BITS, Pilani. Dr. Kotra then moved to the United States of America to pursue Ph.D. from the University of Georgia and underwent postdoctoral training at Wayne State University.

Kotra research program focuses on the interdisciplinary sciences spanning computer modeling, synthetic chemistry, pharmaceutical sciences, biochemistry and animal models addressing the development of novel therapeutic agents. Kotra research group has interests and very active programs in cancer, infectious diseases, diabetes, multiple sclerosis, and related complications. Current research projects in Kotra laboratories in Canada include drugs targeting malaria, thrombocytopenia, diabetic neuropathy, multiple sclerosis, broad-spectrum antivirals, and targeted delivery of anticancer agents. Dr. Kotra has been recently appointed as the

theme lead for health and infectious diseases in the CIRCE initiative by University of Toronto, University of British Columbia and University of Alberta.

Dr. Kotra served on various provincial, national and international initiatives in the areas of drug discovery and development. Dr. Kotra is a recipient of several awards including the Premier's Research Excellence Award from the Province of Ontario, R&D Health Research Foundation Research Career award, GlaxoSmithKline/Canadian Society for Pharmaceutical Sciences Young Investigator Award. Dr. Kotra served on the executive council of the Canadian Society for Pharmaceutical Sciences (2004). Dr. Kotra authored/co-authored over 100 publications including peer-reviewed scientific papers, expert review articles and book chapters, seven patents/patent applications and more than 80 invited talks around the world.

Biography of Ms. Meena K. Purohit

Ms. Meena K. Purohit completed her Bachelor of Pharmacy from The University of Mumbai, in the year 2006 and Master of Pharmaceutical Sciences from Birla Institute of Science and Technology (BITS), Pilani, in 2008. She has been working as BITS exchange research scholar at Toronto General Research Institute (TGRI), University Health Network, Toronto, Canada from 2008-2012 under supervision of Dr. Lakshmi P. Kotra. She has published two scientific publications in international journals. She had presented papers at various national and international conferences.

Table A.3. 1: Neuronal proteins found in the control lane (excluding keratin and repeats) of target deconvolution (serial affinity chromatography) experiment, chapter 3.

Rat		
prot_acc	prot_desc	prot_score
1433B_RAT	14-3-3 protein beta/alpha OS=Rattus norvegicus GN=Ywhab PE=1 SV=3	73
1433E_RAT	14-3-3 protein epsilon OS=Rattus norvegicus GN=Ywhae PE=1 SV=1	149
1433G_RAT	14-3-3 protein gamma OS=Rattus norvegicus GN=Ywhag PE=1 SV=2	100
1433T_RAT	14-3-3 protein theta OS=Rattus norvegicus GN=Ywhaq PE=1 SV=1	127
1433Z_RAT	14-3-3 protein zeta/delta OS=Rattus norvegicus GN=Ywhaz PE=1 SV=1	188
ACTC_RAT	Actin, alpha cardiac muscle 1 OS=Rattus norvegicus GN=Actc1 PE=1 SV=1	545
ACTG_RAT	Actin, cytoplasmic 2 OS=Rattus norvegicus GN=Actg1 PE=1 SV=1	578
ADT1_RAT	ADP/ATP translocase 1 OS=Rattus norvegicus GN=Slc25a4 PE=1 SV=3	144
ADT2_RAT	ADP/ATP translocase 2 OS=Rattus norvegicus GN=Slc25a5 PE=1 SV=3	119
AN32A_RAT	Acidic leucine-rich nuclear phosphoprotein 32 family member A OS=Rattus norvegicus GN=Anp32a PE=2 SV=1	37
ANXA2_RAT	Annexin A2 OS=Rattus norvegicus GN=Anxa2 PE=1 SV=2	98
AP2M1_RAT	AP-2 complex subunit mu-1 OS=Rattus norvegicus GN=Ap2m1 PE=1 SV=1	100
ATPA_RAT	ATP synthase subunit alpha, mitochondrial OS=Rattus norvegicus GN=Atp5a1 PE=1 SV=2	65
ATPB_RAT	ATP synthase subunit beta, mitochondrial OS=Rattus norvegicus GN=Atp5b PE=1 SV=2	57
ATPG_RAT	ATP synthase subunit gamma, mitochondrial OS=Rattus norvegicus GN=Atp5c1 PE=1 SV=2	80
CDIPT_RAT	CDP-diacylglycerol--inositol 3-phosphatidyltransferase OS=Rattus norvegicus GN=Cdipt PE=1 SV=1	45
CN37_RAT	2~,3~-cyclic-nucleotide 3~-phosphodiesterase OS=Rattus norvegicus GN=Cnp PE=1 SV=2	302
DHE3_RAT	Glutamate dehydrogenase 1, mitochondrial OS=Rattus norvegicus GN=Glud1 PE=1 SV=2	209

Appendix

DNM1L_RAT	Dynamin-1-like protein OS=Rattus norvegicus GN=Dnm1l PE=1 SV=1	38
ECHB_RAT	Trifunctional enzyme subunit beta, mitochondrial OS=Rattus norvegicus GN=Hadhb PE=1 SV=1	97
EF1A1_RAT	Elongation factor 1-alpha 1 OS=Rattus norvegicus GN=Eef1a1 PE=2 SV=1	77
EF1A2_RAT	Elongation factor 1-alpha 2 OS=Rattus norvegicus GN=Eef1a2 PE=2 SV=1	94
EF1G_RAT	Elongation factor 1-gamma OS=Rattus norvegicus GN=Eef1g PE=2 SV=3	206
EFTU_RAT	Elongation factor Tu, mitochondrial OS=Rattus norvegicus GN=Tufm PE=1 SV=1	58
EIF3E_RAT	Eukaryotic translation initiation factor 3 subunit E OS=Rattus norvegicus GN=Eif3e PE=2 SV=1	102
ELAV2_RAT	ELAV-like protein 2 OS=Rattus norvegicus GN=Elavl2 PE=2 SV=1	86
FLOT1_RAT	Flotillin-1 OS=Rattus norvegicus GN=Flot1 PE=2 SV=2	90
FLOT2_RAT	Flotillin-2 OS=Rattus norvegicus GN=Flot2 PE=1 SV=1	105
GBLP_RAT	Guanine nucleotide-binding protein subunit beta-2-like 1 OS=Rattus norvegicus GN=Gnb2l1 PE=1 SV=3	127
H10_RAT	Histone H1.0 OS=Rattus norvegicus GN=H1f0 PE=2 SV=2	87
H12_RAT	Histone H1.2 OS=Rattus norvegicus GN=Hist1h1c PE=1 SV=3	87
H1T_RAT	Histone H1t OS=Rattus norvegicus GN=Hist1h1t PE=1 SV=2	48
H2AZ_RAT	Histone H2A.Z OS=Rattus norvegicus GN=H2afz PE=2 SV=2	44
H4_RAT	Histone H4 OS=Rattus norvegicus GN=Hist1h4b PE=1 SV=2	42
HNRPC_RAT	Heterogeneous nuclear ribonucleoprotein C (Fragment) OS=Rattus norvegicus GN=Hnrnpc PE=2 SV=1	76
HNRPF_RAT	Heterogeneous nuclear ribonucleoprotein F OS=Rattus norvegicus GN=Hnrnpf PE=1 SV=3	37
HNRPG_RAT	Heterogeneous nuclear ribonucleoprotein G OS=Rattus norvegicus GN=Rbmx PE=1 SV=1	94
IF4A2_RAT	Eukaryotic initiation factor 4A-II OS=Rattus norvegicus GN=Eif4a2 PE=1 SV=1	88
ITPR2_RAT	Inositol 1,4,5-trisphosphate receptor type 2 OS=Rattus norvegicus GN=Itpr2 PE=2 SV=1	36
KCRU_RAT	Creatine kinase, ubiquitous mitochondrial	76

Appendix

	OS=Rattus norvegicus GN=Ckmt1 PE=1 SV=1	
MAP1A_RAT	Microtubule-associated protein 1A OS=Rattus norvegicus GN=Map1a PE=1 SV=1	66
MBP_RAT	Myelin basic protein S OS=Rattus norvegicus GN=Mbp PE=1 SV=3	326
MK15_RAT	Mitogen-activated protein kinase 15 OS=Rattus norvegicus GN=Mapk15 PE=1 SV=2	40
MLRA_RAT	Myosin regulatory light chain 2-A, smooth muscle isoform OS=Rattus norvegicus GN=Rlc-a PE=2 SV=2	81
MLRS_RAT	Myosin regulatory light chain 2, skeletal muscle isoform OS=Rattus norvegicus GN=Mylpf PE=2 SV=2	115
MPCP_RAT	Phosphate carrier protein, mitochondrial OS=Rattus norvegicus GN=Slc25a3 PE=1 SV=1	57
MYP0_RAT	Myelin P0 protein OS=Rattus norvegicus GN=Mpz PE=1 SV=1	552
NEST_RAT	Nestin OS=Rattus norvegicus GN=Nes PE=1 SV=2	41
NFH_RAT	Neurofilament heavy polypeptide OS=Rattus norvegicus GN=Nefh PE=1 SV=4	85
NFL_RAT	Neurofilament light polypeptide OS=Rattus norvegicus GN=Nefl PE=1 SV=3	130
NFM_RAT	Neurofilament medium polypeptide OS=Rattus norvegicus GN=Nefm PE=1 SV=4	50
PABP1_RAT	Polyadenylate-binding protein 1 OS=Rattus norvegicus GN=Pabpc1 PE=2 SV=1	48
PDC10_RAT	Programmed cell death protein 10 OS=Rattus norvegicus GN=Pdcd10 PE=2 SV=1	38
PDIA6_RAT	Protein disulfide-isomerase A6 OS=Rattus norvegicus GN=Pdia6 PE=1 SV=2	46
PERI_RAT	Peripherin OS=Rattus norvegicus GN=Prph PE=1 SV=1	69
PHB_RAT	Prohibitin OS=Rattus norvegicus GN=Phb PE=1 SV=1	69
PLAK_RAT	Junction plakoglobin OS=Rattus norvegicus GN=Jup PE=1 SV=1	110
PPAL_RAT	Lysosomal acid phosphatase OS=Rattus norvegicus GN=Acp2 PE=1 SV=1	36
PPIB_RAT	Peptidyl-prolyl cis-trans isomerase B OS=Rattus norvegicus GN=Ppib PE=2 SV=2	63
PRAX_RAT	Periaxin OS=Rattus norvegicus GN=Prx PE=1 SV=2	72
QCR2_RAT	Cytochrome b-c1 complex subunit 2, mitochondrial OS=Rattus norvegicus	70

Appendix

	GN=Uqerc2 PE=1 SV=2	
RAC1_RAT	Ras-related C3 botulinum toxin substrate 1 OS=Rattus norvegicus GN=Rac1 PE=1 SV=1	42
RL11_RAT	60S ribosomal protein L11 OS=Rattus norvegicus GN=Rpl11 PE=1 SV=2	120
RL12_RAT	60S ribosomal protein L12 OS=Rattus norvegicus GN=Rpl12 PE=2 SV=1	118
RL13_RAT	60S ribosomal protein L13 OS=Rattus norvegicus GN=Rpl13 PE=1 SV=2	100
RL17_RAT	60S ribosomal protein L17 OS=Rattus norvegicus GN=Rpl17 PE=2 SV=3	106
RL18_RAT	60S ribosomal protein L18 OS=Rattus norvegicus GN=Rpl18 PE=2 SV=2	63
RL18A_RAT	60S ribosomal protein L18a OS=Rattus norvegicus GN=Rpl18a PE=2 SV=1	122
RL21_RAT	60S ribosomal protein L21 OS=Rattus norvegicus GN=Rpl21 PE=1 SV=3	65
RL23A_RAT	60S ribosomal protein L23a OS=Rattus norvegicus GN=Rpl23a PE=2 SV=1	132
RL24_RAT	60S ribosomal protein L24 OS=Rattus norvegicus GN=Rpl24 PE=1 SV=1	236
RL26_RAT	60S ribosomal protein L26 OS=Rattus norvegicus GN=Rpl26 PE=1 SV=1	64
RL27A_RAT	60S ribosomal protein L27a OS=Rattus norvegicus GN=Rpl27a PE=1 SV=3	48
RL28_RAT	60S ribosomal protein L28 OS=Rattus norvegicus GN=Rpl28 PE=1 SV=4	39
RL3_RAT	60S ribosomal protein L3 OS=Rattus norvegicus GN=Rpl3 PE=1 SV=3	99
RL35_RAT	60S ribosomal protein L35 OS=Rattus norvegicus GN=Rpl35 PE=1 SV=3	36
RL4_RAT	60S ribosomal protein L4 OS=Rattus norvegicus GN=Rpl4 PE=2 SV=3	102
RL7_RAT	60S ribosomal protein L7 OS=Rattus norvegicus GN=Rpl7 PE=1 SV=2	361
RL7A_RAT	60S ribosomal protein L7a OS=Rattus norvegicus GN=Rpl7a PE=1 SV=2	374
RL8_RAT	60S ribosomal protein L8 OS=Rattus norvegicus GN=Rpl8 PE=2 SV=2	130
RLA0_RAT	60S acidic ribosomal protein P0 OS=Rattus norvegicus GN=Rplp0 PE=1 SV=2	39
RS11_RAT	40S ribosomal protein S11 OS=Rattus norvegicus GN=Rps11 PE=1 SV=3	69
RS2_RAT	40S ribosomal protein S2 OS=Rattus norvegicus GN=Rps2 PE=1 SV=1	50
RS3_RAT	40S ribosomal protein S3 OS=Rattus norvegicus GN=Rps3 PE=2 SV=1	222
RS3A_RAT	40S ribosomal protein S3a OS=Rattus norvegicus GN=Rps3a PE=1 SV=2	52

Appendix

RS4X_RAT	40S ribosomal protein S4, X isoform OS=Rattus norvegicus GN=Rps4x PE=2 SV=2	282
RS6_RAT	40S ribosomal protein S6 OS=Rattus norvegicus GN=Rps6 PE=1 SV=1	297
RS8_RAT	40S ribosomal protein S8 OS=Rattus norvegicus GN=Rps8 PE=1 SV=2	206
RS9_RAT	40S ribosomal protein S9 OS=Rattus norvegicus GN=Rps9 PE=1 SV=4	43
RSSA_RAT	40S ribosomal protein SA OS=Rattus norvegicus GN=Rpsa PE=1 SV=3	456
SC16B_RAT	Protein transport protein Sec16B OS=Rattus norvegicus GN=Sec16b PE=2 SV=1	35
SC5A6_RAT	Sodium-dependent multivitamin transporter OS=Rattus norvegicus GN=Slc5a6 PE=2 SV=1	45
SEPT2_RAT	Septin-2 OS=Rattus norvegicus GN=Sept2 PE=1 SV=1	44
SEPT7_RAT	Septin-7 OS=Rattus norvegicus GN=Sept7 PE=1 SV=1	51
SET_RAT	Protein SET OS=Rattus norvegicus GN=Set PE=1 SV=2	42
SMC3_RAT	Structural maintenance of chromosomes protein 3 OS=Rattus norvegicus GN=Smc3 PE=1 SV=1	36
TBA1A_RAT	Tubulin alpha-1A chain OS=Rattus norvegicus GN=Tuba1a PE=1 SV=1	164
TBA4A_RAT	Tubulin alpha-4A chain OS=Rattus norvegicus GN=Tuba4a PE=2 SV=1	110
TBB2A_RAT	Tubulin beta-2A chain OS=Rattus norvegicus GN=Tubb2a PE=1 SV=1	463
TBB2B_RAT	Tubulin beta-2B chain OS=Rattus norvegicus GN=Tubb2b PE=1 SV=1	388
TBB2C_RAT	Tubulin beta-2C chain OS=Rattus norvegicus GN=Tubb2c PE=1 SV=1	404
TBB3_RAT	Tubulin beta-3 chain OS=Rattus norvegicus GN=Tubb3 PE=1 SV=1	393
TBB5_RAT	Tubulin beta-5 chain OS=Rattus norvegicus GN=Tubb5 PE=1 SV=1	459
THY1_RAT	Thy-1 membrane glycoprotein OS=Rattus norvegicus GN=Thy1 PE=1 SV=1	47
TRY1_RAT	Anionic trypsin-1 OS=Rattus norvegicus GN=Prss1 PE=1 SV=1	367
TRY2_RAT	Anionic trypsin-2 OS=Rattus norvegicus GN=Prss2 PE=1 SV=2	81
TRY3_RAT	Cationic trypsin-3 OS=Rattus norvegicus GN=Try3 PE=2 SV=1	56
VAPB_RAT	Vesicle-associated membrane protein- associated protein B OS=Rattus norvegicus	150

Appendix

	GN=Vapb PE=1 SV=3	
VDAC2_RAT	Voltage-dependent anion-selective channel protein 2 OS=Rattus norvegicus GN=Vdac2 PE=1 SV=2	82
VIME_RAT	Vimentin OS=Rattus norvegicus GN=Vim PE=1 SV=2	163
YBOX1_RAT	Nuclease-sensitive element-binding protein 1 OS=Rattus norvegicus GN=Ybx1 PE=1 SV=3	162

Table A.3. 2: Neuronal proteins found in the T1lane (excluding keratin and repeats) of target deconvolution (serial affinity chromatography) experiment, chapter 3.

Rat		
UniprotID	prot_desc	Prot_Score
RL30_RAT	60S ribosomal protein L30 OS=Rattus norvegicus GN=Rpl30 PE=2 SV=2	246
RLA2_RAT	60S acidic ribosomal protein P2 OS=Rattus norvegicus GN=Rplp2 PE=1 SV=2	212
MYL6_RAT	Myosin light polypeptide 6 OS=Rattus norvegicus GN=Myl6 PE=1 SV=3	146
RS14_RAT	40S ribosomal protein S14 OS=Rattus norvegicus GN=Rps14 PE=2 SV=3	145
RS19_RAT	40S ribosomal protein S19 OS=Rattus norvegicus GN=Rps19 PE=2 SV=3	132
RS16_RAT	40S ribosomal protein S16 OS=Rattus norvegicus GN=Rps16 PE=1 SV=2	127
RL22_RAT	60S ribosomal protein L22 OS=Rattus norvegicus GN=Rpl22 PE=2 SV=2	125
RS20_RAT	40S ribosomal protein S20 OS=Rattus norvegicus GN=Rps20 PE=3 SV=1	120
H2A1C_RAT	Histone H2A type 1-C OS=Rattus norvegicus PE=1 SV=2	120
RL23_RAT	60S ribosomal protein L23 OS=Rattus norvegicus GN=Rpl23 PE=2 SV=1	110
RL36_RAT	60S ribosomal protein L36 OS=Rattus norvegicus GN=Rpl36 PE=1 SV=2	105
RS26_RAT	40S ribosomal protein S26 OS=Rattus norvegicus GN=Rps26 PE=3 SV=3	103
RS20_RAT	40S ribosomal protein S20 OS=Rattus norvegicus GN=Rps20 PE=3 SV=1	120
RS15A_RAT	40S ribosomal protein S15a OS=Rattus norvegicus GN=Rps15a PE=1 SV=2	98
HBB2_RAT	Hemoglobin subunit beta-2 OS=Rattus norvegicus PE=1 SV=2	93
H4_RAT	Histone H4 OS=Rattus norvegicus GN=Hist1h4b PE=1 SV=2	88
RSSA_RAT	40S ribosomal protein SA OS=Rattus norvegicus GN=Rpsa PE=1 SV=3	84
ATPD_RAT	ATP synthase subunit delta, mitochondrial OS=Rattus norvegicus GN=Atp5d PE=1 SV=2	83
MYL3_RAT	Myosin light chain 3 OS=Rattus norvegicus GN=Myl3 PE=1 SV=2	82

Appendix

HBA_RAT	Hemoglobin subunit alpha-1/2 OS=Rattus norvegicus GN=Hba1 PE=1 SV=3	79
HBB1_RAT	Hemoglobin subunit beta-1 OS=Rattus norvegicus GN=Hbb PE=1 SV=3	75
PRAX_RAT	Periaxin OS=Rattus norvegicus GN=Prx PE=1 SV=2	74
RS12_RAT	40S ribosomal protein S12 OS=Rattus norvegicus GN=Rps12 PE=1 SV=2	69
RL31_RAT	60S ribosomal protein L31 OS=Rattus norvegicus GN=Rpl31 PE=2 SV=1	66
RS25_RAT	40S ribosomal protein S25 OS=Rattus norvegicus GN=Rps25 PE=2 SV=1	57
COX41_RAT	Cytochrome c oxidase subunit 4 isoform 1, mitochondrial OS=Rattus norvegicus GN=Cox4i1 PE=1 SV=1	51
RS23_RAT	40S ribosomal protein S23 OS=Rattus norvegicus GN=Rps23 PE=2 SV=3	49
H2B1_RAT	Histone H2B type 1 OS=Rattus norvegicus PE=1 SV=2	47
RL34_RAT	60S ribosomal protein L34 OS=Rattus norvegicus GN=Rpl34 PE=1 SV=3	46
KLH24_RAT	Kelch-like protein 24 OS=Rattus norvegicus GN=Klh24 PE=1 SV=1	45
RL35A_RAT	60S ribosomal protein L35a OS=Rattus norvegicus GN=Rpl35a PE=3 SV=1	43
ELOB_RAT	Transcription elongation factor B polypeptide 2 OS=Rattus norvegicus GN=Tceb2 PE=1 SV=1	39
RS17_RAT	40S ribosomal protein S17 OS=Rattus norvegicus GN=Rps17 PE=2 SV=3	39
CIP4_RAT	Cdc42-interacting protein 4 OS=Rattus norvegicus GN=Trip10 PE=1 SV=3	38
KIF3C_RAT	Kinesin-like protein KIF3C OS=Rattus norvegicus GN=Kif3c PE=2 SV=1	35
MLRN_RAT	Myosin regulatory light chain 2, smooth muscle isoform OS=Rattus norvegicus GN=Myl9 PE=2 SV=2	153
TMM35_RAT	Transmembrane protein 35 OS=Rattus norvegicus GN=Tmem35 PE=2 SV=1	117
UBIQ_RAT	Ubiquitin OS=Rattus norvegicus GN=Rps27a PE=1 SV=1	96
SSRG_RAT	Translocon-associated protein subunit gamma OS=Rattus norvegicus GN=Ssr3 PE=1 SV=2	91
MCPT1_RAT	Mast cell protease 1 OS=Rattus norvegicus GN=Mcpt1 PE=1 SV=3	87
RS5_RAT	40S ribosomal protein S5 OS=Rattus norvegicus GN=Rps5 PE=2 SV=3	86
RS8_RAT	40S ribosomal protein S8 OS=Rattus norvegicus GN=Rps8 PE=1 SV=2	82

Appendix

TMEDA_RAT	Transmembrane emp24 domain-containing protein 10 OS=Rattus norvegicus GN=Tmed10 PE=1 SV=2	81
MLE1_RAT	Myosin light chain 1, skeletal muscle isoform OS=Rattus norvegicus GN=My11 PE=1 SV=2	78
ATPO_RAT	ATP synthase subunit O, mitochondrial OS=Rattus norvegicus GN=Atp5o PE=1 SV=1	70
SKP1_RAT	S-phase kinase-associated protein 1 OS=Rattus norvegicus GN=Skp1 PE=2 SV=3	69
TM109_RAT	Transmembrane protein 109 OS=Rattus norvegicus GN=Tmem109 PE=2 SV=1	60
ARF5_RAT	ADP-ribosylation factor 5 OS=Rattus norvegicus GN=Arf5 PE=1 SV=2	58
COF1_RAT	Cofilin-1 OS=Rattus norvegicus GN=Cfl1 PE=1 SV=3	58
H1T_RAT	Histone H1t OS=Rattus norvegicus GN=Hist1h1t PE=1 SV=2	55
RER1_RAT	Protein RER1 OS=Rattus norvegicus GN=Rer1 PE=2 SV=1	54
RL13_RAT	60S ribosomal protein L13 OS=Rattus norvegicus GN=Rpl13 PE=1 SV=2	50
RS7_RAT	40S ribosomal protein S7 OS=Rattus norvegicus GN=Rps7 PE=1 SV=1	46
RL32_RAT	60S ribosomal protein L32 OS=Rattus norvegicus GN=Rpl32 PE=1 SV=2	45
COX2_RAT	Cytochrome c oxidase subunit 2 OS=Rattus norvegicus GN=Mtco2 PE=2 SV=2	44
RS20_RAT	40S ribosomal protein S20 OS=Rattus norvegicus GN=Rps20 PE=3 SV=1	41
ANXA2_RAT	Annexin A2 OS=Rattus norvegicus GN=Anxa2 PE=1 SV=2	40
RAP1A_RAT	Ras-related protein Rap-1A OS=Rattus norvegicus GN=Rap1a PE=1 SV=1	40
CDC42_RAT	Cell division control protein 42 homolog OS=Rattus norvegicus GN=Cdc42 PE=1 SV=2	38
RS18_RAT	40S ribosomal protein S18 OS=Rattus norvegicus GN=Rps18 PE=1 SV=3	38
HPCL4_RAT	Hippocalcin-like protein 4 OS=Rattus norvegicus GN=Hpcal4 PE=2 SV=2	37
MYPR_RAT	Myelin proteolipid protein OS=Rattus norvegicus GN=Plp1 PE=1 SV=2	37
VISL1_RAT	Visinin-like protein 1 OS=Rattus norvegicus GN=Vsnl1 PE=1 SV=2	37
RL10_RAT	60S ribosomal protein L10 OS=Rattus norvegicus GN=Rpl10 PE=1 SV=3	176
RL9_RAT	60S ribosomal protein L9 OS=Rattus norvegicus GN=Rpl9 PE=1 SV=1	176

Appendix

MLE1_RAT	Myosin light chain 1, skeletal muscle isoform OS=Rattus norvegicus GN=My11 PE=1 SV=2	150
UCHL1_RAT	Ubiquitin carboxyl-terminal hydrolase isozyme L1 OS=Rattus norvegicus GN=Uchl1 PE=1 SV=2	129
TPIS_RAT	Triosephosphate isomerase OS=Rattus norvegicus GN=Tpi1 PE=1 SV=2	125
RL19_RAT	60S ribosomal protein L19 OS=Rattus norvegicus GN=Rpl19 PE=1 SV=1	116
MYADM_RA T	Myeloid-associated differentiation marker OS=Rattus norvegicus GN=Myadm PE=2 SV=1	113
RS8_RAT	40S ribosomal protein S8 OS=Rattus norvegicus GN=Rps8 PE=1 SV=2	98
PEBP1_RAT	Phosphatidylethanolamine-binding protein 1 OS=Rattus norvegicus GN=Pebp1 PE=1 SV=3	88
RL15_RAT	60S ribosomal protein L15 OS=Rattus norvegicus GN=Rpl15 PE=1 SV=2	87
RL13A_RAT	60S ribosomal protein L13a OS=Rattus norvegicus GN=Rpl13a PE=1 SV=2	76
RL14_RAT	60S ribosomal protein L14 OS=Rattus norvegicus GN=Rpl14 PE=1 SV=3	74
RS5_RAT	40S ribosomal protein S5 OS=Rattus norvegicus GN=Rps5 PE=2 SV=3	70
HSPB1_RAT	Heat shock protein beta-1 OS=Rattus norvegicus GN=Hspb1 PE=1 SV=1	62
SC22B_RAT	Vesicle-trafficking protein SEC22b OS=Rattus norvegicus GN=Sec22b PE=1 SV=3	62
PIMT_RAT	Protein-L-isoaspartate(D-aspartate) O- methyltransferase OS=Rattus norvegicus GN=Pcmt1 PE=1 SV=2	60
NDUV2_RAT	NADH dehydrogenase [ubiquinone] flavoprotein 2, mitochondrial OS=Rattus norvegicus GN=Ndufv2 PE=1 SV=2	59
RL10A_RAT	60S ribosomal protein L10a OS=Rattus norvegicus GN=Rpl10a PE=1 SV=2	58
MCPT1_RAT	Mast cell protease 1 OS=Rattus norvegicus GN=Mcpt1 PE=1 SV=3	55
RTN3_RAT	Reticulon-3 OS=Rattus norvegicus GN=Rtn3 PE=1 SV=1	55
GPSN2_RAT	Synaptic glycoprotein SC2 OS=Rattus norvegicus GN=Gpsn2 PE=2 SV=1	54
AT5F1_RAT	ATP synthase subunit b, mitochondrial OS=Rattus norvegicus GN=Atp5f1 PE=1 SV=1	50
PRDX1_RAT	Peroxiredoxin-1 OS=Rattus norvegicus GN=Prdx1 PE=1 SV=1	49

Appendix

PSB4_RAT	Proteasome subunit beta type-4 OS=Rattus norvegicus GN=Psmb4 PE=1 SV=2	45
ACTB_RAT	Actin, cytoplasmic 1 OS=Rattus norvegicus GN=Actb PE=1 SV=1	43
PRDX6_RAT	Peroxiredoxin-6 OS=Rattus norvegicus GN=Prdx6 PE=1 SV=3	43
ATP5H_RAT	ATP synthase subunit d, mitochondrial OS=Rattus norvegicus GN=Atp5h PE=1 SV=3	42
H12_RAT	Histone H1.2 OS=Rattus norvegicus GN=Hist1h1c PE=1 SV=3	39
RS7_RAT	40S ribosomal protein S7 OS=Rattus norvegicus GN=Rps7 PE=1 SV=1	37
RL29_RAT	60S ribosomal protein L29 OS=Rattus norvegicus GN=Rpl29 PE=1 SV=3	36
UBIQ_RAT	Ubiquitin OS=Rattus norvegicus GN=Rps27a PE=1 SV=1	36
VAPA_RAT	Vesicle-associated membrane protein-associated protein A OS=Rattus norvegicus GN=Vapa PE=1 SV=3	106
ACTB_RAT	Actin, cytoplasmic 1 OS=Rattus norvegicus GN=Actb PE=1 SV=1	43
GPSN2_RAT	Synaptic glycoprotein SC2 OS=Rattus norvegicus GN=Gpsn2 PE=2 SV=1	54
ACTA_RAT	Actin, aortic smooth muscle OS=Rattus norvegicus GN=Acta2 PE=1 SV=1	69
TPM2_RAT	Tropomyosin beta chain OS=Rattus norvegicus GN=Tpm2 PE=2 SV=1	66
TPM4_RAT	Tropomyosin alpha-4 chain OS=Rattus norvegicus GN=Tpm4 PE=1 SV=3	66
ANXA5_RAT	Annexin A5 OS=Rattus norvegicus GN=Anxa5 PE=1 SV=3	65
TXTP_RAT	Tricarboxylate transport protein, mitochondrial OS=Rattus norvegicus GN=Slc25a1 PE=1 SV=1	65
TPM1_RAT	Tropomyosin alpha-1 chain OS=Rattus norvegicus GN=Tpm1 PE=1 SV=3	61
HMGB1_RAT	High mobility group protein B1 OS=Rattus norvegicus GN=Hmgb1 PE=1 SV=2	49
ANXA2_RAT	Annexin A2 OS=Rattus norvegicus GN=Anxa2 PE=1 SV=2	40
NB5R3_RAT	NADH-cytochrome b5 reductase 3 OS=Rattus norvegicus GN=Cyb5r3 PE=1 SV=2	46
RL6_RAT	60S ribosomal protein L6 OS=Rattus norvegicus GN=Rpl6 PE=1 SV=5	43
CAPZB_RAT	F-actin-capping protein subunit beta OS=Rattus norvegicus GN=Capzb PE=1 SV=1	40

Appendix

TM175_RAT	Transmembrane protein 175 OS=Rattus norvegicus GN=Tmem175 PE=2 SV=1	40
TM16G_RAT	Transmembrane protein 16G OS=Rattus norvegicus GN=Tmem16g PE=2 SV=1	38
TM55B_RAT	Transmembrane protein 55B OS=Rattus norvegicus GN=Tmem55b PE=2 SV=1	37
HNRPK_RAT	Heterogeneous nuclear ribonucleoprotein K OS=Rattus norvegicus GN=Hnrpk PE=1 SV=1	36
LXN_RAT	Latexin OS=Rattus norvegicus GN=Lxn PE=1 SV=1	36
ODFP2_RAT	Outer dense fiber protein 2 OS=Rattus norvegicus GN=Odf2 PE=1 SV=2	36
PSME1_RAT	Proteasome activator complex subunit 1 OS=Rattus norvegicus GN=Psm1 PE=2 SV=1	36
ABCB7_RAT	ATP-binding cassette sub-family B member 7, mitochondrial OS=Rattus norvegicus GN=Abcb7 PE=2 SV=1	44
ACADL_RAT	Long-chain specific acyl-CoA dehydrogenase, mitochondrial OS=Rattus norvegicus GN=Acadl PE=1 SV=1	78
AINX_RAT	Alpha-internexin OS=Rattus norvegicus GN=Ina PE=1 SV=2	39
ALDOA_RAT	Fructose-bisphosphate aldolase A OS=Rattus norvegicus GN=Aldoa PE=1 SV=2	60
AT1B1_RAT	Sodium/potassium-transporting ATPase subunit beta-1 OS=Rattus norvegicus GN=Atp1b1 PE=1 SV=1	61
CD48_RAT	CD48 antigen OS=Rattus norvegicus GN=Cd48 PE=1 SV=1	53
CSK21_RAT	Casein kinase II subunit alpha OS=Rattus norvegicus GN=Csnk2a1 PE=2 SV=2	43
ELAV4_RAT	ELAV-like protein 4 OS=Rattus norvegicus GN=Elavl4 PE=1 SV=1	153
GNAS2_RAT	Guanine nucleotide-binding protein G(s) subunit alpha isoforms short OS=Rattus norvegicus GN=Gnas PE=1 SV=1	39
HS90A_RAT	Heat shock protein HSP 90-alpha OS=Rattus norvegicus GN=Hsp90aa1 PE=1 SV=3	37
IDHC_RAT	Isocitrate dehydrogenase [NADP] cytoplasmic OS=Rattus norvegicus GN=Idh1 PE=1 SV=1	49
ILF2_RAT	Interleukin enhancer-binding factor 2 OS=Rattus norvegicus GN=Ilf2 PE=2 SV=1	58
KCRB_RAT	Creatine kinase B-type OS=Rattus norvegicus GN=Ckb PE=1 SV=2	49
KCRM_RAT	Creatine kinase M-type OS=Rattus norvegicus GN=Ckm PE=1 SV=2	41

Appendix

MK01_RAT	Mitogen-activated protein kinase 1 OS=Rattus norvegicus GN=Mapk1 PE=1 SV=3	46
MK03_RAT	Mitogen-activated protein kinase 3 OS=Rattus norvegicus GN=Mapk3 PE=1 SV=5	64
MRP_RAT	MARCKS-related protein OS=Rattus norvegicus GN=Marcks11 PE=2 SV=3	74
OAT_RAT	Ornithine aminotransferase, mitochondrial OS=Rattus norvegicus GN=Oat PE=1 SV=1	46
ODPA_RAT	Pyruvate dehydrogenase E1 component subunit alpha, somatic form, mitochondrial OS=Rattus norvegicus GN=Pdha1 PE=1 SV=2	73
PELO_RAT	Protein pelota homolog OS=Rattus norvegicus GN=Pelo PE=2 SV=1	39
QCR2_RAT	Cytochrome b-c1 complex subunit 2, mitochondrial OS=Rattus norvegicus GN=Uqcrc2 PE=1 SV=2	136
ROA3_RAT	Heterogeneous nuclear ribonucleoprotein A3 OS=Rattus norvegicus GN=Hnrnpa3 PE=1 SV=1	41
SAHH_RAT	Adenosylhomocysteinase OS=Rattus norvegicus GN=Ahcy PE=1 SV=3	36
SCPDH_RAT	Probable saccharopine dehydrogenase OS=Rattus norvegicus GN=Sccpdh PE=2 SV=1	43
SFRS5_RAT	Splicing factor, arginine/serine-rich 5 OS=Rattus norvegicus GN=Sfrs5 PE=2 SV=1	47
WDR18_RAT	WD repeat-containing protein 18 OS=Rattus norvegicus GN=Wdr18 PE=2 SV=1	36
TBA1B_RAT	Tubulin alpha-1B chain OS=Rattus norvegicus GN=Tuba1b PE=1 SV=1	261
SERPH_RAT	Serpin H1 OS=Rattus norvegicus GN=Serpinh1 PE=1 SV=1	110
QCR1_RAT	Cytochrome b-c1 complex subunit 1, mitochondrial OS=Rattus norvegicus GN=Uqcrc1 PE=1 SV=1	86
LA_RAT	Lupus La protein homolog OS=Rattus norvegicus GN=Ssb PE=2 SV=1	84
ODO2_RAT	Dihydrolipoyllysine-residue succinyltransferase component of 2- oxoglutarate dehydrogenase complex, mitochondrial OS=Rattus norvegicus GN=Dlst PE=1 SV=2	74
PDIA3_RAT	Protein disulfide-isomerase A3 OS=Rattus norvegicus GN=Pdia3 PE=1 SV=2	63
GNA12_RAT	Guanine nucleotide-binding protein alpha-12 subunit OS=Rattus norvegicus GN=Gna12	59

Appendix

	PE=2 SV=3	
GNAL_RAT	Guanine nucleotide-binding protein G(olf) subunit alpha OS=Rattus norvegicus GN=Gnal PE=2 SV=2	59
ACTB_RAT	Actin, cytoplasmic 1 OS=Rattus norvegicus GN=Actb PE=1 SV=1	43
CDC37_RAT	Hsp90 co-chaperone Cdc37 OS=Rattus norvegicus GN=Cdc37 PE=1 SV=2	41
ELAV4_RAT	ELAV-like protein 4 OS=Rattus norvegicus GN=Elavl4 PE=1 SV=1	153
ACTA_RAT	Actin, aortic smooth muscle OS=Rattus norvegicus GN=Acta2 PE=1 SV=1	69
FUMH_RAT	Fumarate hydratase, mitochondrial OS=Rattus norvegicus GN=Fh PE=1 SV=1	37
NEUA_RAT	N-acylneuraminate cytidyltransferase OS=Rattus norvegicus GN=Cmas PE=2 SV=1	37
K0174_RAT	Uncharacterized protein KIAA0174 homolog OS=Rattus norvegicus PE=2 SV=1	36
VIP_RAT	VIP peptides OS=Rattus norvegicus GN=Vip PE=1 SV=2	36
ADCY5_RAT	Adenylate cyclase type 5 OS=Rattus norvegicus GN=Adcy5 PE=2 SV=2	35
GP116_RAT	Probable G-protein coupled receptor 116 OS=Rattus norvegicus GN=Gpr116 PE=1 SV=1	35
TBA1B_RAT	Tubulin alpha-1B chain OS=Rattus norvegicus GN=Tuba1b PE=1 SV=1	261
SERA_RAT	D-3-phosphoglycerate dehydrogenase OS=Rattus norvegicus GN=Phgdh PE=1 SV=3	122
LMNA_RAT	Lamin-A OS=Rattus norvegicus GN=Lmna PE=1 SV=1	120
CALR_RAT	Calreticulin OS=Rattus norvegicus GN=Calr PE=1 SV=1	102
FACR1_RAT	Fatty acyl-CoA reductase 1 OS=Rattus norvegicus GN=Mlstd2 PE=2 SV=1	101
SYDC_RAT	Aspartyl-tRNA synthetase, cytoplasmic OS=Rattus norvegicus GN=Dars PE=2 SV=1	101
CV028_RAT	UPF0027 protein C22orf28 homolog OS=Rattus norvegicus PE=2 SV=1	94
HNRH1_RAT	Heterogeneous nuclear ribonucleoprotein H OS=Rattus norvegicus GN=Hnrnph1 PE=1 SV=2	89
PTRF_RAT	Polymerase I and transcript release factor OS=Rattus norvegicus GN=Ptrf PE=1 SV=1	89
ALBU_RAT	Serum albumin OS=Rattus norvegicus GN=Alb PE=1 SV=2	87
PDIA3_RAT	Protein disulfide-isomerase A3 OS=Rattus	83

Appendix

	norvegicus GN=Pdia3 PE=1 SV=2	
TCPB_RAT	T-complex protein 1 subunit beta OS=Rattus norvegicus GN=Cct2 PE=1 SV=3	83
DESM_RAT	Desmin OS=Rattus norvegicus GN=Des PE=2 SV=2	82
PDIA1_RAT	Protein disulfide-isomerase OS=Rattus norvegicus GN=P4hb PE=1 SV=2	80
PTBP1_RAT	Polypyrimidine tract-binding protein 1 OS=Rattus norvegicus GN=Ptbp1 PE=1 SV=1	67
VATB2_RAT	Vacuolar ATP synthase subunit B, brain isoform OS=Rattus norvegicus GN=Atp6v1b2 PE=1 SV=1	59
ALDH2_RAT	Aldehyde dehydrogenase, mitochondrial OS=Rattus norvegicus GN=Aldh2 PE=1 SV=1	56
AINX_RAT	Alpha-internexin OS=Rattus norvegicus GN=Ina PE=1 SV=2	39
ERF1_RAT	Eukaryotic peptide chain release factor subunit 1 OS=Rattus norvegicus GN=Etf1 PE=2 SV=3	52
TCPD_RAT	T-complex protein 1 subunit delta OS=Rattus norvegicus GN=Cct4 PE=1 SV=3	52
HNRPQ_RAT	Heterogeneous nuclear ribonucleoprotein Q OS=Rattus norvegicus GN=Syncrip PE=2 SV=1	47
MOT1_RAT	Monocarboxylate transporter 1 OS=Rattus norvegicus GN=Slc16a1 PE=1 SV=1	45
RUFY3_RAT	Protein RUFY3 OS=Rattus norvegicus GN=Rufy3 PE=1 SV=1	41
ODO2_RAT	Dihydrolipoyllysine-residue succinyltransferase component of 2-oxoglutarate dehydrogenase complex, mitochondrial OS=Rattus norvegicus GN=Dlst PE=1 SV=2	39
AP2M1_RAT	AP-2 complex subunit mu-1 OS=Rattus norvegicus GN=Ap2m1 PE=1 SV=1	38
DYH7_RAT	Dynein heavy chain 7, axonemal OS=Rattus norvegicus GN=Dnah7 PE=2 SV=2	38
PLEC1_RAT	Plectin-1 OS=Rattus norvegicus GN=Plec1 PE=1 SV=2	37
PTBP2_RAT	Polypyrimidine tract-binding protein 2 OS=Rattus norvegicus GN=Ptbp2 PE=2 SV=1	35